Investigation of thyroid hormone-dependent molecular changes in the bullfrog back skin with special emphasis on the innate immune system

By

Lorissa May Corrie

A Thesis Submitted in Partial Fulfillment of the Requirements for the Degree of

MASTER OF SCIENCE

in the Department of Biochemistry and Microbiology

We acknowledge and respect the lək̓ʷəŋən peoples on whose traditional territory the university stands and the Songhees, Esquimalt and W̱SÁNEĆ peoples whose historical relationships with the land continue to this day.

Supervisory Committee

Investigation of thyroid hormone-dependent molecular changes in the bullfrog back skin with special emphasis on the innate immune system

By

Lorissa May Corrie

Supervisory Committee

Dr. Caren C. Helbing

Supervisor, *Department of Biochemistry and Microbiology*

Dr. Caroline Cameron

Departmental Member, *Department of Biochemistry and Microbiology*

Dr. Fraser Hof

Outside Member, *Department of Chemistry*

Abstract

As the aquatic tadpole undergoes metamorphosis to become a terrestrial juvenile frog, its innate immune system must adapt to its new environment. Skin is a primary line of defense in the innate immune system since it acts as an important physical, microbial, and chemical barrier that is constantly in contact with a microbially diverse environment throughout its life cycle. In amphibians, skin undergoes complex remodelling during postembryonic development. Metamorphosis is regulated by thyroid hormone (TH) initiated gene expression that leads to the start of the metamorphic programming. This can be induced by the addition of exogenous TH. While different tissues respond to TH in distinctive ways during metamorphosis, how these tissues respond to TH is poorly understood. Temperature modulation, which regulates metamorphic timing, is a unique way to uncover early TH-induced transcriptomic events related to a molecular memory. Using RNA-sequencing analysis, American bullfrog (*Rana [Lithobates] catesbeiana*) back skin transcripts were profiled during natural and temperature-modulated induced metamorphosis. During natural metamorphosis, significant differential expression was observed in over 6,500 transcripts. Premetamorphic tadpoles maintained at 5^{o}C, a temperature that is non-permissive for inducing morphological changes, showed 83 differentially expressed transcripts within 48 h after TH administration. Of note is the induction of *thibz* that has previously been identified as a molecular memory component in other tissues. Over 3,600 differentially expressed transcripts were detected in TH-treated tadpoles compared to the controls at permissive temperature (24^{o}C) after 48 h or when tadpoles were held at 5^{o}C and then shifted to 24^{o}C. We identified several innate immune system components: keratins, mucins, and antimicrobial peptides (AMPs) whose transcript levels changed during natural and TH-induced metamorphosis. A bioinformatics AMP identification pipeline, rAMPage, was applied to these RNA-seq data sets to identify 489 novel AMP candidates. AMPs have direct acting and immune stimulatory antimicrobial abilities and are promising antibiotic alternatives in public health and agricultural sectors. We synthesized and tested un-amidated and amidated C-terminal versions of 111 top-scoring novel AMP candidates for their antimicrobial activity and cell toxicity with a focus on agriculturally relevant pathogens (avian pathogenic *Escherichia coli* (APEC) and

Salmonella enterica serovar Enteritidis (SE)). We found that 28 peptides were moderately or highly active (Minimum inhibitory concentration ≤ 32 μg/mL) against APEC and six against SE, most of which displayed low cell toxicity. Active AMPs were physicochemically classified as positively charged, alpha helices with amphipathic characteristics. These AMPs are candidates for further testing as therapeutics to prevent or treat disease in poultry. While the present work is focused on the identification of amphibian AMPs, it has far-reaching applications, and the approach can be used to identify AMPs as an antibiotic alternative from any genomic resource.

Table of Contents

List of Figures

List of Tables

Acknowledgments

To Caren, thank you for your wisdom, kindness, encouragement, and laughter. From work experience until now has been a wonderful, frog filled ride that I will always treasure. Thank you for filling the lab with so many people who I am honoured to count as friends.

To my Supervisory Committee, thank you for your insight, support, and patience during this journey. Most importantly, thank you for laughing at my tadpole puns during my Committee meetings.

To the members of the Helbing Lab (both past and present), thank you for the joy you instilled in the lab. The support, encouragement, and laughs rescued many a hard science day and made pushing through so much easier.

To Vanessa, Teagan, Bita, Shae, Haley, Emma, and Anita… thank you for the roles you have played in this project. From tadpoles to chickens, I could not have done it without you.

To Alana, my PeptAid partner in crime, thank you for everything… you are an amazing scientist and even better person.

To my fellow graduate students (Ellis, Haley, Mike, and Neha), thank you for being my fellow grad grotto gremlins. Our terrible puns, lack of sunlight, and printer fumes will bind us together forever!

To Jacob, thank you for your bioinformatics wisdom.

To Josie aka the bestest of roommates, as per our roommate publication pact, I am to refer the readers of this thesis to a wonderful paper co-authored by the even more wonderful Josie: “Natural Biomaterials and Their Use as Bioinks for Printing Tissues”.

To my family and friends, thank you for being by my side and for listening to me talk endlessly about tadpoles. I could not have done it without you.

To Chad the Tad, it has been rad!

List of Abbreviations

AA	Amino acid
AMP	Antimicrobial peptide
AMR	Antimicrobial resistance
APD	Antimicrobial peptide database
APEC	Avian pathogenic *E. coli* 317
ATCC	American Type Culture Collection
BP	Biological process
bw	Body weight
CC	Cellular component
CC50	Cytotoxic concentration needed to reduce cell viability by 50%
CFU	Colony forming units
CRH	Corticotropin-releasing hormone
DE	Differential expression
DEGs	Differentially expressed genes
DEPC-dH2O	Diethyl pyrocarbonate treated water
E. coli ATCC	*Escherichia coli* ATCC 25922
EK	Eberth-Kastschenko Layer
FC	Fold change
FDR	False discovery rate
GO	Gene ontology
GRAVY	Grand Average of Hydropathy
HC50	Hemolytic concentration needed to lyse 50% of the cells
HPT axis	Hypothalamic-pituitary-thyroid axis
HSP	Heat shock protein
inva	Invasion gene
LBP	Lipopolysaccharide binding protein
LC-MS/MS	Liquid chromatography tandem mass spectrometry
LPS	Lipopolysaccharide
MBC	Minimum bactericidal concentration
MF	Molecular function
MHB	Mueller-Hinton Broth
MIC	Minimum inhibitory concentration
MucXS	*Xenopus* skin mucin
NaOH	Sodium hydroxide
nr	Non-redundant
nt	Nucleotide
Otogl	Otogelin-like
PAMPs	Pathogen associated molecular patterns

PC	Principal component
PCA	Principal component analysis
PRR	Pattern recognition receptor
RAK	*Rana* adult keratin
RBCs	Red blood cells
RK	*Rana* keratin
RLK	*Rana* larval keratin
RNA-seq	RNA sequencing
RPMI	Roswell Park Memorial Institute medium
RXR	Retinoic acid receptor
SE ATCC	*Salmonella enterica* serovar Enteritidis ATCC 4931
SE avian	Avian *Salmonella enterica* serovar Enteritidis
spvC	*Salmonella* plasmid virulence gene
T_3	3,5',5-triiodothyronine
T_4	Thyroxine
TH	Thyroid hormone
thibz	Thyroid hormone-induced basic region leucine zipper
thra	Thyroid hormone receptors alpha
thrb	Thyroid hormone receptors beta
TK	Taylor Kollros
TLR	Toll like receptors
TPO	Thyroid peroxidase
TR	Thyroid hormone receptors
TRE	Thyroid hormone response elements
TRH	Thyrotropin-releasing hormone
TSH	Thyroid hormone stimulating hormone
VIDO	Vaccine and Infectious Disease Organization-International Vaccine Centre

Manuscript Planning

Chapter 1: In preparation

Transcriptomic analysis of *Rana* [*Lithobates*] *catesbeiana* tadpole back skin during natural metamorphosis and thyroid hormone-induced precocious metamorphosis under different temperature conditions with particular emphasis on innate immune system components

Lorissa Corrie, Haley Kuecks-Winger, Hossein Ebrahimikondori, Inanc Birol, and Caren C. Helbing

Chapter 2: In preparation

Characterization and validation of novel antimicrobial peptides against pathogens important in the poultry industry: Avian pathogenic *E. coli* (APEC) and *Salmonella enterica* serovar Enteritidis (SE)

Lorissa Corrie, Alana Babcock, Hossein Ebrahimikondori, Amelia Richter, Ali Salehi, Vanessa Thompson, Anat Yanai, Fraser Hof, Inanc Birol, and Caren C. Helbing

1. Introduction

1.1. Thyroid hormone basics

1.1.1.1. TH synthesis, transport, and signalling

Thyroid hormones (TH) play a vital role in the growth, development, and metabolism of vertebrates (Mullur et al., 2014; Paul et al., 2022). THs act on most cells to alter gene expression and misregulation of TH has serious consequences (Nussey & Whitehead, 2001). TH production is under the neuroendocrine control of the hypothalamic-pituitary-thyroid axis (HPT axis), which is generally conserved in vertebrates (Brown & Cai, 2015; Nussey & Whitehead, 2001). When triggered by environmental cues, the hypothalamus can stimulate the thyrotrophs of the pituitary gland to synthesize and secrete TH stimulating hormone (TSH) through the action of thyrotropin-releasing hormone (TRH) in mammals or corticotropin-releasing hormone (CRH) in amphibians (Shi, 2000). TSH produced by the anterior pituitary regulates the activity of the TH gland and stimulates the production of TH (Brown & Cai, 2015; Shi, 2000). Endogenous TH levels are tightly regulated by a negative feedback loop between the thyroid gland, the pituitary, and the hypothalamus (Nussey & Whitehead, 2001).

TH production occurs in follicular cells of the thyroid gland. Iodide is taken up into the follicular cell from the bloodstream by the ATPase sodium-iodide symporter and then oxidized by thyroid peroxidase (TPO) to active iodine (Nussey & Whitehead, 2001). It is then exported to the follicular lumen along with tyrosine rich thyroglobulin. Once iodinated, the coupling of pairs of iodinated tyrosine molecules is catalyzed by TPO and can form thyroxine (T_4) or 3,5',5-triiodothyronine (T_3) depending on the number of iodinated positions (Nussey & Whitehead, 2001). The thyroglobulin is then taken back into the follicular cell where fusion with lysosomes releases the THs which can be secreted to the plasma (more T_4 secreted than T_3) (Nussey & Whitehead, 2001). Once in the blood stream, the THs are transported to peripheral tissues by binding plasma transporter proteins or, rarely, circulate in free form (Nussey & Whitehead, 2001). In peripheral tissues, the conversion of T_4 to T_3 by type I and type II 5'-deiodinases can

occur depending on tissue specific deiodinase presence (Maher et al., 2016). T_3 is five times more biologically active than T_4 (Maher et al., 2016). Conversion of T_4 and T_3 to other active metabolites or to inactive forms is also mediated by deiodinases (Shi, 2000). Different deiodinases have varying properties and distribution in mammal tissues, allowing for fine-tuning of the thyroid response (Maher et al., 2016).

TH action is predominately through genomic signalling although THs can act non-genomically. In the genomic pathway, THs binding TH receptors (TR) regulates gene expression (Nussey & Whitehead, 2001). Two genes encode for TRs alpha and beta (Nussey & Whitehead, 2001). TRs are nuclear transcription factors that dimerize, often with retinoic acid receptors (RXR), and bind the TH response elements (TRE) most often found in the promoter regions of TH responsive genes (Nussey & Whitehead, 2001). In the absence of THs, TRs supress gene expression by recruiting histone deacetylase containing co-repressor protein complexes that repress transcription through histone deacetylation (Shi, 2013). Once bound by TH however, these co-repressors are released, co-activators containing histone acetyltransferases and methyltransferases are recruited, chromatin acetylation increases, and transcription of TH-responsive genes begins (Shi, 2009). This repression in the absence of TH and activation in the presence of TH is called the dual function model which helps to regulate developmental timing (Figure 1.2.1-1).

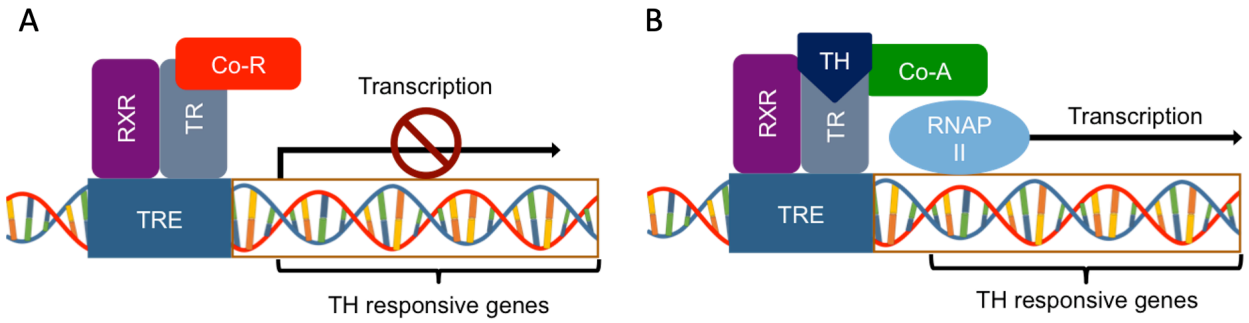

Figure 1.2.1-1 TH Signaling via the Dual Function Model. When TH is not present, corepressors (Co-R) bound by TH receptors (TRs) at the TH response elements (TRE) repress transcription of the response transcripts. In the presence of TH, co-repressors are released, and co-activators (Co-A) are recruited. This leads to the expression of the TH responsive genes such as the receptor transcripts TH receptor beta (*thrb*) and TH-induced basic region leucine zipper-containing transcription factor (*thibz*).

The transcriptomic response to the TH induction of gene expression is thought to be biphasic in nature with an induction and an execution phase (Das et al., 2009; Koide et al., 2022; Wang & Brown, 1993). During the induction phase, direct response genes such as the TRs are induced rapidly after TH exposure. Genes involved in transcriptional regulation and initiation of the cell cycle have been found to be enriched in this stage (Das et al., 2009). The initial induction phase is followed by a delayed secondary execution phase that executes the TH signalling programs. Expression of transcripts related to phenotypic responses such as DNA replication and apoptotic programming have been identified in this phase (Das et al., 2009). The expression of the TRs, as well as early response genes, can be good indicators of TH activity (Brown & Cai, 2015; Poulsen et al., 2023; Shi, 2000).

Non-genomic TH signalling is another mechanism of TH action through the binding of cytosolic or cell surface receptors. A cytosolic TH-TRβ complex has been shown to play a role in cellular glucose metabolism and the expression of related genes (Moeller et al., 2006). The integrin αVβ3 has been identified as a cell surface receptor for T_4 that can activate intracellular signalling cascades (Bergh et al., 2005). Non-genomic signalling can impact transcription, post-transcriptional modifications, and ion transport (Bergh et al., 2005; Moeller et al., 2006; Nussey & Whitehead, 2001). The genomic and non-genomic signalling pathways highlight the complexity of TH signalling.

1.2. TH regulates metamorphosis in amphibians

1.2.1. Amphibian metamorphosis

Amphibian metamorphosis from an aquatic larval stage to a terrestrial juvenile frog is regulated by tissue-dependent TH activity that leads to structural and functional changes in larval tissues (Brown & Cai, 2015). As seen in Figure 1.2.1-1, this process can be divided into three stages prior to becoming froglets: premetamorphosis, prometamorphosis, and metamorphic climax (Thambirajah et al., 2019). Premetamorphic tadpoles have virtually undetectable levels of TH (Brown & Cai, 2015; Poulsen et al., 2023; Shi, 2000). As the thyroid gland develops and produces TH, the prometamorphic period of development begins, initiating changes in virtually every tissue, and is visually characterized by toe differentiation and *de novo* hind limb

development (Shi, 2000; Thambirajah et al., 2019). The metamorphic climax is characterized by reabsorption of the tail and gills, as well as the highest levels of endogenous TH (Poulsen et al., 2023; Shi, 2000; Thambirajah et al., 2019). TH levels are reduced to suprabasal levels in the froglet (Poulsen et al., 2023; Shi, 2000).

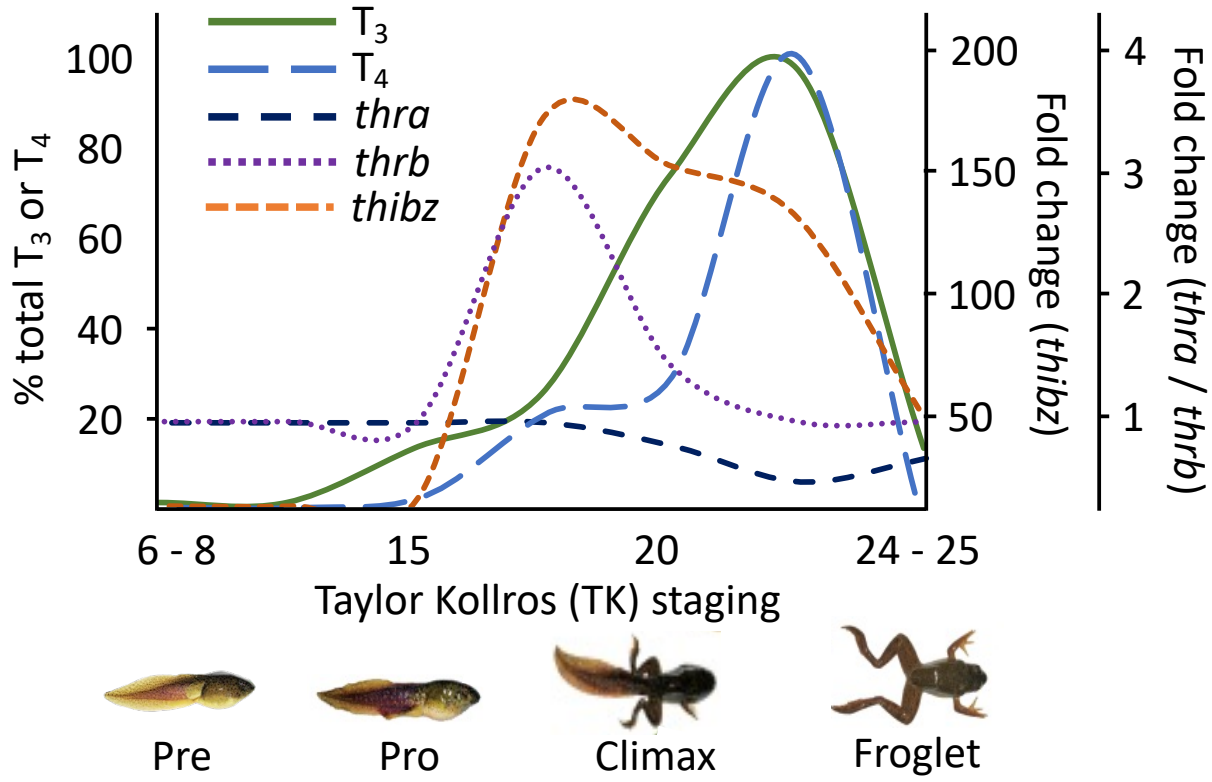

Figure 1.2.1-1 Serum TH levels (T_3 and T_4) and TH-responsive gene expression (*thra*, *thrb*, and *thibz*) in the back skin of the American bullfrog, *Rana [Lithobates] catesbeiana*, during metamorphosis. Stages of development include premetamorphosis (Pre; TK stage 6 - 8), prometamorphosis (Pro; TK stage 15), metamorphic climax (Climax; TK stage 20), and froglets (TK stage 24 - 25). Adapted from Poulsen et al. (2023).

During metamorphosis, there is coordinated physical or biochemical development of essentially every tissue and organ which can be classified in three categories: remodelling, resorption, and *de novo* development (Brown & Cai, 2015; Maher et al., 2016). Examples of this include the biochemical remodelling of the liver from ammonotelism to ureotelism, the complete resorption of the tail fin, the *de novo* development of the limb, and restructuring of the back skin (Brown & Cai, 2015; Poulsen et al., 2023; Shi, 2000; Thambirajah et al., 2019).

These metamorphic changes can be induced by the addition of exogenous TH or prevented by blocking TH synthesis (Shi, 2000). In both *in vivo* and *in vitro* experiments where samples were exposed to exogenous TH, external and internal development was observed (Shi, 2000). Given the different developmental fates of the tadpole tissues, there are tissue-dependent changes during amphibian metamorphosis that are regulated by transcriptional activity and sensitivity to TH (Brown & Cai, 2015; Poulsen et al., 2023; Shi, 2000). As seen in Figure 1.2.1-1, induced-metamorphosis leads to the expression of TH-responsive genes such as those encoding the TRs *thra* and *thrb* and transcription factors like TH-induced basic region leucine zipper (*thibz*), which can be studied to understand tissue specific responses to TH signalling (Maher et al., 2016; Poulsen et al., 2023; Wang & Brown, 1993). This TH sensitivity makes amphibian models ideal for the study of transcriptomic events during experimentally induced metamorphosis.

1.2.2. Amphibian skin during metamorphosis

Like many tadpole tissues, the skin undergoes remodelling during metamorphosis both structurally and functionally (Figure 1.2.2-1). This remodelling leads to enough difference that skin grafts from premetamorphic tadpoles were rejected when transplanted onto the backs of froglets (Yoshizato, 1992). Skin development is region specific with the tailfin skin regressing during metamorphosis, where as the head and trunk remain but undergo substantial restructuring (Yoshizato, 1992). Herein we focus on predominately the head and trunk skin composition. In tadpole skin, the epidermis is composed of four to six replicating cell layers on a basement membrane supported by thin collagenous lamella (Furlow et al., 1997; Miyatani et al., 1986). These cells include the apical cells with microvilli on the outer layer, the skein cells with large keratin bundles (Figures of Eberth) in the middle, and larval basal cells on the basement membrane (Furlow et al., 1997; Robinson & Heintzelman, 1987; Watanabe et al., 2001; Yoshizato, 1992). As TH levels increase, DNA synthesis of the larval-specific apical and skein cells is suppressed and they undergo apoptosis during early to middle metamorphic climax (Yoshizato, 1992). During early metamorphosis, DNA-synthesis of larval basal cells is stimulated and they differentiate into frog basal cells, proliferating becoming cells in the germinative layer (Yoshizato, 1992). At metamorphic climax, the

cell composition is distinct from both that of the premetamorphic larva and of the adult frog with a mix of larval and frog specific as well as differentiating cells (Yoshizato, 1992). By late metamorphic climax, the head and trunk skin has fully developed into the frog epidermis (Yoshizato, 1992).

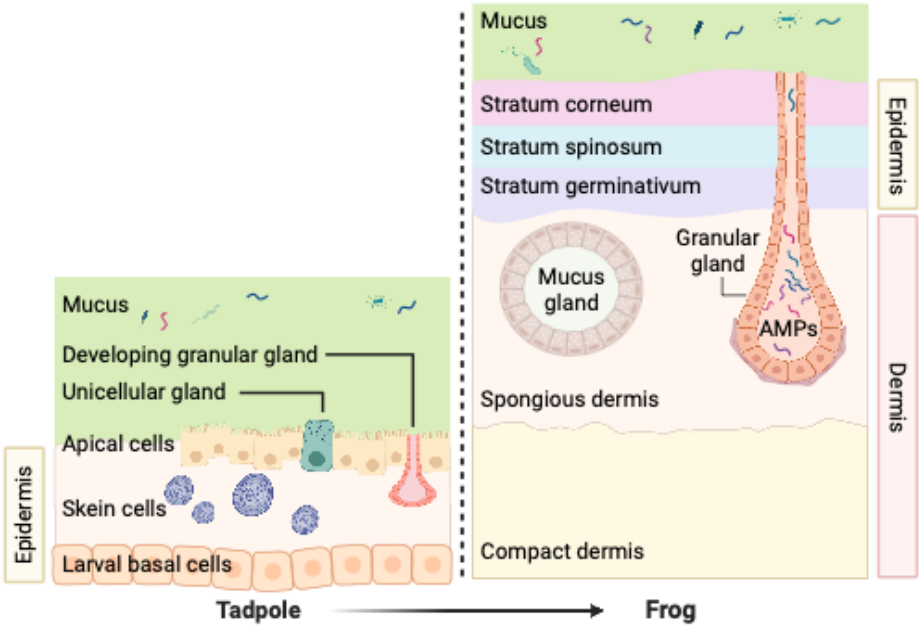

Figure 1.2.2-1 Amphibian skin changes during metamorphosis. The presence of the unicellular gland and developing granular gland are hypothesized as potential sources of AMP production in tadpoles but this has not been confirmed. Adapted from Varga et al. (2019), Akat et al. (2023), and Yoshizato (1992).

Frog skin is composed of two layers: the epidermis and the dermis. The epidermis is composed of three layers of stratified squamous epithelial cells: the stratum corneum, the stratum spinosum, and the stratum germinativum. The stratum corneum is made up of a thin layer of keratinized cells. The stratum spinosum is primarily terminally differentiated cells. The stratum germinativum connects to the dermis and composed of immune cells, chromatophores, and epithelial cells. The dermis is composed of two layers of primarily connective tissue: the spongious dermis (loose connective tissue) and the compact dermis (collagenous layer). Terrestrial frogs will often have a non-cellular Eberth-Kastschenko layer between the spongious and compact dermal layers. During metamorphosis mucus and granular glands develop in the spongious dermal layer. Collagenous fibers are responsible for anchoring the dermis to the hypodermis. In turn, hemidesmosomes anchor the cytoskeletal filaments of the epidermis to the

collagenous fibrils in the dermal layer. The outermost layer of the skin is covered in a mucosal layer that is associated with commensal bacteria.

The development of glands in the spongious dermal layer of the skin is one of the most significant changes that occurs in this tissue during metamorphosis. Mucosal and granular glands are common constituents of the skin and play important roles in osmotic regulation and defense. Both mucus and granular glands are sac-like structures lined with secretory cells that release their granular contents and myoepithelial cells that contract when stimulated. While prevalent all over the organism, mucosal and granular glands tend to be more densely distributed on the dorsal skin. Mucosal glands secrete mucus, which is required for thermoregulation, maintaining moisture and elasticity, and gas exchange in the skin (Lillywhite & Licht, 1975; Varga et al., 2019). Granular glands are the site of toxin production and secretion via an apical pore. Granular gland are observed in the bullfrog, *Rana [Lithobates] catesbeiana*, premetamorphic tadpoles as early as Taylor and Kollros (TK) stage 7 (Robinson & Heintzelman, 1987). They produce a diverse array of bioactive molecules like toxic alkaloids, amines, or antimicrobial peptides (AMPs) that are implicated in antimicrobial and antipredator defense. Granular glands tend to be less dense than mucosal glands although the two follow a similar density pattern. Granular glands can also form clusters in certain areas of the body (Toledo & Jared, 1995; Varga et al., 2019; Wanninger et al., 2018). Gland development and contents varies based on frog species and developmental stage (Gunzburger & Travis, 2005).

1.2.3. Temperature regulation of metamorphosis in the bullfrog

R. catesbeiana tadpoles can overwinter, thereby extending their larval stage until conditions favour undergoing metamorphosis (Wright et al., 1999). Abiotic factors such as temperature can significantly influence metamorphic timing (Ashley et al., 1968; Frieden et al., 1965; Hammond et al., 2015). In 1965, Frieden et al. demonstrated the temperature sensitivity of *Rana grylio*, a related species, during metamorphosis. The rate of metamorphic programming (measured using tail regression) slowed in premetamorphic tadpoles injected with T_3 at temperatures below 25°C and was completely halted at 5°C. The half-life of T_3 is also influenced by temperature,

increasing from 22 h at 25°C to 10 to 15 d at 5°C (Yamamoto et al., 1966). Frieden et al. (1965) also showed that premetamorphic tadpoles injected with T_3 at 5°C, maintained at this cold temperature, and then transferred to 25°C after the exogenous TH would have been cleared from the body despite the increase in half-life could still undergo metamorphosis. Even after 80 days post injection, the tadpoles underwent metamorphosis when transferred to 25°C (Frieden et al., 1965). This shift of cold-acclimated TH-treated tadpoles to a warm metamorphically permissive temperature resulted in an accelerated metamorphosis that abolished the typical 2-day lag period after TH treatment before measurable tail decrease is observed (Frieden et al., 1965). Like tailfin regression, urea production after TH injection is also temperature dependent with no production at 5°C, but accelerated production following a shift to 25°C even after 80 days post injection (Ashley et al., 1968). TH exposure at cold temperatures appears to establish a sort of molecular memory that allows the tadpole to resume its metamorphic programming at metamorphically permissive temperatures. Because *R. catesbeiana* can tolerate low temperatures, they are a good model organism in which to study the initial stages of anuran metamorphosis.

The mechanisms underlying the low-temperature arrest of metamorphic programming are not fully understood. At 4°C, T_3 affinity to the serum TH transporter protein transporter transthyretin is increased, which may create a reservoir of bound T_3 that is not available to target cells (Murata & Yamauchi, 2005). Additionally, uptake into *R. catesbeiana* red blood cells is slowed, which may decrease accumulation within the cell (Murata & Yamauchi, 2005). Once in the cell, T_3 incorporation into the nucleus and the ability to bind THRs was not significantly arrested at 4°C (Murata & Yamauchi, 2005).

Given that THs retain their ability to enter target cell nuclei and bind TRs, TH action once in the nucleus at non-permissive (4-5°C) temperatures and the changes in transcriptomic response have become the focus of recent studies. To this end, studies analyzing TH-responsive transcript expression at metamorphically non-permissive, permissive, or shifting temperatures in tissues with different metamorphic endpoints including the blood, liver, back skin, brain, and tailfin have been performed (Hammond et al., 2016; Hammond et al., 2015; Mochizuki et al., 2012; Murata & Yamauchi, 2005).

Transcriptomic data supports accelerated metamorphosis that occurs when tadpoles treated with TH at 5°C are transferred to permissive temperatures (Ashley et al., 1968; Frieden et al., 1965). In the liver, back skin, and tailfin, there is a greater increase in abundance of TH-responsive transcripts following TH treatment when shifted from 5°C to 24°C compared to tadpoles held only at 24°C (Hammond et al., 2015; Koide et al., 2022).

Herein we focus on the transcriptomic profile of the back skin after TH induction of metamorphosis in temperature modulated conditions. Whole animal premetamorphic *R. catesbeiana* exposures in permissive (24°C; 2 days), non-permissive (5°C; 8 days), or temperature shift (5 – 24°C; 7 days – 1 day respectively) conditions after a 10 pmol/g body weight injection to induce metamorphosis were performed by Hammond et al. (2015). In the back skin, there was a significant up-regulation of *thra*, *thrb*, and *thibz* expression in both the non-permissive and shift conditions after TH injection while, in the premissive condition, *thrb* expression was significantly up-regulated after TH injection. A similar experiment with tadpole back skin was performed over a shorter term (2 day exposure) to further define initial transcriptomic events and early aspects of temperature control (Hammond et al., 2016). In the whole animal exposures, expression of *thra* and *thrb* is abolished at 5°C. Conversely, the TH-dependent upregulation of *thibz* transcript abundance is maintained at 5°C. A significant increase in transcript abundance for all three transcripts was observed in the shift condition.

These targeted mRNA studies strongly implicate *thibz* in early metamorphic program initiation and there may be a hierarchy to early TH response genes. The role of *thibz* in molecular memory remains unknown. Research in cultured *R. catesbeiana* tail fin shows that TH-responsive transcript *thibz* abundance after TH treatment occurs in the presence of the transcription inhibitor actinomycin D, suggesting an alternate mechanism for increased abundance of this transcript (Koide et al., 2022). Temperature sensitivity of *R. catesbeiana* during metamorphosis can be utilized to analyze the transcriptomic response to TH when metamorphosis is paused at cold temperatures, or during accelerated metamorphosis and can help elucidate initial stages of TH-responsive gene expression.

1.2.4. The immune system during metamorphosis

Amphibians have both innate and adaptive immune systems. However, like many organs in anurans, there are large differences in immune systems when comparing different postembryonic stages and many physiological and immunological changes including immunosuppression are observed during this time (Grogan et al., 2018; Humphries et al., 2022; Robert & Ohta, 2009; Rollins-Smith, 1998). While the immune system in tadpoles is competent, it is immature compared to the immune system that develops post-metamorphosis (Rollins-Smith, 1998). During metamorphosis, the major histocompatibility complex profile (which is limited in tadpoles) expands, the thymus involutes and reforms, and glands develop in the skin for the secretion of innate immune molecules such as AMPs (Robert & Ohta, 2009; Varga et al., 2019). The profile of these innate immune secretions evolves in type and quantity during the anuran life cycle (Helbing et al., 2019; Woodhams et al., 2016).The T and B cell repertoires also differ between larval and fully developed adult anurans (Grogan et al., 2018; Robert & Ohta, 2009). It has been shown that amphibians with a longer larval stage such as *R. catesbeiana* develop more defense mechanisms as tadpoles (Gosavi et al., 2014; Woodhams et al., 2016).

During metamorphosis, the immune system is repressed while remodelling occurs until about six months post-metamorphosis (Grogan et al., 2018; Robert & Ohta, 2009). Most larval lymphocytes are lost and T-cell function is impaired during metamorphosis (Robert & Ohta, 2009). Adult lymphocytes emerge that self-tolerate to the new proteins expressed during metamorphosis (Robert & Ohta, 2009; Rollins-Smith, 1998). Additionally, innate immune physical barriers like the skin are undergoing complex remodelling (Schreiber & Brown, 2003; Shih & Vanable, 1975; Suzuki et al., 2001; Varga et al., 2019). Metamorphs are more susceptible to certain infections than larvae and frogs, which highlights the importance of these immunological changes (Humphries et al., 2022; Sauer et al., 2020). While most organisms survive development, uncoordinated development or environmental stressors can increase the risk associated with metamorphosis (Humphries et al., 2022; Robert & Ohta, 2009; Rollins-Smith, 1998; Sauer et al., 2020).

Environmental conditions during the larval stages and metamorphosis affect the immune system of the adult frog (Krynak et al., 2015). Post-metamorphic AMP production was affected by both shade and pH (Krynak et al., 2015). Stress, temperature, and environmental contaminates have all been shown to increase amphibian's susceptibility to infection (Rollins-Smith, 2017; Rollins-Smith et al., 2011). For example, temperature impacts the amphibian immune system. In adult *Rana pipiens*, long term exposure to cold temperature (5°C) decreased in lymphocyte proliferation and complement activity (Maniero & Carey, 1997). Cold temperatures also inhibited the ability of *Xenopus tropicalis* to express the AMP preprocaerulien type iii precursor after infection (Ribas et al., 2009). Therefore, the immune system of a tadpole is malleable by both TH and by environmental conditions including temperature.

1.2.5. The role of amphibian skin in the immune system

Amphibian skin plays many crucial functions including respiration, ion and water regulation, predator defense, and innate immunity at all life stages of the animal (Varga et al., 2019). Given that the skin is in constant contact with diverse, microbially laden environments throughout the anuran life cycle, it must be able to protect from and react to a wide variety of challenges.

The physical skin barrier is composed of a tough outer layer of keratinized cells, with cellular junctions allowing for both selective permeability and integrity to be maintained, covered by a mucus layer (Varga et al., 2019). This mucus layer, in turn, acts as both a physical and chemical barrier by trapping and removing pathogens and acting as a sink for AMPs, antibodies, enzymes, and the symbiotic microbiome (Grogan et al., 2018; Humphries et al., 2022). AMPs kill invading pathogens, stimulate the host immune systems, and can help with wound healing. The amphibian microbiome is developmental stage and environment dependent and contributes to the skin immune system by competing with pathogenic organisms, interacting with the host immune system, and secreting antimicrobial compounds (Bates et al., 2018; Grogan et al., 2018; Helbing et al., 2019; Humphries et al., 2022; Woodhams et al., 2015). The skin also contains a number of immune cells including antigen presenting cells, dendritic epidermal T cells, mast cells (Varga et al., 2019). Intermittent skin sloughing can also

act as a way to control the number of skin-associated pathogens (Varga et al., 2019). Epithelial cells are microbial sensors and initiators of innate immunity through their recognition of stress or infection. They use pattern recognition receptors (PRRs) to identify pathogen-associated molecular patterns (PAMPS), or stress-related damage associated molecular patterns (DAMPs) (Grogan et al., 2018; Humphries et al., 2022; Varga et al., 2019). The binding of the PRRs leads to signalling cascade that can initiate the transcription of inflammatory signals, chemo attractive substances, or anti-pathogenic response molecules (Varga et al., 2019). The adaptive immune response in the skin, which is more specialized but slower to respond than the innate immune system, includes a lymphocyte response and the development of immunological memory (Grogan et al., 2018; Humphries et al., 2022; Robert & Ohta, 2009; Varga et al., 2019).

The skin, which is thought of as the first line of defense in the innate immune system, acts as a protective physical, chemical, and microbiological barrier. Keratins, mucus, and AMPs are all key components of the innate immune system in the skin. However, our knowledge of how these are impacted during development or in changing environmental conditions in *R. catesbeiana* is limited.

Keratins are functionally and structurally important intermediate filaments expressed in the skin. This diverse class of polypeptides can be classified as two types: type I keratins (typically smaller and more acidic) or type II keratins (often larger and more basic to neutral) (Miyatani et al., 1986; Watanabe et al., 2001). Both types are essential for filament formation (Fuchs, 1988). Keratins can be differentially expressed in different tissue types, epithelial locations, and developmental stages (Ellison et al., 1985). In *Xenopus laevis*, embryonic and larval keratin genes are exclusively expressed in these stages and are not expressed in the adult skin, which possesses a distinct repertoire of keratin genes (Jonas et al., 1985; Miyatani et al., 1986; Watanabe et al., 2001). This has also been observed in *R. catesbeiana* development. Suzuki et al. (2001) identified *Rana* larval keratin (*rlk*: type II), which is expressed during pre and prometamorphosis in the larval specific skein cells and is down-regulated as metamorphic climax approaches until it is no longer expressed in the adult epidermis (TK22). While *Rana* adult keratin (*rak*: type I) transcripts are expressed in both the larval

basal cells (weak expression) and by the germinative cells in the adult frog (strong expression), their expression is up-regulated by TH exposure in the back skin (Suzuki et al., 2001). Domanski and Helbing (2007) discovered a second novel *rlk* (type I) in the tail fin of *R. catebesiana* that was expressed at a steady state during pre- and prometamorphosis and then significantly decreased by 3.1-fold at metamorphic climax. This transcript was detected and found to be temperature sensitive after TH induction in the tail fin and back skin by Hammond et al. (2015). Not all keratins are developmentally regulated. Suzuki et al. (2001) found that the expression of *Rana* keratin (rk) 8 did not change in the back skin or tail fin during development. The developmentally regulated patterns of keratin expression are a useful tool for understanding skin development during metamorphosis.

Mucus, which coats the outermost layer of skin, acts as both a physical and chemical barrier (Dubaissi et al., 2018; Varga et al., 2019). Mucus is composed of a wide variety of proteins with the O-linked glycoprotein mucins being a major structural component (Dubaissi et al., 2018). Mucins form a network that can trap and eliminate pathogens, bind ions or water, and provides a framework for protein interactions (Dubaissi et al., 2018; Lang et al., 2007; Thornton et al., 2008). Ciliated cells within the epidermis help to clear these trapped pathogens (Dubaissi et al., 2014). Mucins are classified as either membrane bound or gel forming and at least 25 gel forming mucins have been identified in *X. laevis* (Alves et al., 2018; Lang et al., 2007). Mucins can be expressed in specialized epithelial cells (goblet cells) or mucus glands at constitutive levels or can be stored and released when stimulated (Dubaissi & Papalopulu, 2011; Thornton et al., 2008). The expression of mucin genes is inducible by pathogen exposure (Dohrman et al., 1998).

Not much is known about how mucus and its composition changes during metamorphosis as mucus glands develop (Shih & Vanable, 1975). In marine turbot (*Scophthalmus maximus*), there was a distinct difference in mucus cell contents before and after metamorphosis that reflects larval (viscous) versus adult (lubricating) animal behaviour (Landeira-Dabarca et al., 2021). An increase in mucus secreting cells, the expression of mucin transcripts during metamorphosis, as well as a shift from neutral to a mix of neutral and acidic mucins has been identified during Atlantic halibut

(*Hippoglossus hippoglossus*) metamorphosis (Alves et al., 2018; Ottesen & Olafsen, 1997). In *X. tropicalis*, the tadpole epidermis contains motile, multi-ciliated cells that generate fluid flow of a mucus-like protective layer thought to be secreted by secretory cells (goblet and small secretory cells) (Dubaissi et al., 2018; Dubaissi et al., 2014). Recently the glycoprotein Otogelin-like (Otogl), now called *Xenopus* Skin Mucin (MucXS), has been identified and characterized as a gel-forming mucin that forms that forms a physical barrier on the surface of tadpole skin in *X. tropicalis* (Dubaissi et al., 2018; Dubaissi et al., 2014). When the secretory cells or MucXS is depleted, embryos or tadpoles succumb to infection (Dubaissi et al., 2018; Dubaissi et al., 2014). The framework provided by the mucus layer can contain other gland secretions, thereby also setting the stage for chemical defenses.

The chemical defenses of amphibian skin are predominately secreted toxins and antimicrobial molecules. Toxic alkaloids can be secreted as predator defense and deterrence. AMPs are some of the best studied defensive peptides produced in the skin. These short, typically positively charged, and amphipathic peptides are produced in granular glands and secreted when stimulated by stress, injury, or pathogen or predator challenge. Amphibian AMPs are often alpha-helical and amphipathic in nature (Wang, 2020). A common motif in amphibian AMPs is the “Rana box” (Haney et al., 2009; Wang, 2020). This unique structure is usually formed by two cysteines that are approximately 4 to 6 amino acid (AA) residues apart in the C-terminal region of the peptide, allowing for the creation of a loop via a disulphide bond (Zasloff, 2002). Many AMPs that contain this feature are derived from the Ranids, such as ranalexins.

Adult frogs have been the most studied source of AMPs to date with 42.4% of the AMPs in the Antimicrobial Peptide Database (APD) belonging to frogs [as of January 2023] (Wang et al., 2015). Amphibians have developed a rich AMP repertoire to survive the diverse array of water and soil pathogens they encounter during metamorphosis from aquatic tadpoles into terrestrial frogs (Woodhams et al., 2016). While adult frog AMP profiles have been well characterized, the AMP profile during postembryonic development or under certain challenge conditions is still relatively unknown and remains a possible source for the identification of novel AMPs (Figure 1.2.2-1) (Helbing

et al., 2019). These AMPs, both known and novel, are critical for amphibian defense and have potential applications as possible therapeutics for other organisms.

1.3. AMP physicochemical characteristics and mechanisms of action

While the global threat of antibiotic resistance continues to increase, no new classes of antibiotics have been discovered since the 1980s (Durand et al., 2019). This disparity between increasing antibiotic resistance and the lack of antibiotic discovery drives the need for innovation in the discovery and application of novel antimicrobials. AMPs are one group of promising antibiotic alternatives. This diverse group of peptides is an important component of the innate immune system of multicellular organisms that can provide defense against bacteria, fungi, viruses, and protozoa (Cruz et al., 2014; Zasloff, 2002). Additionally, some AMPs have anti-cancer properties, are immune stimulatory, and can promote wound healing (Hancock & Sahl, 2006). These immune peptides are typically produced on epithelial surfaces or in phagocytic cells and are thought to be the first line of defense in the innate immune system (Bahar & Ren, 2013; Shai, 2002).

AMPs are typically positively charged, range from 5 to 100 amino acids in length, and are often amphipathic, although exceptions do exist in this diverse group of peptides (Hancock & Sahl, 2006; Seyfi et al., 2020). AMPs can be classified structurally as alpha-helices, beta-sheets, extended, loop, or as a mix of the above (Bahar & Ren, 2013; Seyfi et al., 2020). While the active region of AMP sequences are highly diverse and do not tend to be conserved even in closely related species, the prepro-region, which is proteolytically cleaved to activate the peptide, is often conserved within a species or even within a class of AMP (Hancock & Sahl, 2006; Helbing et al., 2019; Simmaco et al., 1998; Zasloff, 2002). This proteolytic activation means that their regulation is dependent on both expression and availability of proteases (Lai & Gallo, 2009). AMP expression can be induced by exposure to cytokines or PAMPs or expression can be constitutively on with the inactive AMPs being stored until infection or inflammation signals release and activation (Lai & Gallo, 2009; Mahlapuu et al., 2016).

AMPs have a broad spectrum of antimicrobial activity including directly killing microbes and modulating the host immune system (Brogden et al., 2016; Seyfi et al.,

2020). AMPs can act directly against invading pathogens. In bacteria, positively charged AMPs are attracted to the negatively charged lipopolysaccharide (LPS: Gram negative) or teichoic acids (Gram positive) on the microbial cell surface (Bahar & Ren, 2013; Hancock & Sahl, 2006; Shai, 2002). The cationic AMP displaces the divalent cations necessary for membrane integrity leading to the disruption of the lipid bilayer (Friedrich et al., 2000). The amphipathic nature of many AMPs also supports the electrostatic interaction of the hydrophilic phospholipids followed by the hydrophobic insertion into the lipid membrane interior (Bahar & Ren, 2013). This can cause rapid cell death through the loss of essential molecules and/or the proton motor force or it can allow the AMP intracellular access (Shai, 2002). There are multiple models for the mechanism of action of membrane-active AMPs summarized in Bahar & Ren (2013) and in Jenssen et al. (2006). One benefit of this membrane targeting mechanism is that the AMPs preferentially bind the bacterial membrane over eukaryotic cells, which have a higher cholesterol level and a net neutral charge on the outer leaflet (Hancock & Sahl, 2006; Mahlapuu et al., 2016; Shai, 2002).

AMPs inhibit critical cellular functions in conjunction with or without disrupting membrane activity. These include disrupting cell membrane protein function (signaling, transport, etc.), DNA, RNA, protein, and cell wall synthesis and expression, and enzymatic activity (Bahar & Ren, 2013; Benincasa et al., 2017; Jenssen et al., 2006). The AMP buforin II enters the cell and binds genetic material (RNA and DNA) in the cytoplasm of *E. coli* without disrupting the membrane, even at five times its minimum inhibitory concentration (MIC) (Park et al., 1998). The AMP pyrrhocidin prevents protein folding in *E. coli* through the inhibition of the ATPase activity of the heat shock protein DnaK, leading to a buildup of misfolded proteins and cell death (Kragol et al., 2001). In addition to its pore-forming ability, the AMP nisin can block cell wall synthesis, even in some antibiotic resistance bacteria (Brumfitt et al., 2002). These intracellular mechanisms of AMPs are performed through uptake into the cell. This can occur through endocytosis (macropinocytosis and receptor mediated endocytosis) or direct penetration across the membrane (Jones, 2007; Shai, 2002). Some AMPs can have multiple targets or have different effects depending on the target microbes, AMP

concentration, or environment, thus adding another tool to their already impressive antimicrobial repertoire (Jenssen et al., 2006).

AMPs also have immune system modulatory abilities, often at concentrations orders of magnitude lower than their MICs (Lai & Gallo, 2009). They can stimulate chemotaxis, modulate inflammation, neutralize pathogenic toxins, promote wound healing, and have anti-cancer properties (Lai & Gallo, 2009; Mahlapuu et al., 2016). AMP immunomodulation can occur through binding the receptors themselves and inducing a signaling cascade, by disrupting the membrane so the receptor availability is altered, by causing the release of membrane bound factors allowing them to bind receptors, or by binding the endotoxins directly (Mahlapuu et al., 2016). AMPs can directly (via chemotaxis) or indirectly (through the stimulation of cytokine and chemokine release via receptor-dependent mechanisms) recruit immune cells (Lai & Gallo, 2009). AMPs modulate the inflammatory response by preventing an excessive proinflammatory signaling cascade to bacterial stimuli (Lai & Gallo, 2009). The AMPs LL-37 and lactoferrin inhibit proinflammatory cytokine release in LPS-treated human monocytes through the toll like receptors (TLR) signaling pathways (Håversen et al., 2002; Mookherjee et al., 2006). Lactoferrin can also bind LPS directly and compete with LPS binding protein (LBP) to prevent the activation of monocytes and macrophages via LBP-mediated binding of LPS to CD14 (Elass-Rochard et al., 1998). AMPs can promote wound healing through the stimulation of endothelial cell proliferation, migration, and tube formation (Lai & Gallo, 2009). The anti-cancer activity of AMPs is thought to come from the ability to selectively target the negatively charged phosphatidylserine on the outer leaflet of tumor cell membranes (Tornesello et al., 2020). Additionally, membrane fluidity is often elevated in cancer cells due to decreased cholesterol, which makes the cells more susceptible to AMP attack (Tornesello et al., 2020). Thus, AMPs can be powerful immune regulators that can signal, rally, and regulate the innate and adaptive immune response on top of their direct antimicrobial effects.

AMPs can have synergistic effects with other antimicrobials including other AMPs and conventional antibiotics (Bahar & Ren, 2013; Brandenburg et al., 2012). For example, Naghmouchi et al. (2012) found that a significant synergistic inhibitory effect was observed when treating resistant *Pseudomonas fluorescens* with a combination of

peptide (multiple bacteriocins) and antibiotic. Synergistic effects could decrease the quantity of antimicrobials needed and increase speed of antimicrobial activity, both of which help to limit the development of resistance. In addition, the speed in which AMPs can act, the employment of the multi-hit mechanisms, the conserved lipid bilayer structure of bacterial membranes, and the lack of a conserved AMP amino acid target to develop defenses against makes the development of resistance more difficult compared to conventional antibiotics, often with only one mechanism of action (Bahar & Ren, 2013; Hancock & Sahl, 2006; Spohn et al., 2019).

1.4. Challenges of AMPs as therapeutics

AMPs have long been acknowledged as potential therapeutics; however, there are several hurdles that hamper the AMP discovery to therapeutic pipeline. Initial discovery of AMPs has traditionally been slow and labour intensive. AMP identification using analytical chemistry methods like liquid chromatography and/or mass spectrometry to isolate new AMPs from excretions, body fluids, or tissue samples and coupling this with antimicrobial susceptibility assays, peptide sequencing, or *de novo* synthesis is a low throughput process that has slowed AMP discovery. This is being overcome with the emergence of new methods such as bioinformatic AMP identification (Bahar & Ren, 2013; Helbing et al., 2019). These can use AMP characteristics to identify putative AMPs in genomic material from virtually any organisms in a high-through put manner, significantly decreasing the effort required to identify putative AMPs, as well as increasing the number of AMPs identified. The physical characteristics of AMPs can also be a barrier to their use of therapeutics. AMPs are expensive to synthesize, prone to proteolytic cleavage, and could be toxic for host cells (Bahar & Ren, 2013). Many of these issues can be addressed through truncations to shorten length and decrease synthesis costs or through modifications to increase stability and antimicrobial activity while decreasing cell toxicity.

C-terminal amidation is a post-translational modification of AMPs that can occur naturally and is common in amphibians (Wang, 2020). Amidation of AMPs can significantly enhance AMP activity and increase their efficacy as antimicrobial agents (Dennison et al., 2015; Huan et al., 2020; Strandberg et al., 2007). When a peptide is

amidated, its carboxyl group at the C-terminus is converted into an amide group which removes the negative charge on the carboxyl group and increases the overall peptide charge by +1 (Mura et al., 2016). Charge is essential for AMP membrane permeability; the increase in charge facilitates improved electrostatic interactions with negatively charged features on the bacterial surface. Amidated AMPs can possess improved membrane-penetrating abilities. Molecular dynamics simulations have also suggested the presence of the NH_2 group at the C-terminus improves the penetration of the peptide into membranes compared to their carboxylated counterparts (Kim et al., 2011; Mura et al., 2016; Sforça et al., 2004). The presence of the amidated C-terminus facilitates stronger interactions with the lipid bilayer (Mura et al., 2016). As a result, the peptide can more easily disrupt and permeabilize the microbial cell membranes. Amidation enhances the stability of AMPs, making them more resistant to degradation by exopeptidases and increases serum stability. This increased stability allows the AMPs to remain active for a longer duration, thereby extending their antimicrobial effects and improving their overall efficacy.

1.5. Bioinformatic antimicrobial peptide discovery

AMP identification methods are rapidly evolving with the creation of new *in silico* bioinformatic tools that allow for the high throughput discovery of putative AMPs from a variety of sources. rAMPage is a scalable bioinformatic AMP discovery pipeline that uses input RNA sequencing (RNA-seq) data to identify AMP sequences (Lin et al., 2022). rAMPage speeds up the discovery stage of finding novel AMPs as possible therapeutics. rAMPage has been applied to insect and amphibian data sets and the novel putative AMPs therein showed activity against a panel of Gram positive and negative pathogens while incurring low cell toxicity (Richter et al., 2022). The rAMPage pipeline applies the AMPlify tool, a deep learning model that applies sequence-aware attention mechanisms for AMP prediction *in silico* (Li et al., 2022). AMPlify has been used to identify AMPs active against WHO priority pathogens (Li et al., 2022), as well as used to evaluate site-directed mutagenesis and truncation of AMPs *in silico* (unpublished data). AMPs are expressed in every living organism, which means that

any transcriptomic material, be it human, amphibian, plant, or bacteria, could be mined as a potential source of AMPs using these tools.

1.6. Antibiotics and agriculture

Antibiotics are commonly used in agricultural sectors to increase food production and to fight and prevent infections in livestock (Barlam & Gupta, 2015; Mathew et al., 2007). These practices exert a selective pressure towards bacteria with a resistance to antibiotics that has serious implications for animal and human health. Consistent exposure to antibiotics can decrease their therapeutic effectiveness in agriculture and public health, threaten food safety, and create potential reservoirs of resistance in the environment due to human and agricultural run-off (Chantziaras et al., 2014; Finley et al., 2013; McCubbin et al., 2021). As awareness of antibiotic resistance grows, steps towards antibiotic-stewardship have been taken such as decreasing antibiotic use for growth promotion or limiting/banning medically important antibiotics in many countries. However, a lack of reporting, difficulties in antibiotic regulation, increased global food demands, and lack of antibiotic alternatives are all roadblocks to decreasing antibiotic use in agricultural settings globally (Van Boeckel et al., 2015). Despite the World Health Organization's warning that antibiotics resistance is "one of the biggest threats to global health, food security, and development today", global antibiotic use is expected to increase by 8% by 2030 (Mulchandani et al., 2023).

Poultry is one of the most commonly consumed animal products worldwide, with flocks often raised in close quarters and given antibiotics to control disease and improve growth (Nhung et al., 2017). Development of resistance in these environments can lead to large economic losses and can pose a public health risk due to resistance gene transfer or products contaminated with zoonotic pathogens. Two of the leading causes of disease in the global poultry industry are colibacillosis and salmonellosis, whose causative agents are avian pathogenic *Escherichia coli* (APEC) and *Salmonella enterica* serovar Enteritidis (SE) respectively (Kabir, 2010; Nhung et al., 2017). Both are gram negative bacterium that can be spread by contaminated eggs, feces, feed, and more, and that result in massive economic losses and a decrease in animal welfare due to mortality and the decrease in production associated with morbidity. APEC can present

in a septicemic acute form or as sub-acute pericarditis, air sacculitis, and perihepatitis. SE can cause local or systemic infections and the chicks that survive become potential asymptomatic carriers. These pathogens also have zoonotic importance as they can contaminate animal products, contributing to foodborne illness and the spread of antibiotic resistance genes. Antibiotic resistance has been identified in both APEC and SE (Nhung et al., 2017). While good husbandry practices are key in limiting disease, the development of new antimicrobials that prevent or treat disease while mitigating the development of resistance is an important step in securing the future of food production in the poultry industry.

In both public health and agricultural sectors, implementation of tighter antibiotic restrictions, increasing global reporting of antibiotic use, and the discovery for antibiotic alternatives that are not as susceptible to the development of resistance will all be critical steps in slowing the spread of antibiotic resistance.

1.7. Hypothesis

My hypothesis is that transcripts related to the innate immune functions of the back skin of *R. catesbeiana* will be differentially expressed during natural metamorphosis and TH-induced temperature modulated metamorphosis. Furthermore, I hypothesize that novel AMP candidates with antimicrobial activity against the poultry related pathogens APEC and SE can be bioinformatically identified using RNA-seq data in these conditions.

1.8. Objectives

Overall objective: To better understand the gene expression changes in *R. catesbeiana* back skin during TH-dependent post-embryonic development, with a particular emphasis on the innate immune system.

Specific objective 1: Generate and analyze gene expression profiles of amphibian skin with a focus of the innate immune system during postembryonic development and in tadpoles induced by TH under different temperature conditions using RNA-seq.

Specific objective 2: Determine the antimicrobial activity and cell toxicity of anuran-derived bioinformatically identified novel AMP candidates in the context of the poultry related pathogens APEC and SE.

2. Transcriptomic analysis of *R. catesbeiana* tadpole back skin during natural metamorphosis and TH-induced precocious metamorphosis under different temperature conditions with particular emphasis on innate immune system components

2.1. Abstract

Amphibians are crucial indicator species that provide insight into general ecosystem health, endocrine disrupting chemical impacts, and the influence of changing environments from natural and anthropogenic factors. As the aquatic tadpole undergoes metamorphosis to become a terrestrial frog, its innate immune system must adapt to pathogens present in the new environment. Amphibians use skin as a primary line of defense in the innate immune system since it acts as an important physical, microbial, and chemical barrier throughout its life cycle, yet this organ undergoes extensive remodelling during metamorphosis. Metamorphosis is regulated by thyroid hormone (TH) initiated gene expression that leads to the start of the metamorphic programming. This can be induced by the addition of exogenous TH. While different tissues respond to TH in distinctive ways during metamorphosis, how these tissues respond to TH is poorly understood. Temperature modulation, which regulates metamorphic timing, is a unique way to uncover early TH-induced transcriptomic events. Precocious metamorphosis of premetamorphic tadpoles is induced by exogenous TH administration at a permissive (24^{o}C) temperature. However, tadpoles exposed to TH at a non-permissive (5^{o}C) temperature do not display physical changes yet retain a “molecular memory” for TH exposure that results in an accelerated metamorphosis upon shifting to the permissive temperature. Gene expression changes at the non-permissive temperature may indicate components of the molecular memory. We used RNA-sequencing to identify changes in *R. catesbeiana* back skin gene expression during natural metamorphosis and temperature modulated responses to TH-induced metamorphosis. During natural metamorphosis, significant differential expression was observed in over 6,500 transcripts including classic TH-responsive transcripts (*thrb* and *thibz*), heat shock

protein 30, and innate immune system components: keratins, mucins, and antimicrobial peptides (AMPs). Premetamorphic tadpoles maintained at the non-permissive temperature showed 83 differentially expressed transcripts within 48 h after TH administration. Of note is the 52-fold increase in *thibz* transcript that has previously been identified as a molecular memory component in other tissues. Over 3,600 differentially expressed transcripts were detected in TH-treated tadpoles compared to the controls at permissive temperature or when tadpoles were held at 5^{o}C and then shifted to 24^{o}C. Gene ontology (GO) terms related to transcription, RNA metabolic processes, and translation were enriched in both datasets and immune related GO terms were observed in the temperature-modulated experiment. We show that the back skin is a TH-responsive and temperature sensitive tissue whose innate immune elements are differentially expressed during metamorphosis and that their expression can be temperature sensitive. We also show that broadening the conditions in which we search for novel AMPs can lead to increased discovery. This has implications in amphibian survival as natural and anthropogenetic factors continue to threaten amphibians worldwide.

2.2. Introduction

Thyroid hormone (TH) is critical for vertebrate growth, development, and metabolism (Mullur et al., 2014; Paul et al., 2022). Anuran metamorphosis from a premetamorphic aquatic larval tadpole to a terrestrial juvenile froglet is regulated by tissue-dependent TH activity that leads to extensive remodelling of larval tissues (Hammond et al., 2015; Poulsen et al., 2023; Shi, 2000). TH levels gradually increase during prometamorphosis until a peak at metamorphic climax followed by a significant reduction in the frog (Poulsen et al., 2023). Metamorphic programming can be induced by exogenous TH (Shi, 2000). This TH-sensitivity make amphibians such as *R. catesbeiana* ideal model organisms in which to study mechanisms of TH action.

THs can act through genomic or non-genomic signalling pathways, with the former being best understood. In the genomic pathway, TH acts through the nuclear TH receptors (TR) which are encoded by two genes: TR alpha (*thra*) and TR beta (*thrb*) (Mullur et al., 2014; Paul et al., 2022; Shi, 2000). Both TRs have tissue and

developmental stage specific expression patterns (Hammond et al., 2015; Poulsen et al., 2023; Shi, 2000). In the best understood mechanism, TRs repress gene expression in the absence of TH, but once bound, they positively regulate the transcription of early response genes leading to a tissue specific cascade of expression (Buchholz et al., 2007; Das et al., 2009). However, TH-TR complexes can also repress gene expression through mechanisms that are still poorly understood (You et al., 2010).

R. catesbeiana tadpoles can overwinter at the bottom of deep ponds, thereby extending their larval stage until conditions favour undergoing metamorphosis (Wright et al., 1999). Consequently, abiotic factors such as temperature influence metamorphic timing. At cold, non-permissive temperatures (5°C), metamorphic programming is paused (Ashley et al., 1968; Frieden et al., 1965). However, if the tadpole is exposed to TH during this period it will retain a molecular memory of the TH exposure and, once returned to a warmer metamorphically permissive temperature (25°C), development will continue at an accelerated rate (Ashley et al., 1968; Frieden et al., 1965). TH responsive gene expression is biphasic with an initiation phase and an execution phase (Das et al., 2009; Koide et al., 2022). The molecular memory retained at cold temperatures further subdivides the initiation phase (Hammond et al., 20015; Koide et al., 2022) enabling the identification of critical components of early metamorphic signalling events.

Metamorphosis and temperature both impact the immune system of amphibians. In tadpoles the immune system, while competent, is considered immature (Grogan et al., 2018; Humphries et al., 2022). However, amphibians with longer larval stage such as *R. catesbeiana* develop more defense mechanisms (Gosavi et al., 2014). During metamorphosis, the immune system is supressed and, like the rest of the tadpole, undergoes massive remodelling (Grogan et al., 2018; Humphries et al., 2022). Environmental factors such as low temperatures, pollutants, and stress can all inhibit the natural defenses of amphibians and increase the susceptibility to infection (Humphries et al., 2022; Rollins-Smith et al., 2011; Sauer et al., 2020). Therefore, understanding how the amphibian immune system changes during metamorphosis and in challenging environmental conditions is critical for amphibian survival.

Amphibian skin plays many crucial functions including respiration, ion and water regulation, predator defense, and innate immunity (Akat Çömden et al., 2023; Varga et al., 2019). The skin, which is thought of as the first line of defense in the innate immune system, acts as a physical, chemical, and microbiological barrier that is in constant contact with a microbially laden environment. As the aquatic tadpole develops into the terrestrial frog, the skin must adapt to this new environment and the pathogens and challenges that comes with it.

Like many of the other larval tissues, the amphibian skin undergoes remodelling during metamorphosis. Here we focus on the head and trunk skin composition, which has a different metamorphic outcome than the regressing tail fin (Yoshizato, 1992). In tadpole back skin, the epidermis has four to six replicating cell layers composed apical cells, skein cells, and larval basal cells on a basement membrane (Furlow et al., 1997; Robinson & Heintzelman, 1987; Watanabe et al., 2001; Yoshizato, 1992). As TH levels increase during metamorphosis, the larval-specific apical and skein cells undergo apoptosis and larval basal cells are stimulated to differentiate into adult basal cells, proliferating becoming cells in the germinative layer (Yoshizato, 1992). By late metamorphic climax, the head and trunk skin has fully developed into the adult stratified epidermis composed of two layers: the epidermis and the dermis (Yoshizato, 1992). Fully developed terrestrial frog skin is both structurally and functionally different from that of the free-swimming larvae.

The goal of the present study is two-fold. First, we generated and analyzed gene expression profiles of *R. catesbeiana* skin during post-embryonic development and in tadpoles induced by TH under different temperature conditions using RNA-sequencing. We characterize the expression of TH-responsive transcripts as well as perform gene ontology (GO) enrichment analysis for each experiment. The differential expression of transcripts of interest identified in the datasets including heat shock proteins and components of the skin innate immune system including keratin, mucin, and known AMPs were examined.

Second, we apply a novel bioinformatic AMP discovery tool called rAMPage (Lin et al., 2022) to these RNA-sequencing datasets to identify novel putative AMPs and

study their expression during development and in temperature-modulated conditions. Given that TH-dependent metamorphosis itself is perturbed by changes in temperature, we hypothesized that TH-dependent changes to the immune system may also be altered by temperature, providing a broader opportunity to discover novel AMP candidates.

2.3. Materials and methods

2.3.1. Experimental animals

R. catesbeiana tadpoles of mixed sex were caught from local freshwater systems by Westwind Sealab Supplies in Victoria, British Columbia, Canada and housed at the University of Victoria Outdoor Aquatics Unit. Animals were housed in covered outdoor 100-gallon (378.54 L) fiberglass tanks filled with recirculated dechlorinated municipal water at 15 ± 1°C, pH 6.8, and 96-98% dissolved oxygen. The tadpoles are fed daily with Spirulina flakes (Nutrafin Max, Rolf C. Hagen, Montreal, PQ, Canada). Animal care was in accordance with the Canadian Council on Animal Care and the University of Victoria Animal Care Committee guidelines under animal use protocol # 2019-025.

2.3.2. Experimental set-up

2.3.2.1. Natural metamorphosis

Animals were chosen from the University of Victoria Aquatics Care Unit based on their naturally occurring stage of metamorphosis. *R. catesbeiana* were visually assessed using Taylor Kollros (TK) staging (Taylor & Kollros, 1946) and chosen to represent key developmental milestones during metamorphosis, including premetamorphosis (TK stage 6 - 8; n = 5), prometamorphosis (TK stage 15; n = 10), metamorphic climax (TK stage 20; n = 13), and froglets (TK stage 24 - 25; n = 5) (Figure 1.2.1-1).

2.3.2.1. TH-induced metamorphosis under different temperature conditions

This experiment examined *R. catesbeiana* tadpoles undergoing TH-induced metamorphosis in temperature conditions known to influence the rate of development. The tadpoles were injected with T_3 (to induce metamorphosis) or with solvent control and then exposed to three conditions known to influence the rate of metamorphosis:

permissive (24°C), non-permissive (5°C), and temperature-shift (5°C shifted to 24°C) (Figure 2.3.2-1A).

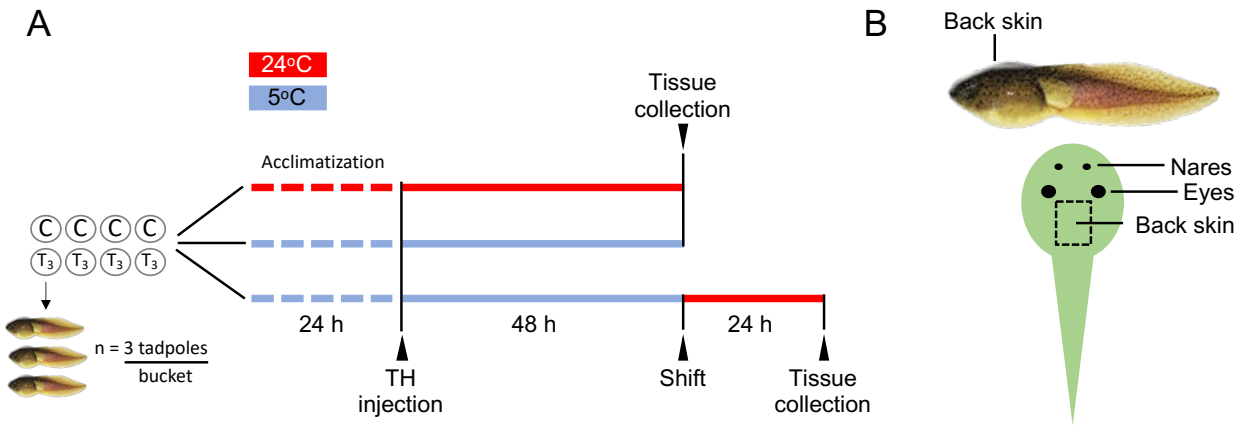

Figure 2.3.2-1 A) The experimental setup of the temperature modulation experiment where tadpoles injected with either T_3 or solvent control and then exposed to one of three temperature conditions: permissive (24°C), non-permissive (5°C), and temperature-shift (5°C shifted to 24°C). B) Location of the back skin tissue collection.

Premetamorphic *R. catesbeiana* tadpoles (n = 12/each temperature treatment/condition) were placed in 12 L high-density polyethylene buckets (3 tadpoles per bucket) containing 8 L of source recirculated dechlorinated water. The buckets were randomized and acclimatized for 24 h in sea trays maintained at either 5±0.6°C for the non-permissive and shift conditions or 24±1°C for the permissive condition. Air stones were placed in each bucket for continual aeration and the tadpoles were not fed for the duration of the experiment.

Injections of 10 pmole T_3/g body weight (bw) in 400nM of NaOH or solvent control (400 nM NaOH) were performed as per Corrie et al. (2021). TH concentration of the 10^{-5} M T_3 stock solution was measured using mass spectrometry. Briefly, TH analytical analysis of T_3 stock solution (CAS # 55-06-1; Alfa Aesar, Ward Hill, MA, US) was performed at the UVic/Genome BC Proteomics Centre using liquid chromatography multiple reaction monitoring mass spectrometry (LC/MRM/MS). Using the measured T_3 concentrations, stocks were diluted to a 10 µM T_3 working stock. After acclimatization, the tadpoles were intraperitoneally injected with 1 µL/g bw rounded to the nearest 0.5

µL of either 10 µM T_3 or an equal volume of 400 nM NaOH using 50 µL Hamilton syringe with 26 G x 1/2 sterile needles.

As per Figure 2.3.2-1, after 48 h exposure at the permissive and non-permissive temperatures respectively, the tadpole tissues were collected. For the non-permissive treatment group, the tissues were collected in a 2°C cold room to always maintain a low tissue temperature. For the temperature shift treatment group, after 48 h at the non-permissive temperature, the tadpoles were moved to buckets pre-warmed to a permissive temperature for 24 h. After 24 h at the permissive temperature, tissue was collected from the temperature shift group. Animal and water quality monitoring (pH [Aquacheck CAS # 27552-50], temperature, ammonia [Aquacheck CAS # 27553-25]) was performed daily throughout the experiment. The pH for each experimental condition independently was 6.8 and the ammonia levels were between 0.25 to 0.5 ppm. The back skin was collected as shown in Figure 2.3.2-2. Results from other collected tissues will be presented in other manuscripts (Field et al., in prep and Kuecks-Winger, et al., in prep). Although n =12 per temperature treatment/condition were prepared for the general study, these animals were shared with other experiments. For the present study, a subset of n = 5 randomly chosen animals were used per temperature condition and hormone/control treatment.

2.3.2.2. Sample collection for RNA-sequencing

This research combines RNA-seq analysis of back skin tissue samples from both the natural metamorphosis (n = 5 during premetamorphosis, n = 10 during prometamorphosis, n = 13 at metamorphic climax, and n = 5 as froglets) and the temperatures shift animals n = 5 at each temperature and hormone or control treatment).

2.3.3. Euthanasia, dissection, and tissue collection

All animals from both the natural metamorphosis and temperature shift experiments were euthanized by immersion in 0.1% (w/v) tricaine methane sulfonate (Syndel Laboratories, BC, Canada) buffered in 25mM sodium bicarbonate (CAS # 144-55-8; Fisher Chemical, Fair Lawn, NJ, US). Immediately following euthanasia, the back skin tissue was collected (Figure 2.3.2-1B) and submerged in 1.25 mL RNA*later* (Ref

AM7021; Thermo Fisher Scientific, Burlington, ON, Canada) according to the manufacturer's standard protocol.

2.3.4. Total RNA extraction

2.3.4.1. Natural metamorphosis

Back skin samples were randomized prior to processing to minimize technical bias. The back skin tissue samples were placed in a 1.5 mL safe-lock microfuge tube (CAS # 022363611; Original Eppendorf, Mississauga, ON, Canada) containing 700 µL TRIzol (CAS # 15596-018; Invitrogen, Carlsbad, CA, US) and a 3 mm tungsten carbide bead and mechanically disrupted using the Retsch MM301 Mixer Mill (Thermo Fisher Scientific, Ottawa, Canada) at 20 Hz for two 3 min cycles separated by a sample rotation of 180° between cycles. RNA was extracted using chloroform, isopropanol, and ethanol treatments as per Heerema et al. (2018). The extracted neat RNA was dissolved in UltraPure RNAse-free water (Invitrogen, CAS # 10977023) and stored at −80 °C.

2.3.4.2. TH-induced metamorphosis under different temperature conditions

Tissue samples (n = 5/each temperature condition and treatment) were randomized prior to RNA extraction. Total RNA extraction was carried out using the miRNeasy Tissue/Cells Advanced Mini Kit (CAS # 217605; QIAGEN, Germantown, MD, US) following the supplier's protocol for 20 - 30 mg of tissue with some modifications. Briefly, the tissue was removed from RNALater, gently blotted to remove excess RNALater residue, and placed in 1.5 mL Safe-Lock microfuge tube (CAS # 022363611; Original Eppendorf, Mississauga, ON, Canada) containing 450 µL Buffer RLT, 0.04 M DTT (CAS # 3483-12-3; Sigma Aldrich), and a 3 mm ALPHA Nanotech stainless-steel lysing bead. If the tissues exceeded the appropriate size, they were cut using a razor blade. The samples were homogenized using the same Mixer Mill protocol above. The samples were centrifuged at 21,000 xg for 3 min using a Microfuge® 16 centrifuge (Beckman Coulter, Indianapolis, US). The supernatant was transferred to a new 1.5 mL Eppendorf tube for storage at -80°C prior to the remainder of the RNA extraction.

Once thawed, the homogenized samples were processed following the manufacturer's protocol with the following modifications: an additional 500 mL 80% ethanol wash step performed prior to the RNA elution and a 2 min spin was used to dry the column. Additionally, to elute the RNA, 50 µL RNase free water was added to column and incubated for 10 min at room temperature before centrifugation for 1 min at 21,000 xg. The isolated RNA samples were stored at -80°C.

2.3.5. RNA sequencing (RNA-seq)

RNA sample integrity and concentration were assessed for both experiments using a Bioanalyzer 2100 (Agilent, Mississauga, Ontario, Canada) and RNA Nano Kit (Cat # 5067-1511, Agilent, Mississauga, Ontario, Canada). Samples with an RNA Integrity Number (RIN) ≥ 7 were selected. The RNA was shipped on dry ice to the Genome Sciences Centre in Vancouver, BC Cancer, BC, Canada where polyA+ mRNA strand-specific library construction and sequencing on the NovaSeq6000 platform (Illumina, San Diego, California, USA) was performed to generate 2 × 150bp paired-end RNA-seq reads (50 million reads per sample).

2.3.6. RNA-seq analyses

RNA-seq analyses were performed on the natural metamorphosis and TH-induction read sets separately but using the same RNA-seq and Gene Ontology (GO) pipeline as described in Jackman et al. (2022), with the exception of using a more complete version (version 4) of the *R. catesbeiana* genome assembly (DOI 10.5281/zenodo.8125199). Briefly the RNA-seq analysis was performed as follows. STAR two-pass alignment (version 2.6.1) (Dobin et al., 2013) was used to align the raw reads to the *R. catesbeiana* genome version 4. StringTie (version 1.3.4) was used to assemble and count transcripts (Pertea et al., 2015). A filter was applied with a cut off of five samples with normalized counts below 0.1 counts per million to eliminate low count false positives. Differential expression analysis from transcript counts was performed using DESeq2 ($p_{adj} \leq 0.05$, FDR ≤ 0.05; version 1.28.1) (Love et al., 2014). Transcripts were annotated with BLASTn (version 5; Blast+/2.13.0) and BLASTx using the National Center for Biotechnology Information (NCBI) nucleotide (nt) and non-redundant (nr) protein databases.

Trinotate was used to annotate differentially expressed genes with gene ontology (GO) terms (version 3.2.0) (Bryant et al., 2017). GO term enrichment ($p_{adj} \leq 0.05$, FDR ≤ 0.05) was identified using GOseq (version 1.38.0) (Young et al., 2010). Cytoscape used the enriched GO terms to generate enrichment maps to facilitate visualization (version 3.8.2) (Shannon et al., 2003). An 'extremes' filter was applied using Gogadget (version 2.1) (Nota, 2017) allowing for the removal of overly specific or general GO terms to improve mapping of the enriched genes.

2.3.7. Antimicrobial peptide identification and differential expression

The differential expression (DE) of novel and known antimicrobial peptides (AMPs) in the natural metamorphosis and TH-induction transcriptomic datasets was examined. Local blastn databases comprising either RNA-seq datasets were created using the makeblastdb command (blast+/2.13.0).

For the known AMPs, the *R. catesbeinana* nucleotide sequences for known AMPs: ranatuerin-1, -5, -7, and -8, for ranalexin, for ranacyclin-Ca, -Cb, and -Cc, and for cathelicidin-RC1 and -RC2, were obtained from NCBI. These sequences were blasted against our local transcript databases for both experiments to identify the contigIDs associated with those sequences. Those contigIDs were then used to query the datasets to determine if these known AMPs were DE in any treatment condition.

To bioinformatically identify novel putative AMPs in the RNA-seq datasets, the homology based Rapid Antimicrobial Peptide Annotation and Gene Estimation (rAMPage) pipeline (Lin et al., 2022) was used as per Richter et al. (2022). For both experiments, rAMPage (version 1.0.1) was employed up to the assembly step, which generated transcriptomics assemblies for each experimental condition separately. Subsequently, for each produced assembly, the remaining steps of the rAMPage pipeline, including translation, homology search, and cleavage, were performed. To prioritize the peptides, specific filters were used by employing the AMPlify tool (Li et al., 2022). Peptides were retained if they satisfied the following criteria: AMPlify score ≥ 10, length ≤ 50 amino acids, and charge ≥ 1.

Peptides that met these criteria were considered putative AMPs. A BLAST search against the National Center for Biotechnology Information (NCBI) non-redundant

(nr) protein databases database was conducted. An AMP is classified as novel if the putative AMP sequence was not the same as any known AMP sequences. The term “putative” was assigned to the bioinformatically identified AMPs since antimicrobial susceptibility testing was not performed to confirm antimicrobial activity.

The rAMPage assembled nucleotide sequences for the novel putative AMPs were blasted against our local blastn databases created for each experiment to identify the local contigIDs for the novel putative AMPs. These were then used to examine the DE of each novel putative AMP. When more than one contig was associated with a novel putative AMP, the contig with the highest abundance was used for DE analysis.

2.4. Results and discussion

2.4.1.1. RNA-seq counts and differential expression analysis

An average of 43.1 million reads were sequenced per library. An average of 77.9% of the reads were successfully mapped to the annotated *R. catesbeiana* genome version 4 (DOI 10.5281/zenodo.8125199) across all libraries. The number of total transcripts identified across each stage comparison ranged from 16,128 to 17,719 transcripts with an average of 96.6% being annotated (Table 2.3.7-1). See Supplementary Table 7-1 for additional information.

Table 2.3.7-1 Total number of transcripts sequenced per developmental stage comparison from the back skin of *R. catesbeiana* undergoing natural metamorphosis. The stages listed here are compared to the premetamorphic tadpoles. Total transcripts include all transcripts identified in either of the stages being compared. Differential expression (DE) of a transcript was denoted as a statistically significant difference in transcript abundance between the stages of development being compared with a $p_{adj} \leq 0.05$ and a false discovery rate (FDR) of 0.05.

Stage Comparison	Total Transcripts	% Annotated	DE Transcripts	% DE Annotated
Prometamorphosis	17,169	96.4	6,548	96.9
Metamorphic climax	17,719	96.4	7,806	96.9
Froglet	16,128	97.0	8,119	97.3

Principal component analysis (PCA) revealed a strong separation of the DE transcriptomic profiles of each developmental stage compared to that of the premetamorphic tadpole (Figure 2.3.7-1). The premetamorphic organisms compared to

the prometamorphic group showed a 60.9% variation across principal component (PC) 1. For the premetamorphosis versus metamorphic climax group, PC1 accounted for 57.2% of the variation. The strongest separation of 74.1% across PC1 was observed in the premetamorphosis to froglet comparison.

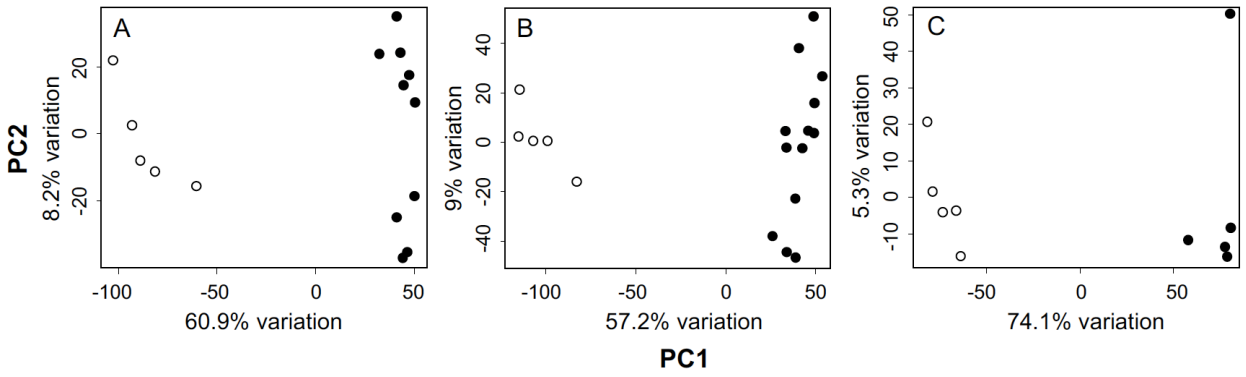

Figure 2.3.7-1 Principal Component Analysis (PCA) of DE transcripts from the back skin of *R. catesbeiana* at key developmental stages of natural metamorphosis: prometamorphosis (A), metamorphic climax (B), and froglets (C) relative to premetamorphosis. The premetamorphic tadpoles are indicated by the open circles, with each circle representing an individual biological replicate. The biological replicates belonging to developmental stage being compared are indicated by the closed circles.

As seen in Figure 2.3.7-2, there was a significant change in transcript expression in all developmental stages tested compared to the premetamorphic tadpoles. In the premetamorphosis to prometamorphosis comparison, there were 3,346 up-regulated transcripts and 3,198 down-regulated transcripts. In the premetamorphosis to metamorphic climax comparison, there were 4,023 up-regulated transcripts and 3,775 down-regulated transcripts. In the premetamorphosis to froglets comparison, there were 3,966 up-regulated transcripts and 4,145 down-regulated transcripts. This suggests that transcript DE is ramping up to a peak at metamorphic climax, which corresponds to the highest level of circulating TH (Poulsen et al., 2023).

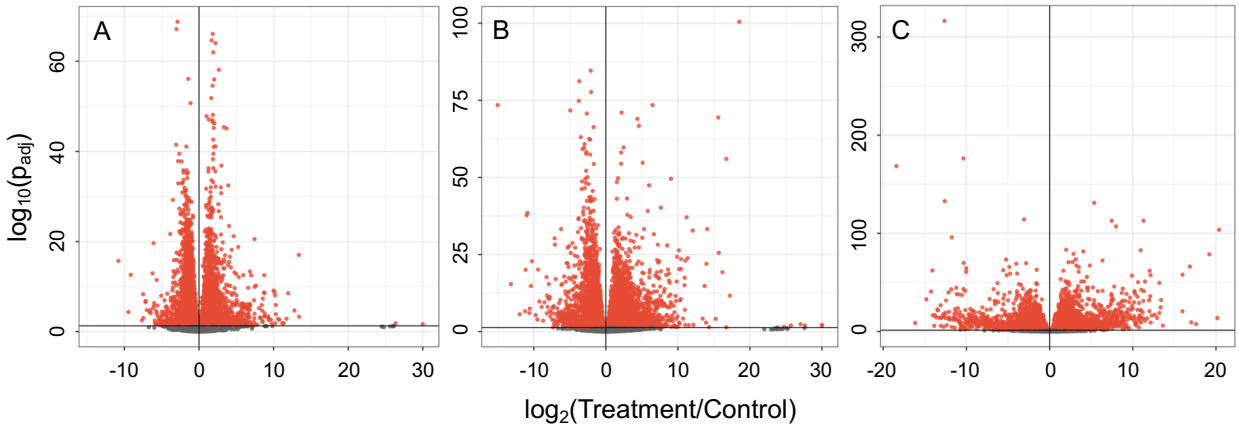

Figure 2.3.7-2 Volcano plots of DE transcripts in the back skin of *R. catesbeiana* at key developmental stages of natural metamorphosis: prometamorphosis (A), metamorphic climax (B), and froglets (C) relative to premetamorphosis. DE of transcripts was determined by DESeq2 analysis (Love et al., 2014). Red dots indicate transcripts that are DE between the stages indicated at the top of the plot and grey dots are the non-DE transcripts ($p_{adj} \leq 0.05$). Transcripts to the left of 0 on the x-axis are down-regulated, while transcripts to the right are up-regulated.

When comparing the transcriptomic response across the developmental stages many of the DE transcripts were affected at all stages; however, there were numerous transcripts that were uniquely affected by developmental stage (Figure 2.3.7-3A). There were 3,904 DE transcripts shared across prometamophosis, at metamorphic climax, and as froglets when compared to the premetamorphic tadpoles (Figure 2.3.7-3A). In contrast there were 876, 1,253, or 1,844 transcripts being expressed during only prometamorphosis, at metamorphic climax, and as froglets respectively (Figure 2.3.7-3A). As the tadpoles underwent metamorphosis, the number of distinct DE transcripts increased with 13.4% of the prometamorphic DE transcripts being unique, followed by 16.1% at metamorphic climax, and finally 22.7% in froglets. The most overlap of DE transcripts was observed between metamorphic climax and froglets and the lowest was observed between prometamorphic tadpoles and froglets (the two most distinct developmental stages). While there was conserved expression in all developmental stages studied, each stage also had a distinct transcriptomic profile during development.

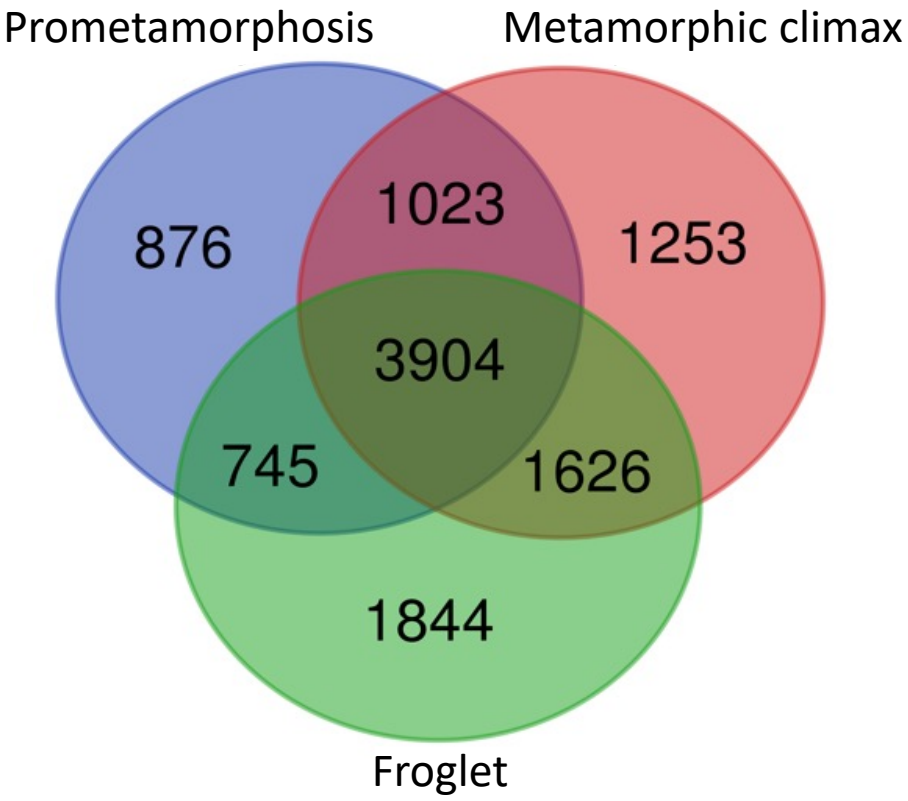

Figure 2.3.7-3 Comparison of the number of DE transcripts in the back skin of *R. catesbeiana* undergoing natural metamorphosis. DE ($p_{adj} \leq 0.05$) during prometamorphosis (blue), at metamorphic climax (red), or as froglets (green) compared to premetamorphic tadpoles as identified by DESeq2. See Supplementary Figure 6-1 for a comparison of the DE genes used in the gene ontology analysis.

2.4.1.2. Classic thyroid hormone indicator transcripts

Thyroid hormone (TH) is a critical regulator of amphibian metamorphosis, primarily by binding the nuclear TH receptors and regulating the expression of early response genes (Shi, 2000). TH bioindicator transcripts such as the TH receptors α (*thra*) and β (*thrb*) or the early response gene TH-induced basic region leucine zipper-containing transcription factor (*thibz*) are often used to understand the changes in TH signalling or perturbations in the system (Thambirajah et al., 2019). In the present study, the expression of those same TH-indicator transcripts was examined as per Table 2.3.7-2 using RNA-seq analysis. This allowed us to verify the staging of the animals by comparing the levels of TH-responsive transcripts to the visually identified developmental stages (see Figure 1.2.1-1 for reference).

Each classic TH indicator transcripts was detected at all stages investigated in this experiment. No significant change in expression of *thra* was observed at any of the developmental stages (Table 2.3.7-2). The expression of both *thrb* and *thibz* transcripts was significantly increased at all three stages, although to a much greater degree for *thibz* compared to *thrb* (Table 2.3.7-2). The highest abundance of *thrb* and *thibz* expression was observed around metamorphic climax. Hence, our results show that the levels of the TH-responsive transcripts *thrb* and *thibz* increased during metamorphosis until they peaked at metamorphic climax and then decreased as the back skin approached its juvenile frog form.

Poulsen et al. (2023) recently published a study comparing serum TH levels and related metabolites determined using liquid chromatography tandem mass spectrometry (LC-MS/MS) to TH-indicator transcript expression in the back skin of the same animals using qPCR. They found that *thra* expression was steady during prometamorphosis and showed a minor significant decrease at metamorphic climax and onwards whereas we found no significant change (Poulsen et al., 2023). This could point to negative feedback of *thra* expression in the back skin. Their results for the abundance of *thrb* and *thibz* transcripts are in line with those found in the present study and support the developmental stages applied herein (Table 2.3.7-2 and see Figure 1.2.1-1 for reference). The patterns of expression of the TH-responsive transcripts identified in Table 2.3.7-2 are consistent with the back skin responding to changing TH levels during metamorphosis.

Table 2.3.7-2 Fold changes of TH-responsive transcripts in *R. catesbeiana* back skin during prometamorphosis, at metamorphic climax, or as froglets compared to the premetamorphic tadpole. All transcripts were detected in the RNA-seq data. The thyroid transcripts indicated are *thra* (TH receptor α), *thrb* (TH receptor β), and *thibz* (TH-induced basic region leucine zipper-containing transcription factor). All fold changes are statistically significant with a $p_{adj} \leq 0.05$. A "-" indicates no significant change was observed.

Transcript	Prometamorphosis	Metamorphic climax	Froglet	Accession #
thra	-	-	-	L06064.1
thrb	⇧ 1.5	⇧ 3.3	⇧ 1.8	XM_040353001.1
thibz	⇧ 4.1	⇧ 507.7	⇧ 32.2	MG459289.1

2.4.1.1. Gene ontology (GO) analysis of natural metamorphosis

Eighty-eight GO terms were identified in the prometamorphic tadpoles, 21 GO terms were identified at metamorphic climax, and 11 GO terms were identified in froglets. Prometamorphic tadpoles had the most enriched GO terms and froglets had the least, indicating more enriched biological pathways early on in development. Significant GO terms associated with molecular functions, biological processes, and cellular components were identified at each developmental stage tested and the most significant can be seen in Figure 2.3.7-4.

GO terms associated with transcription, RNA metabolic processes, and translation were the most prominent clusters as seen in Figure 2.3.7-5. During metamorphosis, larval specific skin cells undergo apoptosis and basal cells proliferate to form the stratified adult epidermis. TH, the initiator of metamorphic programming, regulates many cellular activities including proliferation and apoptosis (Buchholz, 2015; Shi, 2000; Shi et al., 2012; Skirrow et al., 2008; Suzuki et al., 2009).

The premetamorphic to prometamorphic developmental stage transition was responsible for most of the GO nodes indicating an initial surge of activity in the expression and regulation of RNA and proteins as TH begins being produced. Similar trends have been observed in *X. laevis* body skin where transcription and proteolysis GO terms were identified as early as one day post TH exposure and in *R. catesbeiana* back skin where a significant increase in DE of protein encoding genes after T_3 exposure was observed (Das et al., 2009; Hammond et al., 2017; Suzuki et al., 2009). We observed a cluster for epigenetic regulation only in the premetamorphosis to prometamorphosis developmental stage comparison (Figure 2.3.7-5). Chromatin remodelling has been shown to be an important component in TH-induced gene expression (Shi et al., 2012). Thus, epigenetic regulation may play a role in initial stages of skin metamorphosis.

Figure 2.3.7-4 GO enrichment analysis of *R. catesbeiana* back skin during prometamorphosis (blue), at metamorphic climax (red), and as froglets (green) compared to the premetamorphic tadpole. The negative $\log_{10}$ of the p-value for each GO term grouped by molecular function (MF), biological process (BP), or cellular components (CC). Only the top 5 GO terms in each category are shown for prometamorphosis and at metamorphic climax to simplify visualization. All GO terms are shown for froglets. For a full list of GO terms for prometamorphosis and metamorphic climax, see Supplementary Figure 6-2 and Supplementary Figure 6-3.

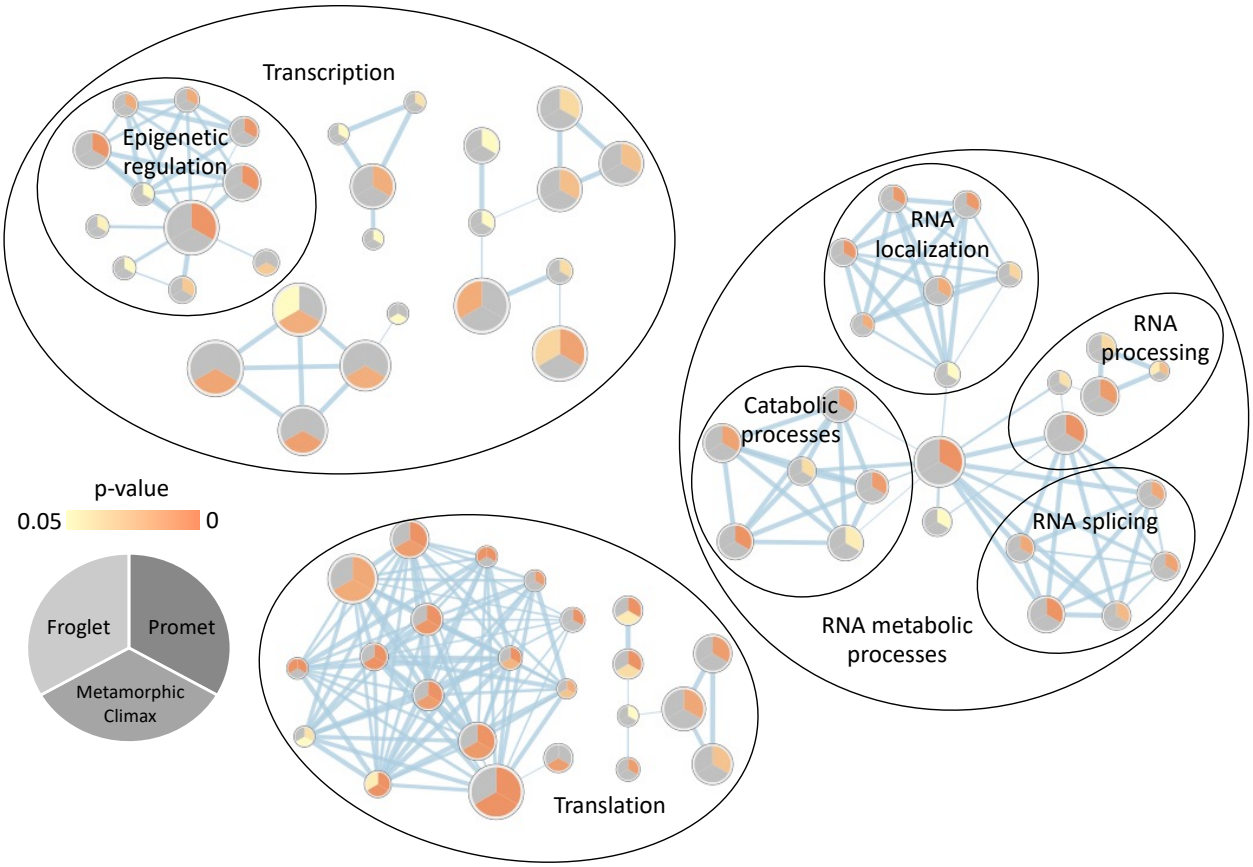

Figure 2.3.7-5 GO enrichment analysis of transcription, RNA metabolic processes, and translation related functions during prometamorphosis (promet), at metamorphic climax, or as froglets compared to premetamorphic tadpoles. GO term enrichment was visualized using the Cytoscape Enrichment Map plugin. Each GO term is represented by a node split into thirds representing a different developmental stage. Orange indicates that that GO term is enriched at that stage with the shade of orange indicating p-value and grey indicating no enrichment. Node size indicates the number of genes associated with each GO term and the thickness of the line indicates the relatedness of the connected nodes.

RNA metabolic processes were enriched almost uniquely during prometamorphosis (Figure 2.3.7-5). This enrichment cluster appears to be tissue specific. In Jackman et al. (2022), GO enrichment analysis was performed on the tail fin, liver, and olfactory epithelium of *R. catesbeiana* after TH exposure and a similar RNA processing related cluster with many of the same nodes identified in the present study were identified in the olfactory epithelium but not in the other two tissues.

Translation, specifically GO terms associated with the ribosome, showed the most overlap between the different stages in development with most GO terms being enriched at both the prometamorphic and metamorphic climax stages (Figure 2.3.7-5).

As metamorphosis progresses, the translation of early direct response transcripts is necessary to produce proteins needed to continue the TH signalling program (Das et al., 2009; Koide et al., 2022). Transcription and translation related GO terms continued to be enriched at metamorphic climax and in froglets, although to a lesser extent than in prometamorphic tadpoles suggesting that transitory changes required for tadpole remodelling were complete once reaching the end of metamorphosis.

2.4.2. Temperature modulated transcriptomic changes during induced metamorphosis

Temperature regulates metamorphic timing, with cold non-permissive temperatures halting the metamorphic program and warm permissive temperatures allow metamorphosis to proceed (Frieden et al., 1965). In tadpoles that have been exposed to TH at cold, non-permissive temperatures, a molecular memory is retained so that, once the tadpole is returned to a permissive temperature metamorphic programming is resumed at an accelerated rate (Ashley et al., 1968; Frieden et al., 1965; Hammond et al., 2015). Utilizing the temperature control of metamorphic timing allows for the investigation of early metamorphic events (Hammond et al., 2016; Koide et al., 2022). Here we employed RNA-seq methods to understand transcriptomic changes of TH-responsive transcripts and components of the innate immune system in the back skin in non-permissive, permissive, and shift temperature conditions after TH injection.

2.4.2.1. RNA-seq counts and DE analysis

The average number of reads per back skin library was 63.5 million, with an average of 78% of filtered RNA-Seq reads mapped to the annotated *R. catesbeiana* genome version 4 (DOI 10.5281/zenodo.8125199). The non-permissive, permissive, and shift temperature conditions generated 15,868, 15,818, and 16,160 transcripts respectively, with approximately 97% of those being annotated in each condition (Table 2.4.2-1). For additional information see Supplementary Table 7-2.

Table 2.4.2-1 Total number of transcripts sequenced from back skin of 10 nM T_3-treated *R. catesbeiana* tadpoles in three temperature conditions: non-permissive, permissive, and shift. Tadpoles at each temperature were injected with a NaOH control or T_3 (n = 5 tadpoles per injection group). Total number of transcripts include all transcripts identified in any control or treatment animals. DE of a transcript was denoted as a statistically significant difference in transcript abundance between the control and treatment groups with a $p_{adj} \leq 0.05$ and FDR of 0.05.

Condition	Total Transcripts	% Annotated	DE Transcripts	% DE Annotated
Non-permissive	15,868	97.4	83	98.8
Permissive	15,818	97.5	3,986	98.9
Shift	16,160	97.2	3,686	98.6

In the non-permissive condition 83 transcripts were DE, 3,986 in the permissive condition, and 3,686 in the temperature shift condition, with ~99% of the DE transcripts annotated in all temperature conditions (Table 2.4.2-1). PCA revealed a strong separation of DE transcripts between the control and T_3 treated *R. catesbeiana* tadpoles in each temperature condition, with a 71 - 72.3% separation on PC1 for all treatment groups (Figure 2.4.2-1). This suggested a reproducible T_3-induced transcriptomic response in each temperature condition.

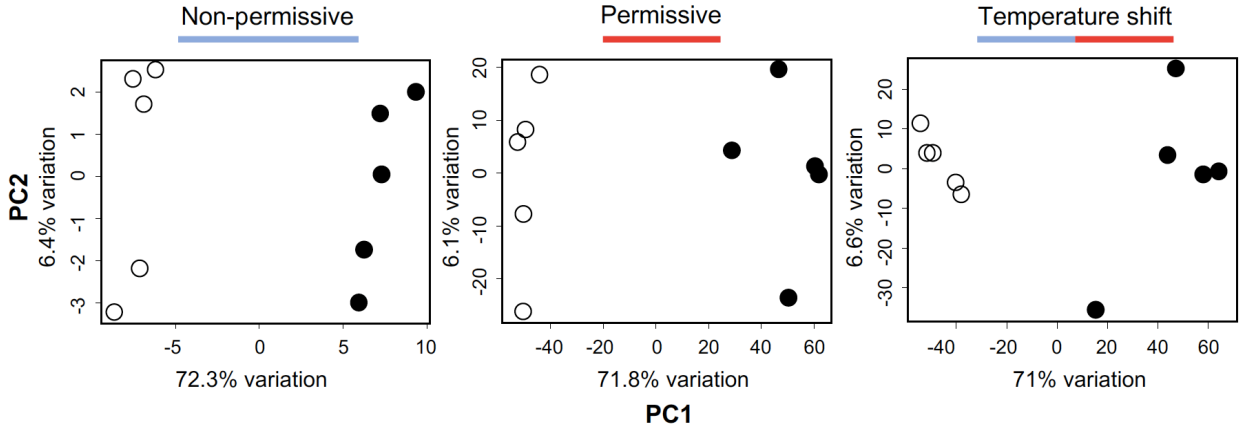

Figure 2.4.2-1 PCA of DE transcripts from the back skin of premetamorphic *R. catesbeiana* tadpoles treated with T_3 at three temperature conditions: non-permissive, permissive, and temperature shift. Control biological replicates (800 nM NaOH) are indicated by the open circles. Biological replicates treated with 10 nM T_3 are indicated by the closed circles.

The back skin tissue showed a markedly higher response to TH treatment in the permissive and shift conditions compared to a significantly smaller number of DE

transcripts observed in the non-permissive condition (Table 2.4.2-1 and Figure 2.4.2-2A). There was very little overlap observed between the non-permissive condition and the permissive and shift conditions. However, the permissive and shift conditions had a comparatively higher amount of overlap consistent with the higher temperature (Figure 2.4.2-2A). In the non-permissive condition, there were approximately three times as many up-regulated DE transcripts (63) as down-regulated transcripts (20) as seen in Figure 2.4.2-2. Similar results have been observed in the tail fin at cold temperatures (Koide et al., 2022). See Supplementary Table 7-3 and Supplementary Table 7-4 for lists of the DE transcripts and genes in the non-permissive condition, respectively.

In the permissive and shift conditions, the number of significantly up- and down-regulated transcripts was more equal with 1,999 and 1,823 transcripts being up-regulated and 1,987 and 1,862 being down-regulated in the permissive and shift conditions respectively (Figure 2.4.2-2). Of the up-regulated transcripts in the non-permissive, permissive, and shift conditions, the percent that were up-regulated over 2-fold were 65.1%, 47.4%, and 35.7% respectively. Of the down-regulated transcripts, 75% in the non-permissive condition, 47.5% in the permissive condition, and 36.5% in the shift condition were down-regulated by 2-fold or more (0.5-fold change). These plots indicate that there was a stronger transcriptomic response to the permissive and shift conditions compared to the non-permissive treatment condition (Figure 2.4.2-2). However, of the transcripts with significant changes in expression, a higher percent of transcripts at the non-permissive temperature had a higher magnitude of fold change compared to the other conditions. This indicates a transcriptomic component in establishing molecular memory at the non-permissive temperature.

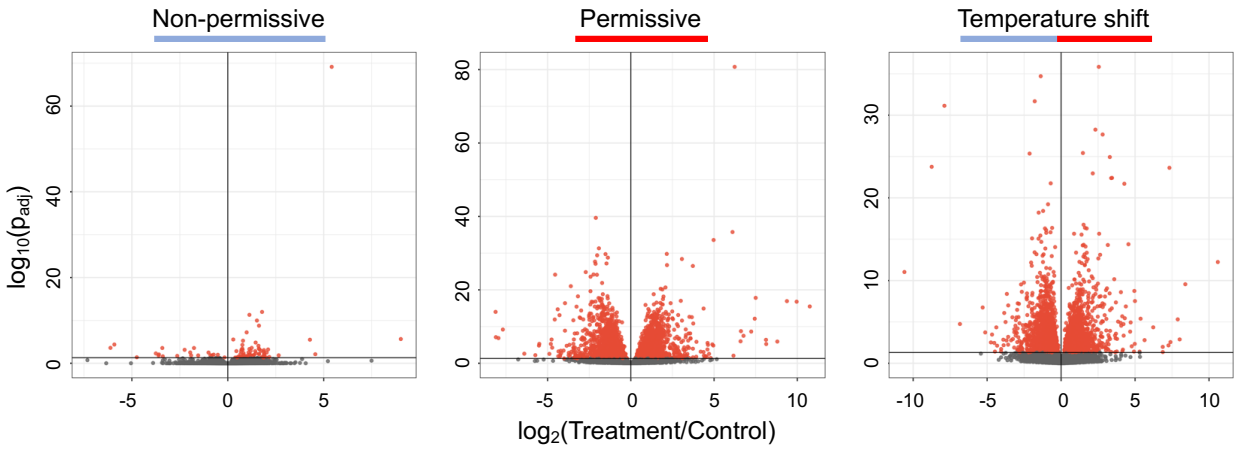

Figure 2.4.2-2 Volcano plots of DE transcripts in the back skin of premetamorphic *R. catesbeiana* tadpoles treated with 10 nM T_3 at three temperature conditions: non-permissive, permissive, and temperature shift. See Figure 2.3.7-2 legend for additional details.

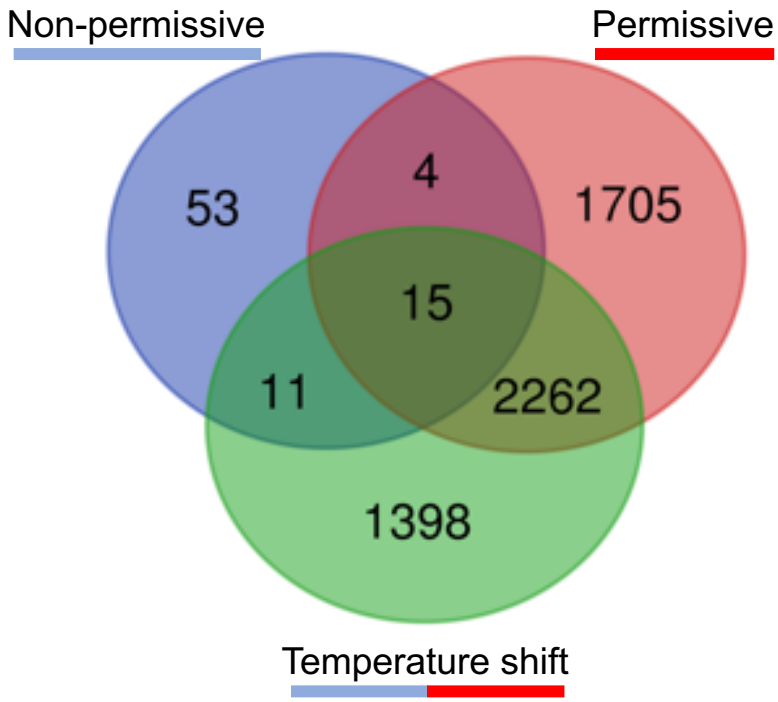

Figure 2.4.2-3 Comparison of the number of DE transcripts in the back skin treated of *R. catesbeiana* tadpoles injected with 10 nM T_3. DE ($p_{adj} \leq 0.05$) in response to non-permissive (blue), permissive (red), or shift (green) conditions were identified by DESeq2. See Supplementary Figure 6-4 for a comparison of the DE genes used in the gene ontology analysis.

2.4.2.1. Classic thyroid hormone indicator transcripts

The expression of TH-responsive transcripts at non-permissive temperatures has been used to study early metamorphic events in a variety of tissues (Hammond et al., 2016; Hammond et al., 2015; Mochizuki et al., 2012; Murata & Yamauchi, 2005). In the present study, we used RNA-seq to further understand transcriptomic changes early in development in the back skin using the classic TH-indicator transcripts *thra, thrb*, and *thibz*. All three transcripts were detected in each temperature condition (Table 2.4.2-2).

A change in expression of *thra* was only observed in the shift condition with a 1.4-fold up-regulation but not in the non-permissive or permissive temperatures. Increased expression of the *thrb* transcripts was observed in both the shift and permissive conditions with respective up-regulation of 2.3- and 2.0-fold changes but not in the non-permissive temperature. No significant changes in abundance of *thra* and *thrb* were observed in the non-permissive temperature where early metamorphic programming was paused; therefore, these transcripts were not part of the molecular memory in the back skin. These trends are consistent with previously reported *thra* and *thrb* literature values in a number of different *R. catesbeiana* tissues after TH exposure (Hammond et al., 2016; Hammond et al., 2015). The change in expression of these TH-responsive transcripts also allowed us to confirm that the tadpoles were responding to the TH injection.

We observed a large up-regulation of *thibz* transcript expression in all temperature conditions with fold changes of 51.9 in the non-permissive condition, 91.9 in the permissive condition, and 215.5 in the shift condition (Table 2.4.2-2). The enhanced induction in the shift condition compared to the permissive condition is consistent with accelerated metamorphosis and has been observed in other tissues (Hammond et al., 2016; Koide et al., 2022). The significant increase in expression of *thibz* in the non-permissive temperature reaffirmed its likely importance as an early initiatior of metamorphic programming in tadpole tissues including the back skin. This signifcant increase in *thibz* abundance has been observed in many *R. catesbeiana* tissues and strongly implicates *thibz* in molecular memory (Hammond et al., 2016;

Hammond et al., 2015; Koide et al., 2022). Futher investigation into the function of *thibz* is warranted.

Other strongly TH-induced transcripts that have not been identified in other tissues were annotated as tuftelin (840.1-fold), semaphorin (18.4-fold), leptin (7.0-fold), and squalene synthase (6.0-fold; Supplementary Table 7-3). Tuftelin is best known for its role in dental enamel mineralization in humans, but it has broad expression with the highest expression in skin (Deutsch et al., 2002; Fagerberg et al., 2014). Its role in mesenchymal stem cell function is more relevant in the context of toothless frogs (Deutsch et al., 2011). Semaphorins are a group of both secreted and membrane proteins expressed in a wide range of tissues with high expression in the skin and that were originally identified for their role in axon growth and guidance (Fagerberg et al., 2014; Gurrapu & Tamagnone, 2016; Koncina et al.). They are also involved in immune regulation, cell adhesion and mobility, angiogenesis, and tumour growth (Chapoval et al., 2022; Gurrapu & Tamagnone, 2016; Lu & Zhu, 2020). These functions may have implications in immune function and cell dynamics at non-permissive temperatures in the skin. Leptin is a protein hormone involved in appetite regulation and energy balance (Pereira et al., 2021). Premetamorphic tadpoles eat continuously to increase body size for metamorphosis (Bender et al., 2018; Crespi & Denver, 2006). Then, during development, leptin expression increases and appetite is supressed. Crespi et al. (2006) found that, in mid-prometamorphic tadpoles and juvenile frogs, leptin exposure inhibited appetite; however, in early prometamorphic tadpoles exogenous leptin exposure induced hindlimb formation and digit differentiation in *X. laevis*. Therefore, leptin may play a role in the initiation of metamorphic programming early on in development, which is consistent with the expression observed in the non-permissive condition of the present study. Squalene synthase is an enzyme in the endoplasmic reticulum that synthesizes squalene and helps protect the cell membrane from lipid peroxidation and oxidative damage. This may also have a protective function in the skin. These transcripts were identifed in the present study as early response transcripts to TH exposure in the back skin and they may be involved in estabilishing a molecular memory in cold temperatures, where the TH signal is initiated but not yet executed.

Table 2.4.2-2 Median fold changes of thyroid hormone-responsive transcripts in T_3 treated *R. catesbeiana* back skin relative to their paired NaOH control across each temperature condition (n = 5 tadpoles/group). All fold changes are statistically significant with a $p_{adj} \leq 0.05$. A "-" indicates no significant change was observed. All transcripts were detected in the RNA-seq data. The thyroid transcripts indicated are *thra (*TH receptor α), *thrb (*TH receptor β), and *thibz* (TH-induced basic region leucine zipper-containing transcription factor).

Transcript	Non-permissive	Permissive	Shift	Accession #
thra	-	-	⇧ 1.4	L06064.1
thrb	-	⇧ 2.0	⇧ 2.3	XM_040353001.1
thibz	⇧ 51.9	⇧ 91.8	⇧ 215.5	MG459289.1

2.4.2.1. GO analysis of temperature modulated induced metamorphosis

There were 22 enriched GO terms in the non-permissive condition after TH exposure. The majority of these were related to an immune response and were classified as biological processes (Figure 2.4.2-4). There were two main clusters observed in the immune GO terms: response to other organisms/viruses and innate immunity. Organisms undergoing metamorphosis are more susceptible to infection than premetamorphic tadpoles and frogs (Humphries et al., 2022; Sauer et al., 2020). Additionally, cold temperatures are known to suppress the amphibian immune response (Robak et al., 2019; Rollins-Smith, 2017; Rollins-Smith et al., 2011). Therefore, the immune system of a tadpole is malleable by both TH and by environmental conditions, both of which may have had an influence the enrichment of immune related GO terms observed in the non-permissive condition of the present study. Similar immune GO enrichment was observed by Koide et al. (2022) at non-permissive temperatures in *R. catesbeiana* tail fin. Given that TH-dependent metamorphosis is perturbed by changes in temperature, the immune response to TH may also be affected by non-permissive temperatures. This may, in turn, affect the immune system of the frog once the metamorphic program is resumed given that environmental conditions during the larval stages and metamorphosis affect the immune system of the adult frog (Krynak et al., 2015).

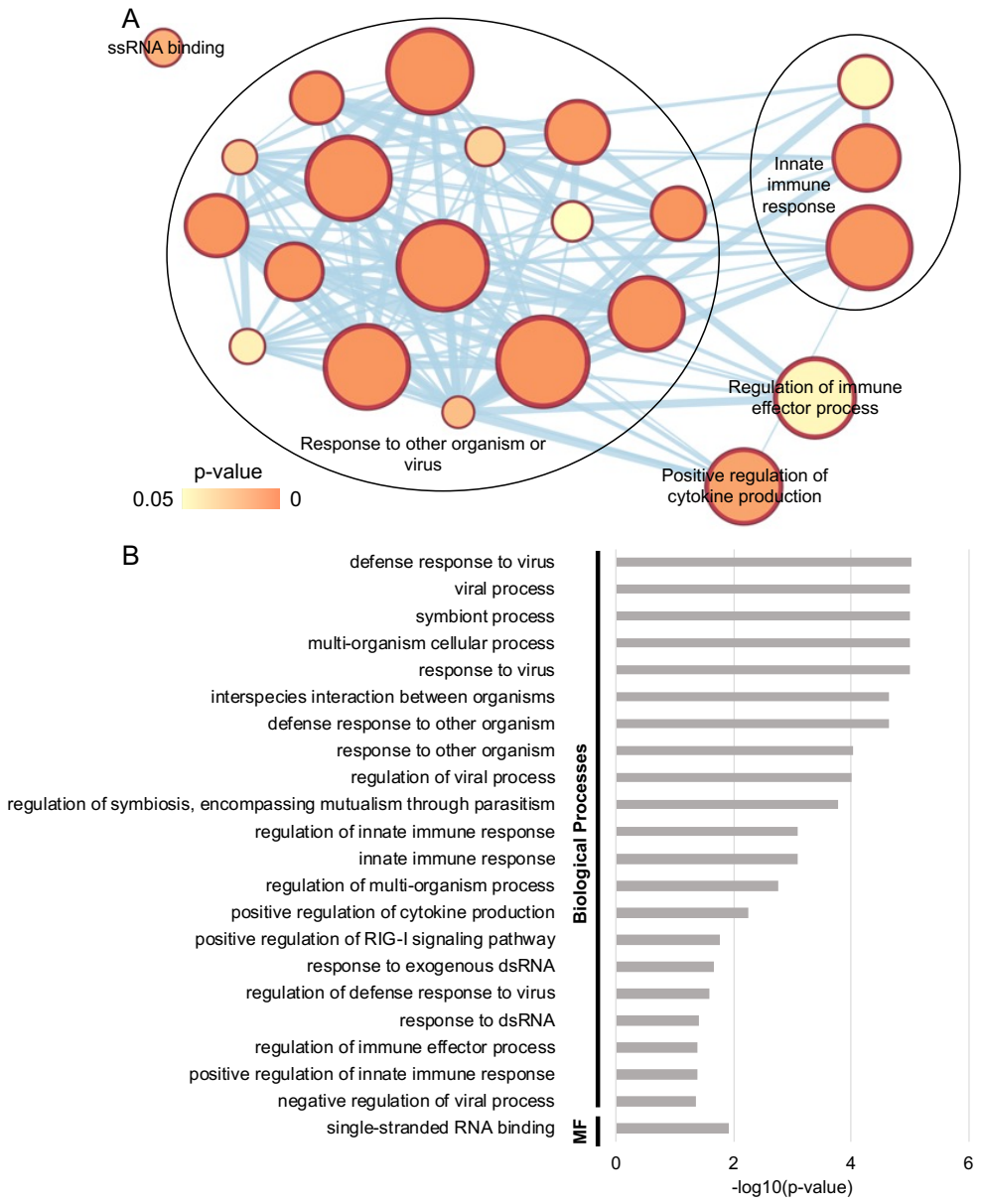

Figure 2.4.2-4 A) GO enrichment analysis of *R. catesbeiana* tadpole back skin in the non-permissive condition after 10 nM T_3 injection. The Cytoscape Enrichment Map plugin was used for visualization. Each GO term is represented by a node, where a darker colour represents a smaller p-value ($p_{adj} \leq 0.05$). Node size is determined by the number of genes associated with that GO term, and the thickness of the connecting lines indicates the relatedness of adjacent nodes. B) The negative $\log_{10}$ of the p-value associated with each GO term grouped by BP or MF designations are on the y-axis. All GO terms are visualized here.

In the permissive temperature condition, there were 83 enriched GO terms, which was the highest of all the temperature conditions. GO terms related to

transcription (3 GO terms), RNA metabolic process (20 GO terms), translation (20 GO terms), and cell division and DNA repair (22 GO terms) were enriched (Figure 2.4.2-5) and were significantly implicated in biological processes, metabolic functions, and cellular component groups. TH and metamorphically permissive temperatures are essential for induction of metamorphosis. TH treatment is known to regulate a wide range of cellular activities including proliferation and apoptosis, which both play a role in the formation of a stratified adult epidermis during metamorphosis (Buchholz, 2015; Shi, 2000; Shi et al., 2012; Skirrow et al., 2008; Suzuki et al., 2009). Hammond et al. (2017) identified nearly 5,000 DE protein encoding genes 48 h after T_3 exposure in *R. catesbeiana* back skin tissue, as well as the enrichment of RNA/DNA processing and cell growth and division GO clusters. These results are consistent with our findings at the permissive temperature. The enrichment of transcription, RNA metabolic process, and translation was like what was observed during the premetamorphosis to prometamorphosis transition during natural metamorphosis in Section 2.4.1.1 as well as what was found Jackman et al. (2022) in the GO enrichment of the olfactory epithelium after TH treatment. Our data showed active TH-induced regulation and expression of both RNA and proteins as well as cell proliferation, as key components of the early metamorphic programming in the back skin. This is consistent with the known activities of TH as a regulator of gene expression and the initiator of metamorphosis (Shi, 2000; Shi et al., 2012).

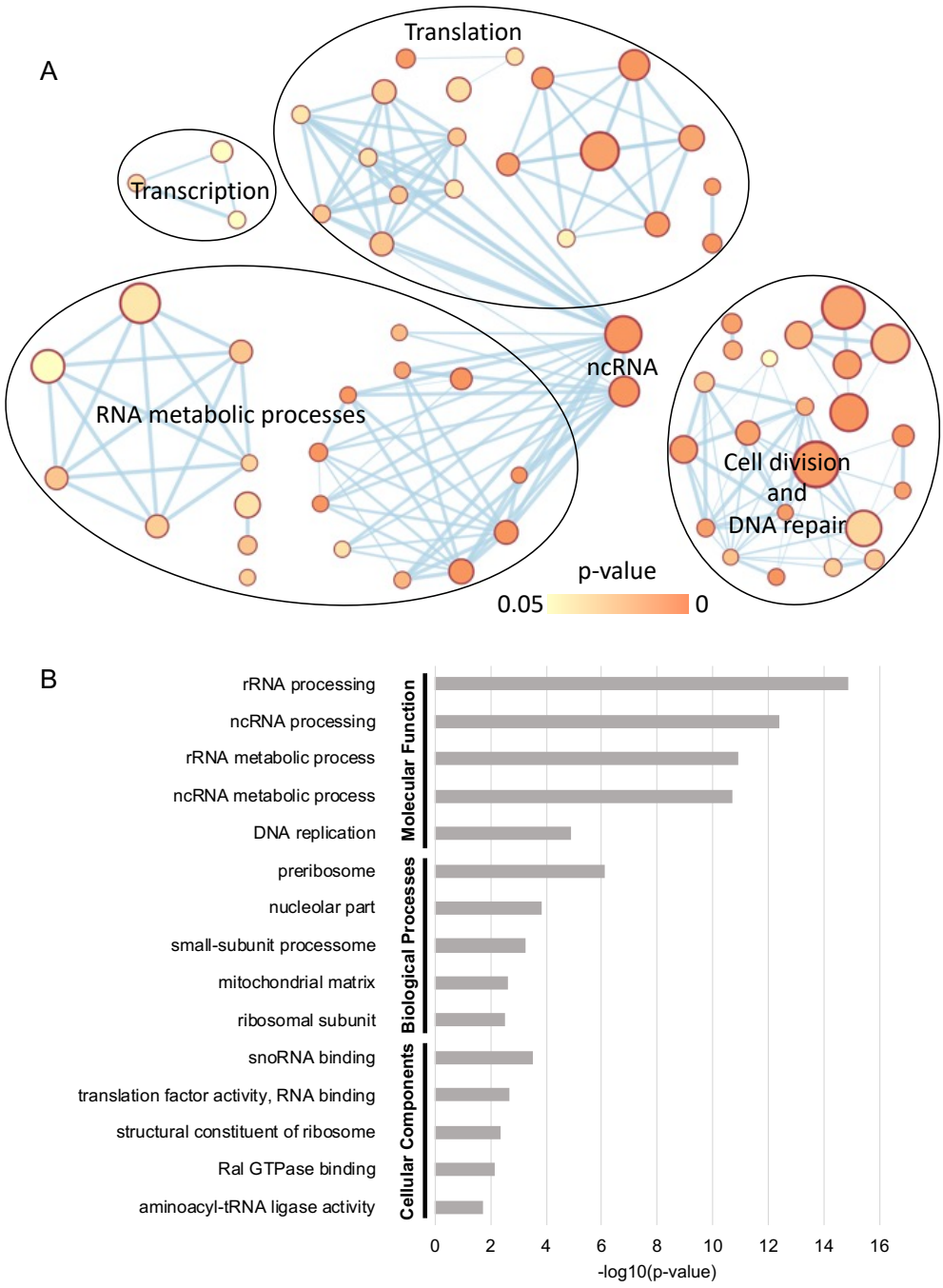

Figure 2.4.2-5 A) GO enrichment analysis of transcription, RNA metabolic process, translation, and cell division and repair in *R. catesbeiana* tadpole back skin in the permissive condition after 10 nM T_3 injection. See Figure 2.4.2-4 legend for more detail. B) The negative $\log_{10}$ of the p-value per GO term grouped by MF, BP, or CC designations are on the y-axis. Only the top 5 GO terms in each category are shown here. Full list of GO terms in Supplementary Figure 6-5.

In the temperature shift condition, 8 GO terms were identified. This was the lowest number of GO terms in any of the temperature conditions. Only GO terms related to biological processes and cellular components were enriched in the shift condition. As seen in Figure 2.4.2-6, there was a small group of rRNA processing GO terms (3 GO terms) with significant enrichment; however, the large clusters of RNA and protein related synthesis observed at the permissive time point were lacking. Suzuki et al. (2009) found that certain GO terms were enriched at different time points. Transcription and proteolysis were enriched one day post TH treatment and cell cycle related GO terms were enriched three days post-treatment. While the expression of TH-responsive transcripts such as *thibz* (a known early response gene) indicated accelerated metamorphosis in the shift condition of the present study, 24 h at a permissive temperature may not have been sufficiently long to allow for the same pattern of GO enrichment observed at the permissive temperature (48 h exposure). A time-course exposure for days following the shift from a non-permissive to a permissive temperature is likely necessary to get a full understanding of GO term enrichment.

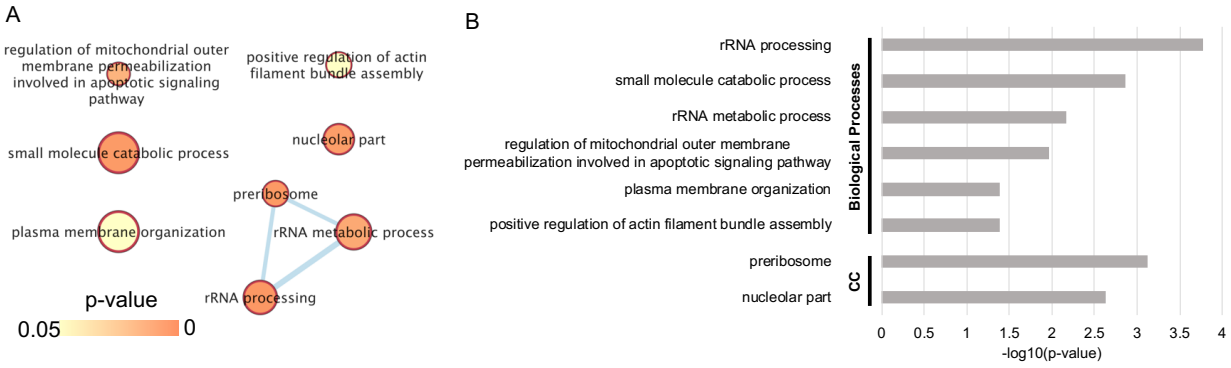

Figure 2.4.2-6 A) GO enrichment analysis of *R. catesbeiana* tadpole back skin in the temperature shift condition after 10 nM T_3 injection. See Figure 2.4.2-4 legend for more detail. B) The negative $\log_{10}$ of the p-value per GO term grouped by BP or CC designations are on the y-axis. All GO terms are visualized here.

2.4.3. Explorative study of stress and innate immune responses in the back skin

2.4.3.1. Differential expression of heat shock proteins during natural and temperature modulated TH-induced metamorphosis

Heat shock proteins are produced by many organisms in response to stress and are primarily regulated at the transcriptional level (Heikkila, 2010). They act as molecular chaperones for protein folding and translocation (Heikkila, 2010). There is a growing body of literature showing that their expression is also linked to development (Heikkila, 2003, 2010; Helbing et al., 1996).

The expression of heat shock protein 30 (*hsp30*) was significantly up-regulated during metamorphosis, with the highest abundance observed in froglets (Table 2.4.3-1). In amphibians, *hsp30* is developmentally regulated in a tissue-dependent manner; however, its expression in the back skin during metamorphosis had yet to be studied (Heikkila, 2003; Helbing et al., 1996; Krone, 2003; Lévesque et al., 2005). We found that *hsp30* was developmentally regulated in the back skin during natural metamorphosis. Therefore, *hsp30* may play a TH-induced role in metamorphosis of the back skin.

Additionally, we examined the expression of other heat shock protein transcripts during metamorphosis. Six other transcripts annotated as heat shock proteins were identified: *hspB* (2 variants), *hsp40* (23 variants), *hsp60* (1 variant), *hsp70* (6 variants), *hsp90* (3 variants), and *hsp110* (1 variant). DE (up or down) was observed in at least some of the variants for all heat shock proteins identified depending on the developmental stage, while the expression of other *hsp* transcripts remained consistent throughout development (see Table 2.4.3-1 for the expression of the *hsp* transcripts with one variant, data for transcripts with multiple variants not shown). Therefore, there appeared to be a degree of developmentally regulated heat shock protein expression depending on the family, variant, and developmental stage.

Table 2.4.3-1 Significant fold change of heat shock proteins 30, 90 and 110 expression in *R. catesbeiana* back skin during prometamorphosis, at metamorphic climax, or as froglets compared to the premetamorphic tadpole. All fold changes are statistically significant with a $p_{adj} \leq 0.05$.

Organism of annotation origin	HSP	Prometamorphosis	Metamorphic climax	Froglet	Developmental trend	Accession #
R. catesbeiana	*hsp30*	⇧ 6.9	⇧ 4.5	⇧ 14.2	⇧	U44894.1
R. temporaria	*hsp60*	-	-	⇩ 1.4	⇩	XM_040357127.1
	hsp110	⇧ 1.6	⇧ 2.1	-	⇧	XM_040340456.1

We analyzed the response of heat shock proteins in the back skin to the temperature and metamorphic stress experienced in our experimental conditions. We found no significant difference in *R. catesbeiana hsp30* expression between the T_3 treated and the temperature matched control in the back skin, which was consistent with the previous literature (Table 2.4.3-2) (Hammond et al., 2016; Hammond et al., 2015). Helbing et al. (1996) noted a tissue specific *hsp30* response to heat shock in other tissues, suggesting that *hsp30* is regulated in a tissue specific manner.

We also expanded our search to analyze the expression of other heat shock proteins in the temperature modulated experiment. Transcripts annotated as *Rana temporia hsp40, hsp60, hsp70,* and *hsp110* were identified in our dataset. Transcript abundance of *hsp60* and *hsp110* increased in the permissive and shift temperatures with a higher fold-change being observed in the permissive condition (Table 2.4.3-2). Five variants of the *hsp40* family (18 distinct variants detected) were significantly up-regulated in both permissive and shift conditions and one variant of the *hsp70* family (6 distinct variants detected) was up-regulated and one was down-regulated in the permissive and shift conditions respectively (data not shown).

No significant *hsp* expression was observed in the non-permissive condition, indicating that heat shock proteins were not early initiators of the metamorphic programming. In both permissive and shift conditions, significant changes in heat shock protein abundance were observed in all identified transcripts except for *hsp30*. Given that TH exposure during development leads to immediate and drastic metamorphic

changes, our results suggested that TH exposure at these temperatures may be considered stressful and lead to the expression of heat shock proteins in response. The expression of *hsp30*, however, appeared to be developmentally regulated on a time scale greater than what was observed in the temperature mediation study.

Table 2.4.3-2 Significant fold changes of heat shock protein transcripts in premetamorphic *R. catesbeiana* tadpole back skin undergoing T_3 induced metamorphosis relative to their NaOH control at the three temperature modulated conditions: non-permissive, permissive, and temperature shift. All fold changes are statistically significant with a $p_{adj} \leq 0.05$. A "-" indicates no significant change was observed.

Organism of annotation origin	HSP	Non-permissive	Permissive	Shift	Accession #
R. catesbeiana	*hsp30*	-	-	-	U44894.1
R. temporaria	*hsp60*	-	⇧ 3.3	⇧ 2	XM_040357127.1
	hsp110	-	⇧ 3.7	⇧ 2.4	XM_040340456.1

2.4.3.1. Differential expression of keratins during natural and temperature modulated TH-induced metamorphosis

During metamorphosis, a tough keratinized outer layer of skin develops that acts as a physical innate immune barrier to protect the frog. Keratins can be DE in different tissue types, epithelial locations, and developmental stages (Ellison et al., 1985; Hammond et al., 2015; Jonas et al., 1985; Miyatani et al., 1986; Watanabe et al., 2001). The developmentally regulated patterns of keratin expression are a useful tool for understanding skin development.

In *R. catesbeiana* skin, two types of *Rana* larval keratin (*rlk* I and *rlk* II*)* genes have been identified that are expressed in the larval but not adult epithelium (Domanski & Helbing, 2007; Suzuki et al., 2001). In the present study, no *rlk* I expression was observed in the back skin during both natural metamorphosis (Table 2.4.3-3) or during TH-induced temperature modulated metamorphosis (Table 2.4.3-4). However, *rlk* I expression was detected in the back skin using qPCR (Hammond et al., 2015). This discrepancy was likely due to the incomplete status of the bullfrog genome assembly.

When examining *rlk* II, we saw the highest level of expression in the premetamorphic stages followed by a 1.9- and 623.9-fold down-regulation of expression during prometamorphosis and at metamorphic climax respectively (Table 2.4.3-3). Finally, in the froglet we saw no expression of the *rlk* II larval specific transcript (Table 2.4.3-3). These results were consistent with previous observations (Suzuki et al., 2001).

In permissive and shift temperature conditions, we saw a significant 16.7-fold and a 9.9-fold down-regulation of *rlk* II expression, respectively (Table 2.4.3-4), consistent with metamorphic induction. The decrease in expression of *rlk II* associated with the permissive and shift conditions and lack of significant change in the non-permissive condition in the present study was consistent with trends observed in *rlk I* (the other larval keratin) expression in both the back skin and tail fin epithelial tissues (Hammond et al., 2015). Overall, *rlk* II expression in the back skin responded to the induced metamorphosis in temperature modulated conditions in a TH-dependent manner.

Table 2.4.3-3 Significant fold changes of keratin transcripts in *R. catesbeiana* back skin during prometamorphosis, at metamorphic climax, or as froglets compared to the premetamorphic tadpole. The expression of *Rana* larval keratin I and II (*rlk* I and *rlk I*), *Rana* adult keratin (*rak*), and *Rana* keratin 8 (*rk8*) transcripts are examined. All fold changes are statistically significant with a $p_{adj} \leq 0.05$. A "-" indicates no significant change was observed, "ND" indicates that the transcript was not detected in the dataset, and "⇩" indicates a significant decrease to zero (no transcripts being expressed) at the froglet developmental stage. In the development trends column, a "⇩", "⇧", or "=" indicates a trend of down-, up-, or steady regulation as metamorphosis progresses respectively.

Keratin	Prometamorphosis	Metamorphic climax	Froglet	Developmental trend	Accession #
rlk I	ND	ND	ND	ND	EF156435.1
rlk II	⇩ 1.9	⇩ 623.9	⇩	⇩	AB050956.1
rak	⇧ 7.3	-	-	⇧	AB050955.1
rk8	⇧ 3.6	⇧ 4.8	⇧ 3.3	=	AB056480.1

In the present study, we observed a significant 7.3-fold up-regulation of *Rana* adult keratin (*rak*) during prometamorphosis; however, no significant change in expression was observed at metamorphic climax or in froglets (Table 2.4.3-3). In previous work, the adult *rak* keratin transcript was expressed in both tadpole and frog skin but was significantly up-regulated as TH-modulated metamorphosis occurred

(Suzuki et al., 2001). While we observed an initial increase in expression during prometamorphosis that was consistent with that found in the literature (Suzuki et al., 2001), the expected continual increase of *rak* expression during development was not observed. At the biological replicate level for the organisms at metamorphic climax and as froglets, the expression of *rak* was either much higher than the median premetamorphic expression levels or was very low (see Supplementary Table 7-5 for raw counts). The high variation accounted for the lack of significance seen later in development. The cause of the different levels of *rak* expression is unknown.

At permissive and shift temperatures, we observed no change in expression of *rak* (Table 2.4.3-4) suggesting that induction of this keratin was not directly dependent upon TH. This is consistent with the observation that *rak* up-regulation has been predominately observed once metamorphic climax had begun (Suzuki et al., 2001).

Not all keratins are developmentally regulated. In the present study we saw a significant 3.6-fold up-regulation of *Rana* keratin 8 (*rk8*) from premetamorphosis to prometamorphosis and then that increased expression stayed approximately consistent with a slight increase of 4.8- and a 3.3-fold up-regulation at metamorphic climax and in froglets respectively (Table 2.4.3-3). Additionally, we saw no significant changes in expression in response to the TH injections in any of the temperature conditions tested (Table 2.4.3-4). This was consistent with the Suzuki et al. (2001) results where *rk*8 expression was not developmentally regulated. Additionally, our results suggest that it does not appear to be temperature sensitive at the temperatures tested.

Finally, none of the keratin transcripts were DE at non-permissive temperatures, indicating that they are not early TH-responsive genes (Table 2.4.3-4).

Table 2.4.3-4 Significant fold changes of keratin transcripts in premetamorphic *R. catesbeiana* tadpole back skin undergoing T_3 induced metamorphosis relative to their NaOH control at the three temperature modulated conditions: non-permissive, permissive, and temperature shift. The expression of *Rana* larval keratin I and II (*rlk* I and *rlk I*), *Rana* adult keratin (*rak*), and *Rana* keratin 8 (RK8) transcripts are examined. All fold changes are statistically significant with a $p_{adj} \leq 0.05$. A "-" indicates no significant change was observed and "ND" indicates that the transcript was not detected in the dataset.

Keratin	Non-permissive	Permissive	Shift	Accession #
rlk I	ND	ND	ND	EF156435.1
rlk II	-	⇩ 16.7	⇩ 9.9	AB050956.1
rak	-	-	-	AB050955.1
rk8	-	-	-	AB056480.1

2.4.3.1. Differential expression of mucins during natural and temperature modulated TH-induced metamorphosis

Mucus, which acts as a physical and chemical component of the innate immune system, is composed of a wide variety of proteins with the O-linked glycoprotein mucins being a major structural component (Dubaissi et al., 2018; Varga et al., 2019). Not much is known about how mucin composition altered during metamorphosis, although there is evidence of mucus cell contents changing during metamorphosis to help adapt to new environments in some species (Landeira-Dabarca et al., 2021; Shih & Vanable, 1975).

The regulation of expression (up, down, and constitutive) of mucin-like transcripts in response to the TH-modulated metamorphic programming appeared to vary at an individual mucin level or, in the case of mucin-like 5AC, at the variant level (Table 2.4.3-5). TH exposure can influence the number and distribution of mucus expressing cells as well as mucin type (Alves et al., 2018; Ottesen & Olafsen, 1997). As the aquatic tadpole becomes a terrestrial juvenile frog, the skin must adapt to a change in pathogens, predators, and environmental circumstance so the variation in mucin expression may be implicated in the immune protection needed for a terrestrial life. Mucin 19-like for example, which was not expressed in the premetamorphic tadpoles in either experiment (Table 2.4.3-5 and Table 2.4.3-6), showed a drastic increase in abundance during development. These findings suggest that mucin 19-like was developmentally regulated, which may have corresponded with the development of

cutaneous mucus glands during TH-regulated metamorphosis and with the needs associated with a new environmental niche (Dubaissi & Papalopulu, 2011; Thornton et al., 2008). Similarly, the mucins whose expression was down-regulated during metamorphosis may have been more suited to aquatic environments and were therefore preferentially expressed during larval stages. The expression of *mucXS*, which was identified in *X. tropicalis* tadpole skin (Dubaissi et al., 2018; Dubaissi et al., 2014), fit that pattern during *R. catesbeiana* development (Table 2.4.3-5).

Table 2.4.3-5 Significant fold changes of predicted mucin transcripts in *R. catesbeiana* back skin during prometamorphosis, at metamorphic climax, or as froglets compared to the premetamorphic tadpole. All fold changes are statistically significant with a $p_{adj} \leq 0.05$. A "-" indicates no significant change was observed, a "⇩" indicates a significant decrease to zero (no transcripts being expressed), and "⇧" indicates a significant increase from zero expression during premetamorphosis. In the development trends column, a "⇩", "⇧", or "=" indicates a trend of down-, up-, or steady regulation as metamorphosis progresses respectively and an "NS" is not significant. The numbers in the brackets indicate the median expression of that transcript as premetamorphic tadpoles did not express the indicated transcript and fold change calculations were not possible.

Organism of annotation origin	Predicted mucin	Prometamorphosis	Metamorphic climax	Froglet	Developmental trend	Accession #
Rana temporaria	mucin 2-like	-	-	-	NS	XM_40355343.1
	mucin 4-like	⇩ 79.9	⇩	⇩	⇩	XM_40349650.1
	mucin 5AC-like	-	⇩ 11.2	⇩ 45	⇩	XM_40323445.1
		⇧ 2.5	⇧ 2.1	⇧ 1.8	=	XR_5749590.1
		-	⇧ 148.1	⇧ 10744	⇧	XM_40327702.1
	mucin 15	-	⇧ 3.7	⇧ 6.6	⇧	XM_40328357.1
	mucin 16-like	-	-	⇩ 21.6	⇩	XM_40344215.1
	mucin 17-like	⇧ 1.5	⇧ 2.3	⇧ 2.0	=	XM_40329875.1
	mucin 19-like	⇧ (434)	⇧ (14995)	⇧ (96818)	⇧	XM_40343594.1
	otogelin-like (mucXS)	-	-	⇧ 5.1	⇧	XM_040344209.1
		-	⇩ 18.5	⇩	⇩	XM_040326638.1

In the temperature mediation dataset, we identified seven predicted mucin-like types that correspond to expressed *R. catesbeiana* transcripts (Table 2.4.3-6). At non-permissive temperatures, TH injection influenced the expression of one mucin transcript compared to the permissive and shift conditions, which had a greater impact on transcript abundance. Both up- and down- regulation of expression were observed depending on the mucin, which suggested independent TH regulation in the different temperature conditions.

The present study showed that mucin expression was responsive to TH in a transcript dependent manner during metamorphosis and that distinct mucins were abundant at different developmental stages. It is likely that mucus composition depends on the needs of the organism. This responsiveness to TH was also observed in the temperature mediation experiment, where some of the predicted mucins appeared to be TH-regulated depending on the environmental temperature. This could have implications on the amphibian immune response as climate change shifts temperatures world-wide. Mucins play an important role in the structure of mucus, which is a critical physical and chemical barrier of the amphibian innate immune system that protects the organism again pathogen challenge, environmental conditions, pollutants, and predators. If temperatures influence TH-mediated expression of mucins, then the tadpole may be especially vulnerable during metamorphic transformation.

Table 2.4.3-6 Significant fold changes of predicted mucin transcripts in *R. catesbeiana* back skin undergoing T_3 induced metamorphosis relative to their NaOH control at the three temperature modulated conditions: non-permissive, permissive, and temperature shift. All fold changes are statistically significant with a $p_{adj} \leq 0.05$. A "-" indicates no significant change was observed, "ND" indicated that the transcript was not detected, and "⇧" indicates a significant increase from zero expression in the NaOH control. The numbers in the brackets indicate the median expression of that transcript in the TH-treated tadpoles since the control tadpoles did not express the indicated transcript and fold change calculations were not possible.

Organism of annotation origin	Predicted mucin	Non-permissive	Permissive	Shift	Accession #
Rana temporaria	mucin 2-like	-	-	-	XM_40327735.1
		-	-	⇩ 1.2	XM_40355343.1
		⇩ 5.4	-	-	XM_040339420.1
	mucin 4-like	-	-	-	XM_40349650.1
	mucin 5AC-like	-	⇩ 2.1	-	XM_40327722.1
		-	-	-	XM_40323445.1
		-	-	⇧ 1.3	XM_40355347.1
		-	⇧ (74)	⇧ (84)	XM_040323436.1
	mucin 5B-like	ND	-	ND	XM_040328507.1
	mucin 15	-	-	-	XM_40328357.1
	mucin 16-like	-	⇩ 11.2	⇩ 68	XM_40344215.1
	mucin 17-like	-	-	-	XM_040329910.1
		-	-	⇧ 1.4	XM_40329875.1
	mucin 19-like	-	-	ND	XM_040327723.1
	otogelin-like (mucXS)	-	-	⇧ 7.9	XM_040344209.1
		-	-	-	XM_040326638.1

2.4.3.1. Differential expression of antimicrobial peptides during natural and temperature modulated TH-induced metamorphosis

AMPs are chemical components of the innate immune system that are produced either constitutively or when stimulated by stress, injury, or pathogen or predator challenge (Akat Çömden et al., 2023; Bahar & Ren, 2013; Varga et al., 2019). AMPs have a broad spectrum of antimicrobial activity including directly killing microbes, modulating the host immune system, and promoting wound healing (Brogden et al., 2016; Seyfi et al., 2020). Adult frogs are the best-known source of AMPs to date;

however, there is limited information on how AMP profiles change during amphibian development or in challenging environmental conditions (Helbing et al., 2019; Wang et al., 2015; Woodhams et al., 2016). In the present study, we used RNA-seq analysis to increase our understanding of the expression of known AMPs during postembryonic development. Given that the tadpole AMP profile is largely unknown (Lin et al., 2022), we also apply rAMPage, a novel bioinformatic AMP identification pipeline, to extract novel putative AMP sequences from the transcriptomic dataset.

Of the known AMPs examined in the current study, only cathelicidin was expressed in our transcriptomic data. A significant down-regulation of cathelicidin expression at both metamorphic climax (⇩ 1.49) and froglets (⇩ 3.85) was observed. Stress influences cathelicidin production so the decrease in AMP abundance during development could have been due to stress induced by the metamorphic process (Aberg et al., 2007; Chambers et al., 2011; Helbing et al., 1996; Lai & Gallo, 2009; Rollins-Smith, 2017). Additionally, the immune system is repressed during metamorphosis, which could account for the down-regulation of cathelicidin observed in the present study (Grogan et al., 2018; Robert & Ohta, 2009). Ranatuerin (1, 5, 7, and 8), ranalexin, and ranacyclin (Ca, Cb, and Cc) were not detected in our transcriptomic dataset. This could be due to a lack of stimulus, or these AMPs not being expressed at these developmental stages. In Helbing et al. (2019), ranacyclin-Ca and ranatuerin-1 expression were not observed in any premetamorphic tissues including the back skin, which is consistent with our findings. However, constitutive expression of ranatuerins (7 and 8) and ranalexin have been shown in the tadpole in other work (Woodhams et al., 2016). This discrepancy could be caused by several factors including differing husbandry practices, pathogen loads, or microbiomes.

Using the rAMPage pipeline, we identified 281 novel putative AMPs in the natural metamorphosis RNA-seq data. Of these AMP candidates, 70 were found in premetamorphic tadpoles, 109 in prometamorphic tadpoles, 85 at metamorphic climax, and 125 in froglets. Twenty-four of these were expressed consistently throughout postembryonic development (Figure 2.4.3-1). However, unique AMP candidate profiles were observed at each developmental stage, with the highest number of AMP

candidates identified in froglets (Figure 2.4.3-1). This supports the hypothesis that the AMP profile changes during metamorphosis from the tadpole to the frog.

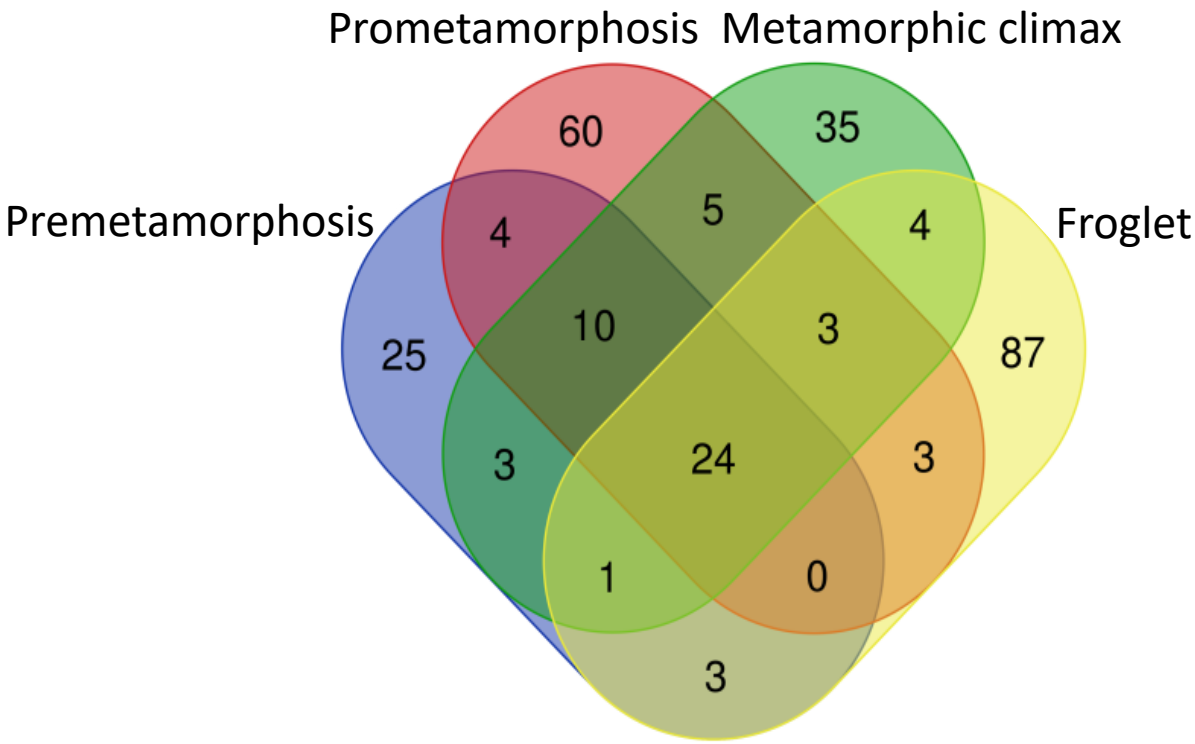

Figure 2.4.3-1 Distribution and overlap of the expression of the bioinformatically identified novel AMP candidates during four stages of natural metamorphosis: premetamorphosis, prometamorphosis, metamorphic climax, and froglet.

During prometamorphosis, DE of the novel putative AMPs was significantly higher (33.1%; 93/281) than during premetamorphosis (Table 2.4.3-7). The percent of DE novel putative AMPs decreased to only 6.8% (19/281) at metamorphic climax and then increased again in froglets to 34.2% (96/281). The percent of significantly up-regulated novel AMP candidates followed the same pattern with the percent of up-regulated novel AMP candidates being high during prometamorphosis (31.7%; 89/281), dipping at metamorphic climax (4.3%; 12/281), and then increasing again in froglets (31.7%; 89/281) (Table 2.4.3-7).

These results are consistent with the secretion levels observed during *R. catesbeiana* development after norepinephrine exposure and with the knowledge that

the amphibian immune system is repressed at metamorphic climax (Woodhams et al., 2016). Additionally, the observed increase in novel putative AMP expression compared to premetamorphic tadpoles may have been due to the development of granular glands. While cutaneous glandular glands have been observed as early as TK7, their development is not complete until the end of metamorphosis (Robinson & Heintzelman, 1987). As the gland density during development increases, it follows that AMP expression would also increase. Finally, terrestrial frogs encounter different pathogens than the aquatic tadpole, requiring a different AMP profile that may be up-regulated during metamorphosis (Helbing et al., 2019). Therefore, developmental stage appeared to influence the expression of a subset of the novel putative AMPs identified.

The number of down-regulated novel putative AMPs remained low and consistent at each stage accounting for 1.4% (4/281) to 2.1% (6/281) of the novel putative AMPs (Table 2.4.3-7). As with cathelicidins, it is possible that these transcripts were stress responsive and were therefore downregulated during metamorphosis.

Table 2.4.3-7 The percent of total, up- and down-regulated significantly DE novel putative AMPs (n = 281) during three stages of natural metamorphosis (prometamorphosis, metamorphic climax, and froglets) compared to premetamorphic tadpoles. A total of 281 novel putative AMPs were bioinformatically identified. The transcript with the highest abundance per novel putative AMP was used to calculate the number of DE novel putative AMPs per stage ($p_{adj} \leq 0.05$). The values in brackets indicate the number of AMPs.

	% significantly DE novel putative AMPs		
Stage comparison	**Total**	**Up-regulated**	**Down-regulated**
Prometamorphosis	33.1% (93)	31.7% (89)	1.4% (4)
Metamorphic climax	6.8% (19)	4.3% (12)	2.1% (6)
Froglet	34.2% (96)	31.7% (89)	2.1% (6)

The temperature shift experiment was performed on premetamorphic tadpoles with immature immune systems as they began to undergo induced metamorphosis in conjunction with a temperature modulated environment. AMP expression and secretion has been shown in the back skin of *R. catesbeiana* tadpoles during premetamorphosis, although at a lower rate than that of an adult frog (Woodhams et al., 2016). However, no

studies have looked at the influence of temperature mediation and TH induction on AMP production in larval *R. catesbeiana*.

Consistent with the natural metamorphosis data, ranatuerin, ranalexin, and ranacyclin were not expressed at measurable levels in any of the temperature conditions in the premetamorphic tadpole experiment. Cathelicidin was expressed in all temperature conditions; however, no DE was observed. Therefore, cathelicidin expression was not affected by temperature at this developmental stage.

In the temperature modulation TH-induction experiment, we identified 151 novel putative AMPs using the rAMPage pipeline. No significant DE was observed in the non-permissive condition in response to TH treatment (Table 2.4.3-8). This suggested that a cold temperature does not influence AMP expression early in the metamorphic programming. Similar results have been observed in the ventral skin of *R. sylvatica*, where brevinine-1SY transcript abundance was not affected after 24 h of freezing compared to the control (Katzenback et al., 2014).

All the significantly DE transcripts in both the permissive and shift conditions were down-regulated in response to TH treatment (Table 2.4.3-8). As previously mentioned, stress response can negatively impact AMP production (Aberg et al., 2007; Lai & Gallo, 2009), and we demonstrated that there was a significant up-regulation in HSPs at both the permissive and shift temperatures (Table 2.4.3-2). It is possible that a subset of the novel putative AMP's expression was down-regulated in response to the heat shock condition. Notably, the temperature shift condition had approximately twice the number of DE contigs than the permissive condition. However, since the permissive condition is not a heat shock condition, the data suggest that TH can influence AMP expression. The current mechanism is not understood.

Table 2.4.3-8 The percent of total, up- and down-regulated significantly DE novel putative AMPs (n = 151) from TH or control injected premetamorphic tadpoles in three temperature conditions: non-permissive, permissive, and temperature shift. A total of 151 novel putative AMPs were bioinformatically identified. The transcript with the highest abundance per novel putative AMP was used to calculate the number of DE novel putative AMPs per stage ($p_{adj} \leq 0.05$). The "-" indicated that no significant DE was observed in that condition. The values in brackets indicate the number of AMPs.

	% significantly DE novel putative AMPs		
Condition	**Total**	**Up-regulated**	**Down-regulated**
Non-permissive	-	-	-
Permissive	23.2% (35)	-	23.2% (35)
Shift	45.7% (69)	-	45.7% (69)

2.5. Conclusion

Amphibians are crucial indicator species that are undergoing mass global decline, predominately due to climate change, pollution, and spreading pathogenic infections. Amphibian skin is in constant in contact with shifting environmental conditions and, as such, it acts as the first line of defense in the innate immune system. The back skin is drastically remodeled during metamorphosis and much remains unknown about the TH-mediated mechanisms of action during that process. In the present study, we investigated transcriptomic changes in the back skin during natural metamorphosis and TH-induced metamorphosis in temperature modulated conditions.

Herein, we show that the back skin is a TH-responsive tissue with a complex and highly inducible transcriptomic profile during natural and temperature modulated TH-induced metamorphosis. We identified *thibz* as an early response gene in metamorphic programming. This result has been repeatedly observed in many *R. catesbeiana* tissues and highlights the importance of this transcript to molecular memory. We also identified four molecular memory candidates (tuftelin, semaphorin, leptin, and squalene synthase) that were significantly up-regulared in the skin at non-perimissive temperatures that have not been identified in other tissues.

The expression of physical and chemical components of the innate immune system in the skin was highly responsive to TH. Although transcripts were individually regulated, many transcripts responsible for critical immune functions were found to be regulated at some level by TH. As the back skin undergoes metamorphosis it is completely remodeled, and this was reflected in the TH-mediated abundance of heat shock proteins, keratins, mucins, and AMPs. Temperature was also found to influence the response to TH exposure of many of the immune transcripts. As environmental temperatures continue to change, this could have implications for the regulation of key innate immune transcripts in amphibian back skin.

Finally, we also identified hundreds of novel putative AMP transcripts. This showed that broadening the scope of experimental conditions used in AMP discovery may help identify more AMPs that may only be expressed in certain conditions. This could have important implications in AMP discovery for both animal and human health.

Our results indicated that the skin response to TH is complex and varied. Many of the components of the innate immune system were TH and temperature sensitive, which has implications on amphibian survival as anthropogenic and natural challenges continue to grow. Further characterization of physical and chemical innate immune response of *R. catesbeiana* is necessary.

3. Characterization and validation of novel antimicrobial peptides against pathogens important in the poultry industry: avian pathogenic *E. coli* (APEC) and *Salmonella enterica* serovar Enteritidis (SE)

3.1. Abstract

Antibiotics are commonly used in the agricultural industry to increase food production and to fight and prevent infections in livestock. With both antibiotic use and antibiotic resistance on the rise worldwide, these practices threaten our food systems and both animal and human health. In response to this rapidly emerging global health threat, there is a need to discover alternatives to antibiotics. The present work aims to characterize and validate 111 novel antimicrobial peptide (AMP) candidates previously discovered from amphibian RNA-sequencing datasets using the rAMPage pipeline and evaluate them for their efficacy against two pathogens important in the poultry industry, avian pathogenic *Escherichia coli* (APEC) and *Salmonella enterica* serovar Enteritidis (SE). AMPs are produced as a part of the innate immune system by all organisms and are small, typically positively charged, and amphipathic peptides with direct acting and immune stimulatory antimicrobial abilities. Un-amidated and amidated C-terminal versions of 111 novel AMP candidates underwent antimicrobial susceptibility and cell toxicity testing. We found that 28 of the AMPs identified were moderately or highly active (Minimum inhibitory concentration (MIC) $\leq$ 32 μg/mL) against APEC and six against SE, most of which displayed low cell toxicity against red blood and HEK293 cells. Additionally, the influence of amidation, charge, secondary structure, and length were also investigated. C-terminal amidation significantly increased AMP activity in 61% of the AMPs against APEC and in 37% of the AMPs against SE. Alpha-helical secondary structure, a positive charge range of +1 to +5, and hydrophobic characteristics were all associated with increased antimicrobial activity. While these AMPs are candidates for further testing as therapeutics to prevent or treat disease in poultry, the present work also provides useful physicochemical information for

incorporation into AMP discovery pipelines to augment the identification of AMPs as an antibiotic alternative from any genomic resource.

3.2. Introduction

Antibiotics have been commonly used in agricultural sectors to increase food production and to fight and prevent infections in livestock (Barlam & Gupta, 2015; Mathew et al., 2007). These practices exert a selective pressure towards bacteria with antibiotic resistance, with serious implications for animal and human health (Chantziaras et al., 2014; Finley et al., 2013; McCubbin et al., 2021). As awareness of antibiotic resistance grows, steps towards antibiotic-stewardship have been taken; however, a lack of reporting, difficulties in antibiotic regulation, increased global food demands, and lack of antibiotic alternatives are all roadblocks to decreasing antibiotic use in agricultural settings globally (Van Boeckel et al., 2015). Despite the World Health Organization's warning that antibiotic resistance is "one of the biggest threats to global health, food security, and development today", global antibiotic use is expected to increase by 8% by 2030 (Mulchandani et al., 2023).

Poultry is one of the most commonly consumed animal products worldwide, with flocks often raised in close quarters and given antibiotics to control disease and improve growth (Nhung et al., 2017). Two of the leading causes of disease in the global poultry industry are colibacillosis and salmonellosis, whose causative agents are avian pathogenic *Escherichia coli* (APEC) and *Salmonella enterica* serovar *Enteriditis* (SE) respectively (Kabir, 2010; Nhung et al., 2017). These pathogens have economic and zoonotic importance as they can decimate flocks and contaminate animal products, contributing to foodborne illness and the spread of antibiotic resistance genes (Nhung et al., 2017). While good husbandry practices are key in limiting disease, the development of new antimicrobials that prevent or treat disease while mitigating the development of resistance is an important step in securing the future of food production in the poultry industry.

Antimicrobial peptides (AMPs) are promising antibiotic alternatives. This diverse group of peptides is an important component of the innate immune system of all organisms. AMPs are typically positively charged, range from 5 to 100 amino acids

long, and are often amphipathic (Hancock & Sahl, 2006; Seyfi et al., 2020). They can be classified structurally as alpha-helices, beta-sheets, extended, loop, or as a mix of these (Bahar & Ren, 2013; Seyfi et al., 2020). AMP characteristics and secondary structure are directly related to their activity.

AMPs are the first line of defense in the innate immune system (Bahar & Ren, 2013; Shai, 2002). These immune peptides can directly attack invading pathogens including bacteria, fungi, viruses, and protozoa, or can modulate the host immune response (Brogden et al., 2016; Cruz et al., 2014; Hancock & Sahl, 2006; Seyfi et al., 2020; Zasloff, 2002). AMPs employ several mechanisms to directly affect invading pathogens. Membrane perforation by AMPs occurs when a positively charged AMP is attracted to the negatively charged bacterial membranes where its amphipathic nature leads to membrane perforation (Bahar & Ren, 2013; Hancock & Sahl, 2006; Shai, 2002). AMPs can also inhibit critical cellular functions with or without disrupting membrane activity. These include disrupting cell membrane protein function (signaling, transport, etc.), DNA, RNA, protein synthesis and expression, and cell wall integrity, and enzymatic activity (Bahar & Ren, 2013; Benincasa et al., 2017; Jenssen et al., 2006). AMPs can have immune system modulatory abilities, often at concentrations orders of magnitude lower than their minimum inhibitory concentrations (Lai & Gallo, 2009). They can stimulate chemotaxis, modulate inflammation, neutralize pathogenic toxins, promote wound healing, and have anti-cancer properties (Lai & Gallo, 2009; Mahlapuu et al., 2016). Thus, AMPs are powerful immune regulators that can signal, rally, and regulate the innate and adaptive immune response in addition to their direct antimicrobial effects.

AMPs often do not incur resistance to the same extent as conventional antibiotics. AMPs can act rapidly and employ multi-hit mechanisms to target pathogens. This means the pathogen has a shorter window in which to develop resistance mechanisms against multiple targets (unlike conventional antibiotics that only have one target) making the development of resistance more difficult (Bahar & Ren, 2013; Hancock & Sahl, 2006; Spohn et al., 2019). This, along with the preferential membrane targeting mechanism for bacterial membranes over eukaryotic cells due to differences in

membrane composition (Hancock & Sahl, 2006; Mahlapuu et al., 2016; Shai, 2002) makes AMPs promising antimicrobial therapeutic candidates.

AMPs have long been acknowledged as potential therapeutics; however, there are several hurdles that hamper the AMP discovery to therapeutic pipeline. Initial discovery of AMPs has traditionally been slow and labour intensive. This is being overcome with the emergence of new methods such as bioinformatic AMP identification (Bahar & Ren, 2013; Helbing et al., 2019). The physical characteristics of AMPs can also be a barrier to their use as therapeutics. AMPs are expensive to synthesize, prone to proteolytic cleavage and degradation in biological systems, and could be toxic for host cells (Bahar & Ren, 2013). Many of these issues can be addressed through AMP modifications. Truncating AMPs is one method to decrease synthesis costs. Modifications like unnatural amino acids confer higher stability against proteases and altering the amino acid composition can impact cytotoxicity. By understanding and altering these physicochemical properties, AMP design and activity can be improved.

C-terminal amidation is a post-translational modification of AMPs that can occur naturally (Wang, 2020). Amidation of AMPs can significantly enhance AMP activity and increase their efficacy as antimicrobial agents (Dennison et al., 2015; Huan et al., 2020; Strandberg et al., 2007). When a peptide is amidated, its carboxyl group at the C-terminus is converted into an amide group which removes the negative charge on the carboxyl group and increases the overall peptide charge by +1 (Mura et al., 2016). Charge is essential for AMP membrane permeability; the increase in charge facilitates improved electrostatic interactions with negatively charged features on the bacterial surface. Amidated AMPs can possess improved membrane-penetrating abilities. Molecular dynamics simulations have also suggested the presence of the NH_2 group at the C-terminus improves the penetration of the peptide into membranes compared to their carboxylated counterparts (Kim et al., 2011; Mura et al., 2016; Sforça et al., 2004). The presence of the amidated C-terminus facilitates stronger interactions with the lipid bilayer (Mura et al., 2016). As a result, the peptide can more easily disrupt and permeabilize the microbial cell membranes. Amidation enhances the stability of AMPs, making them more resistant to degradation by exopeptidases and increases serum stability. This increased stability allows the AMPs to remain active for a longer duration,

thereby extending their antimicrobial effects and improving their overall efficacy. Despite all these advantages, extensive comparisons between the un-amidated and amidated forms of AMPs is lacking in the literature.

In the present study, we examine 111 bioinformatically identified novel AMP candidates from amphibian RNA-seq datasets (Corrie et al., Chapter 2). Un-amidated and amidated versions of the novel putative candidates underwent antimicrobial susceptibility and cell toxicity testing with a focus on agriculturally relevant poultry pathogens (APEC and a clinical avian SE isolate), as well as their respective more susceptible strains *E. coli* ATCC 25922, and *Salmonella enterica* serovar Enteritidis ATCC 4931. The physicochemical properties of the novel putative AMP dataset were also examined and linked to activity to provide a more comprehensive understanding of their structure-function relationships than available to date.

3.3. Materials and methods

3.3.1. Novel AMP identification and selection

The Rapid Antimicrobial Peptide Annotation and Gene Estimation (rAMPage) pipeline (Lin et al., 2022; Richter et al., 2022), a homology based pipeline that uses RNA-seq data to identify putative AMPs for downstream testing, was applied to four amphibian RNA-seq datasets as input (Corrie et al., Chapter 2; Li et al., 2022). From the putative AMPs identified using rAMPage, 111 were selected for *in vitro* validation of activity. These peptides were selected based on an AMPlify score ≥10, length ≤ 30 AA, and charge ≥ 1. The un-amidated peptides are denoted as CCH-# and the amidated forms as CCH-#a (where # = 1 – 111). See Supplementary Table 7-6 for individual novel putative AMP properties. The amidated C-terminus versions of the peptides were synthesized by GenScript (Piscataway, NJ, USA). One putative AMP, CCH-54 was not easily synthesized, eliminating it as a potential therapeutic and was not moved forwards in the experimentation. CCH-54a was successfully synthesized however and was included in analysis.

3.3.2. Bacterial isolates

A panel of Gram-negative bacteria with a focus on pathogens that are critical to the poultry industry were selected to perform antimicrobial susceptibility testing. These include *Escherichia coli* ATCC 25922, and *Salmonella enterica* serovar Enteritidis ATCC 4931 from the American Type Culture Collection (ATCC; Manassas, VA, USA), as well as avian pathogenic *E. coli* 317 (Vaccine and Infectious Disease Organization (VIDO)) and avian *Salmonella enterica* serovar Enteritidis (LS101; VIDO). *Escherichia coli* ATCC 25922 (*E. coli* ATCC) is a non-pathogen strain commonly used for antimicrobial susceptibility testing, while avian pathogenic *E. coli* 317 (APEC) is pathogenic with virulence and resistance genes. *Salmonella enterica* serovar Enteritidis ATCC 4931 (SE ATCC) contains three known antimicrobial resistance genes and is commonly associated with contaminated food or water. *Salmonella enterica* serovar Enteritidis LS101 (SE avian) was isolated by VIDO from their flocks. Bacterial isolates were grown and stored as per Richter et al. (2022).

3.3.3. Antimicrobial susceptibility and cell toxicity testing

The antimicrobial activity of all the novel putative AMPs was measured by broth microdilution assays as per Richter et al. (2022) to determine the minimum inhibitory and bactericidal concentration (MIC and MBC, respectively), as outlined by the Clinical and Laboratory Standards Institute (2015), with some adaptations for testing cationic AMPs as described previously (Hancock & Sahl, 2006). Putative AMPs were considered active if the inhibited growth of any of the bacteria tested was ≤ 128 μg/mL (i.e., MIC ≤ 128 μg/mL). Cell toxicity testing (hemolysis assay and alamarBlue cell viability assay) of the novel putative AMPs proceeded as per protocols laid out in prior publications (Li et al., 2022; Richter et al., 2022). To study the ability of the putative AMPs to rupture eukaryotic membranes, the hemolysis assay on porcine red blood cells (PRBCs; Lampire Biological Laboratories, Pipersville, PA, USA) was performed on all un-amidated and amidated peptides. PRBC were chosen for this assay due to the consistent availability of high-quality cells, which was not the case for chicken RBCs. Hemolytic activity was assessed by determining the AMP concentration needed to lyse 50% of the RBCs (HC50). The alamarBlue cell viability assay to measure cytotoxicity on

the human embryonic kidney cell line HEK293 (ATCC) was performed only on putative AMPs with high antimicrobial activity and/or hemolytic activity plus the un-amidated or amidated counterpart in the PRBCs. This was measured as the concentration of AMP needed to reduce cell viability by 50% (CC50). The antimicrobial activity of the novel putative AMPs was classified using median MIC scores of “No activity” (MIC > 128 μg/mL), “low” (128 μg/mL ≥ MIC >32 μg/mL), “moderate” (32 μg/mL ≥ MIC > 4 μg/mL), or “high” (MIC ≤ 4μg/mL). Any peptide with low, moderate, or high activity (MIC of ≤ 128 μg/mL) against any of the pathogens is denoted as a verified AMP. Hemolytic or cytotoxic activity was classified as follows: no hemolytic or cytotoxic activity (HC50/CC50 = 256 μg/mL; no activity measured in the assay), low (HC50/CC50 ≥ 128 μg/mL), moderate (128 μg/mL > HC50/CC50 ≥ 64 μg/mL), or high (HC50/CC50 < 64 μg/mL).

3.3.4. Physicochemical property analysis

The 3D structures of the putative AMPs were predicted with ColabFold (Mirdita et al., 2022). The ColabFold server generated five structures for each peptide with sub-models of AlphaFold (Jumper et al., 2021). The five estimated structures were relaxed using the Amber force field, to limit stereochemical violations in the predictions. The five structures for each sequence were ranked by the per-residue estimate of AlphaFold’s confidence in its prediction (pLDDT score). The resulting PDB file of the Amber relaxed rank 1 model for each peptide was passed through STRIDE to categorize peptides based on their secondary structure (Frishman & Argos, 1995). The peptides were classified as either: helical (>80% of the residues were assigned as participating in an α-, pi- or 310-helical structure), mainly helical (between 50–80% of the residues were helical), mainly extended (<50% of the residues were helical), extended peptides (only possessing turn secondary structure and/or coils, no helical or beta-strand containing residues), mixed (possessing both helical and beta strand motifs) or β-strand containing (only possessing beta-strand residues and no helical residues present).

To determine the hydrophobicity of the peptides, the Grand Average of Hydropathy (GRAVY) score was calculated using the sum of the hydropathy values for all amino acids (AA) (considering the hydrophilic and hydrophobic properties of the AA

side chains) in the peptide divided by the total number of AAs (Kyte & Doolittle, 1982; Stothard, 2000).

3.3.5. Statistical analyses

All plots except for the Supplementary Figure 6-6 to Supplementary Figure 6-8 boxplots were created in R version 4.3.1 using ggplot2 (version 3.4.2) (Wickham, 2016). The nonparametric Mann-Whitney U (aka Mann-Whitney Wilcoxon) test was used to perform pairwise comparisons of the MIC and cell toxicity technical replicates for each AMP treatment using R version 3.6.3 (R Core Team 2021). A $p_{adj} \leq 0.05$ was deemed to be significant.

3.4. Results and discussion

3.4.1. Antimicrobial activity against APEC and SE avian

A set of 111 novel putative AMPs from amphibia with a length limitation of 30 AA was chosen to undergo *in vitro* antimicrobial susceptibility and cell toxicity testing in both their natural un-amidated and C-terminal amidated forms and with a focus on the agriculturally relevant pathogens APEC and SE avian, as well as their ATCC counterparts. We also performed an in-depth characterization of the novel putative AMP physicochemical properties and how those relate to activity and toxicity. The cost of AMP synthesis is one of the limiting factors of AMP use as therapeutics. By using length as the selection criteria, we aimed to mitigate synthesis costs by identifying short active AMPs with therapeutic potential. Prior studies have focused on the effect of amidation on individual or a low number of peptides (Dennison et al., 2015; Mura et al., 2016), or on AMP database studies (Pirtskhalava et al., 2021; Wang, 2020). To our knowledge, the present study is the first to examine the influence of amidation on a large group of bioinformatically identified novel putative AMPs and to observe the activity of those AMPs against the critical poultry related pathogens APEC and SE.

In the present study, we examined the antimicrobial activity of our novel putative AMPs against the agriculturally relevant gram-negative pathogens APEC and SE avian, as well as their respective ATCC counterparts. APEC and SE avian are both economically important poultry pathogens that pose public health risks. Multiple drug

resistance has been characterized in both pathogens. In poultry litter from controlled feeding trials and commercial farms, 69 *E. coli* were isolated and all isolates from commercial farms were resistant to at least seven antibiotics (Furtula et al., 2010). In 193 *Salmonella* isolates from broiler chicken production facilities in British Columbia, Canada, over 43% were resistance to five antibiotics (Diarra et al., 2014). Additionally, 65% of the SE isolates were found to carry both the invasion gene (*inva*) and the *Salmonella* plasmid virulence gene (*spvC*). Hence, the discovery of antibiotic alternatives for these agriculturally relevant pathogens is critical. A study by Nguyen et al. (2021) using avian derived AMPs showed that AMPs could possess antimicrobial activity against poultry related pathogens including APEC and SE avian, as well as have immunomodulatory effects on the immune system, and offer protection from a yolk sac APEC exposure after *in ovo* injection. In the present study, we aimed to identify novel AMPs from anurans that could be utilized in the poultry industry.

Of the 221 novel putative un-amidated and amidated AMPs tested in the present study, 92 showed some activity (MIC $\leq$ 128 µg/mL) against at least one of the pathogens tested (Table 3.4.1-1). Nine AMPs were classified as highly active, and 43 AMPs were classified as moderately active against at least one pathogen. We successfully identified novel AMPs that were highly active against *E. coli* ATCC (9), APEC (4), and SE ATCC (3) as seen in Table 3.4.1-1. No AMPs were highly active against SE avian, although six AMPs were moderately active against this pathogen.

When comparing the avian pathogens to their respective ATCC strains, we noted that the ATCC strains were more susceptible than their avian pathogen counterparts to AMP treatment. We are in the process of sequencing the APEC and SE avian to determine which antimicrobial resistance genes they may carry. Given that *E. coli* ATCC is a non-pathogenic strain, while APEC is highly pathogenic and often associated with virulence and resistance genes (Furtula et al., 2010), it is understandable that *E. coli* ATCC was more susceptible to AMP treatment. What is noteworthy however, is that four and 24 AMPs were highly or moderately active against the resistant APEC strain (Table 3.4.1-1). A similar pattern was observed in the SE strains with SE ATCC, which contains three known antimicrobial resistance genes. SE ATCC was more susceptible

to AMP treatment than SE avian, which was isolated from broiler flocks at VIDO. While we did not identify any highly active novel AMPs against SE avian, we found six moderately active novel AMPs (Table 3.4.1-1). The AMPs that were active against these critical poultry pathogens are potential targets to undergo further modifications to improve activity and undergo testing as potential agricultural therapeutics. One such modification, C-terminal amidation, was performed in the present study. More active AMPs were found in the amidated group than the un-amidated group for all pathogens. This is discussed further in Section 3.4.1. There was overlap between the AMPs' activity against different pathogens where all the moderate activity AMPs in SE avian were also moderately or highly active against APEC. This indicated that we had identified broad spectrum AMPs in our dataset that may be effective against both critical poultry pathogens. We also identified AMPs that are uniquely active against APEC if a more targeted approach is desired.

Table 3.4.1-1 Antimicrobial activity of the novel AMPs per pathogen. The total (un-amidated + amidated), un-amidated, and amidated numbers of peptides in each activity category per pathogen. AMP activity was determined using median MIC values scored as "No activity" (MIC > 128 µg/mL), "low" (128 µg/mL ≥ MIC >32 µg/mL), "moderate" (32 µg/mL ≥ MIC > 4 µg/mL), or "high" (MIC ≤ 4 µg/mL).

	Activity	*E. coli* ATCC	APEC	SE ATCC	SE avian
Un-amidated	High	1	0	1	0
	Moderate	14	8	2	1
	Low	16	16	10	7
	Total active	31	24	13	8
	No activity	79	86	97	102
Amidated	High	8	4	2	0
	Moderate	20	16	7	5
	Low	27	31	29	21
	Total active	55	51	38	26
	No activity	56	60	73	85
Total	High	9	4	3	0
	Moderate	34	24	9	6
	Low	43	47	39	28
	Total active	86	75	51	34
	No activity	135	146	170	187

3.4.1. AMP characterization

The AMP mode of action is dependent on structural and physicochemical properties (Torres et al., 2019). As we continue to refine high throughput *in silico* AMP discovery methods (e.g., rAMPage), understanding how these properties relate to AMP function and activity can inform the decision-making process regarding which AMPs to test during *in vitro* validation. This relationship also has implications in novel AMP design and AMP modification to improve function.

AMPs can be classified by their secondary structure as alpha-helices, beta-sheets, extended, loop, or mixed (Bahar & Ren, 2013; Seyfi et al., 2020). Most AMPs identified to date do not have an experimentally validated secondary structure, which can be a costly, time consuming, and low throughput process (Chen et al., 2022). In the present study, we performed 3D structure prediction and peptide categorization using ColabFold (Mirdita et al., 2022), and STRIDE (Frishman & Argos, 1995). This allowed us to predict secondary structure in a high throughput manner and make associations with AMP activity.

The predicted 3D structure classification of the 111 un-amidated novel putative AMPs synthesized for *in vitro* validation can be found in Figure 3.4.1-1. This peptide set favoured alpha-helical secondary structure which accounted for 78% of the 111 novel putative AMPs (Figure 3.4.1-1). Interestingly, in a bioinformatic analysis of 1000 amphibian AMPs, they found a linear correlation between peptide length and average leucine content. There was a higher average percent leucine content, an AA implicated in alpha-helical formation, in shorter peptides and, as the peptide length increased, the proportion of the peptide that was composed of leucine decreased (Wang, 2020). The positively charged, often amphipathic alpha-helix is a common amphibian AMP motif associated with membrane disruption (Haney et al., 2009; Islam et al., 2023). This appears to be consistent with the distribution of the novel putative AMPs in our dataset.

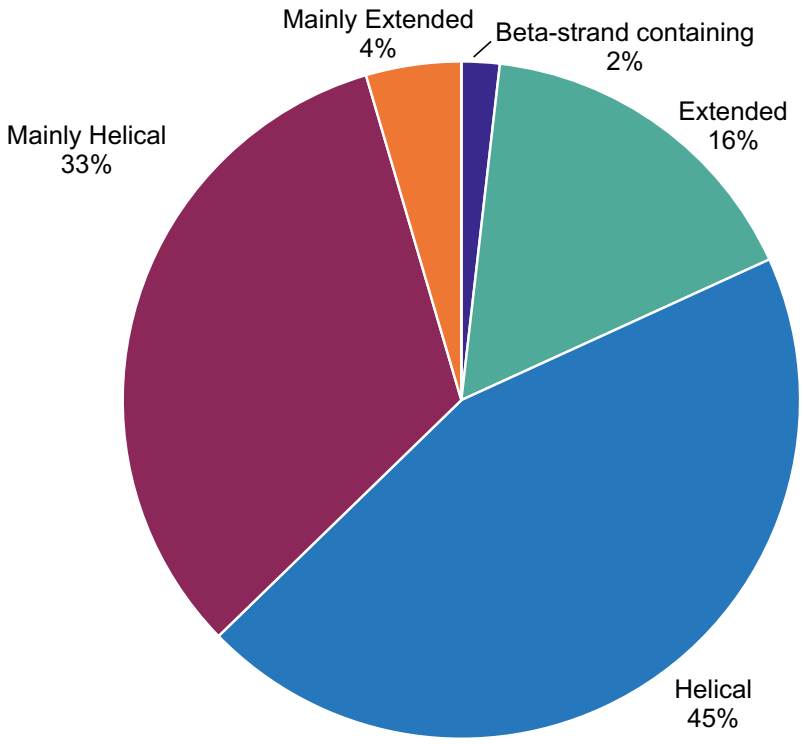

Figure 3.4.1-1 The predicted secondary structure classifications of the 111 novel putative AMPs chosen for antimicrobial susceptibility and toxicity testing. The peptides were classified as: helical (>80% of the residues assigned as participating in a helical structure), mainly helical (50–80% of the residues are helical), mainly extended (<50% of the residues are helical), extended peptides (turn secondary structure and/or coils only, no helical or β-strand containing residues), mixed (both helical and β-strand motifs), or β-strand containing (only beta-strand residues). 3D structure prediction was performed using ColabFold (Mirdita et al., 2022) and STRIDE (Frishman & Argos, 1995).

We explored the relationship between predicted secondary structure and activity by plotting the antimicrobial activity of all the un-amidated AMPs in relation to their percent helical and extended content (Figure 3.4.1-2). The size of the circle correlates to AMP activity and the colour represents the predicted Colabfold secondary structure of the sequences. High helical content was associated with AMP activity in all strains tested; however, this was most important for activity against SE ATCC. *E. coli* ATCC had the most variety in active peptides with one mainly helical peptide having moderate activity. While all highly active AMPs were helical, it is important to note that not all helical peptides were active. Mainly extended or extended peptides in this dataset were either low activity or inactive against the strains tested. Similar results were observed in

Richter et al. (2022), where most validated AMPs from insect and amphibian datasets were predicted to be alpha-helical in nature.

There are limitations to using predicted secondary structure classifications. The majority of known AMPs with determined structures are alpha-helical (Giangaspero et al., 2001). Given that these known AMPs were used to train the machine learning pipeline used in the present study, this could have resulted in a bias towards the identification of such AMPs from our datasets. Additionally, this software cannot account for post-translational modifications including C-terminal amidation. This limited our ability to characterize a portion of our highly active AMPs.

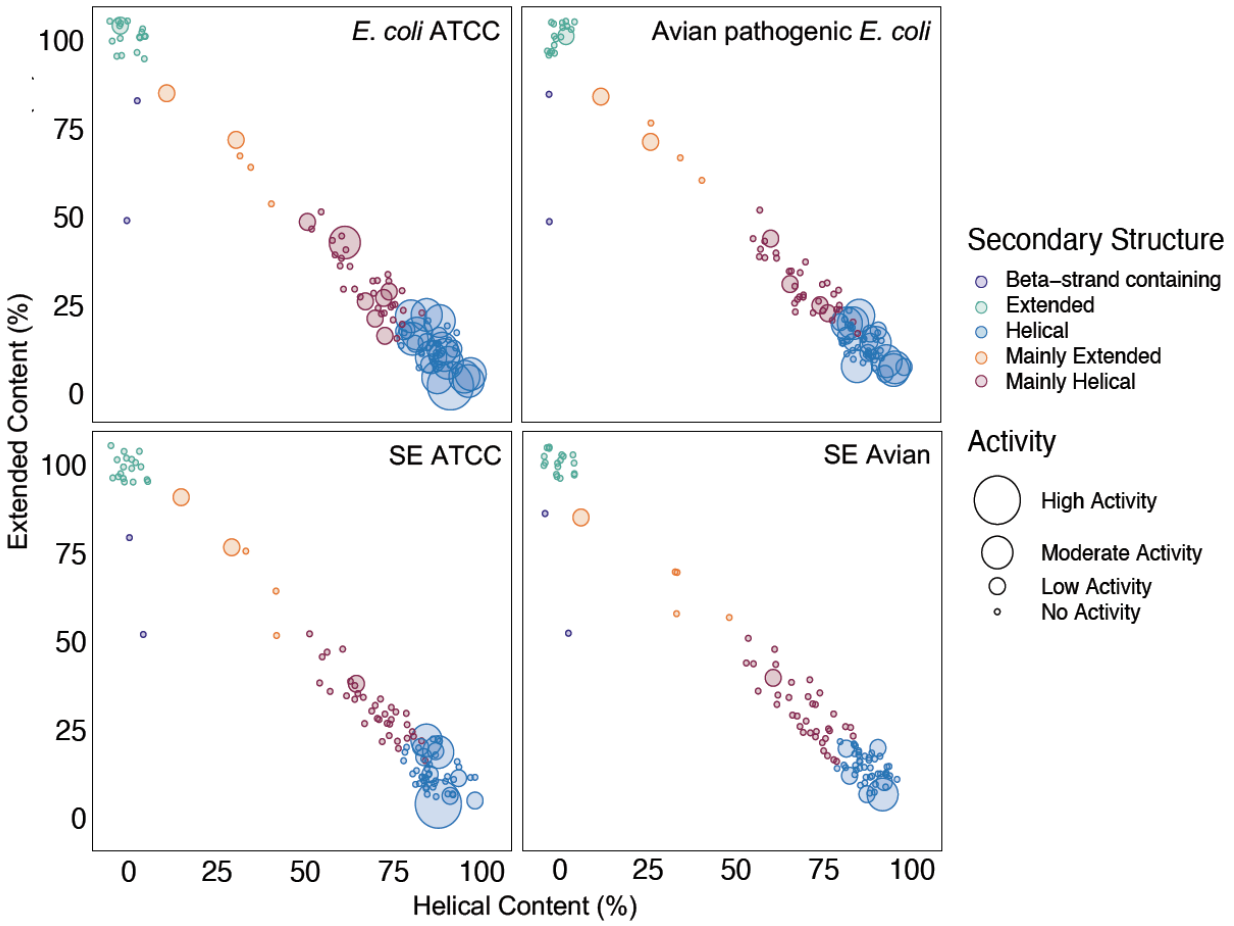

Figure 3.4.1-2 Predicted secondary structure and antimicrobial activity of the un-amidated novel AMPs against *E. coli* ATCC, APEC, SE ATCC, and SE avian. Predicted secondary structure content is indicated by the percentage of residues assigned to participate in the helical (x-axis) vs extended (y-axis) regions. The colour indicates the predicted secondary structure classification of the novel putative AMP and the size of the circles indicates the antimicrobial activity. The distribution of the circles is slightly jittered to improve visualization.

3.4.2. Hydrophobicity, charge, and length distribution

Initial cell membrane interaction is required for membrane-active AMPs as well as for AMPs with intracellular targets. Membrane-active AMPs are often amphipathic in nature with a positive charge allowing for electrostatic interaction with the negatively charged microbial membrane and the hydrophobic part of the AMP contributing to membrane insertion (Bahar & Ren, 2013). Therefore, the hydrophobic and cationic properties of the peptides strongly contribute to these interactions and the activity of the

AMP. The association between hydrophobicity (Figure 3.4.2-1), charge (Figure 3.4.2-2), and length (Figure 3.4.2-3) of the putative AMPs and their MICs have been investigated to determine their respective effects on antimicrobial activity and cell toxicity.

To elucidate the relationship between hydrophobicity of our un-amidated AMPs and their antimicrobial activity, the Grand Average of Hydropathy (GRAVY) score was calculated (Stothard, 2000). This score provided a hydropathy index for the peptide by dividing the summation of the AA hydropathy values by the peptide sequence length (Kyte & Doolittle, 1982). Hydrophilic peptides have a negative GRAVY score, and hydrophobic peptides have a positive GRAVY score. All AMPs with moderate to high antimicrobial activity had positive GRAVY scores between zero and two in all pathogens ($\log_2 MIC \leq 5$; Figure 3.4.2-1). Hydrophobicity influences membrane permeability and cell targeting (Kustanovich et al., 2002; Zelezetsky et al., 2005). Possessing hydrophobic characteristics appears to be linked with activity against the target pathogens in the present study. As previously mentioned, hydrophobicity is commonly found in AMPs, especially those with membrane perforating positively charged, alpha-helical characteristics. Indeed, increasing hydrophobicity of AMPs has been found to increase their lytic activity (Lee et al., 2006).

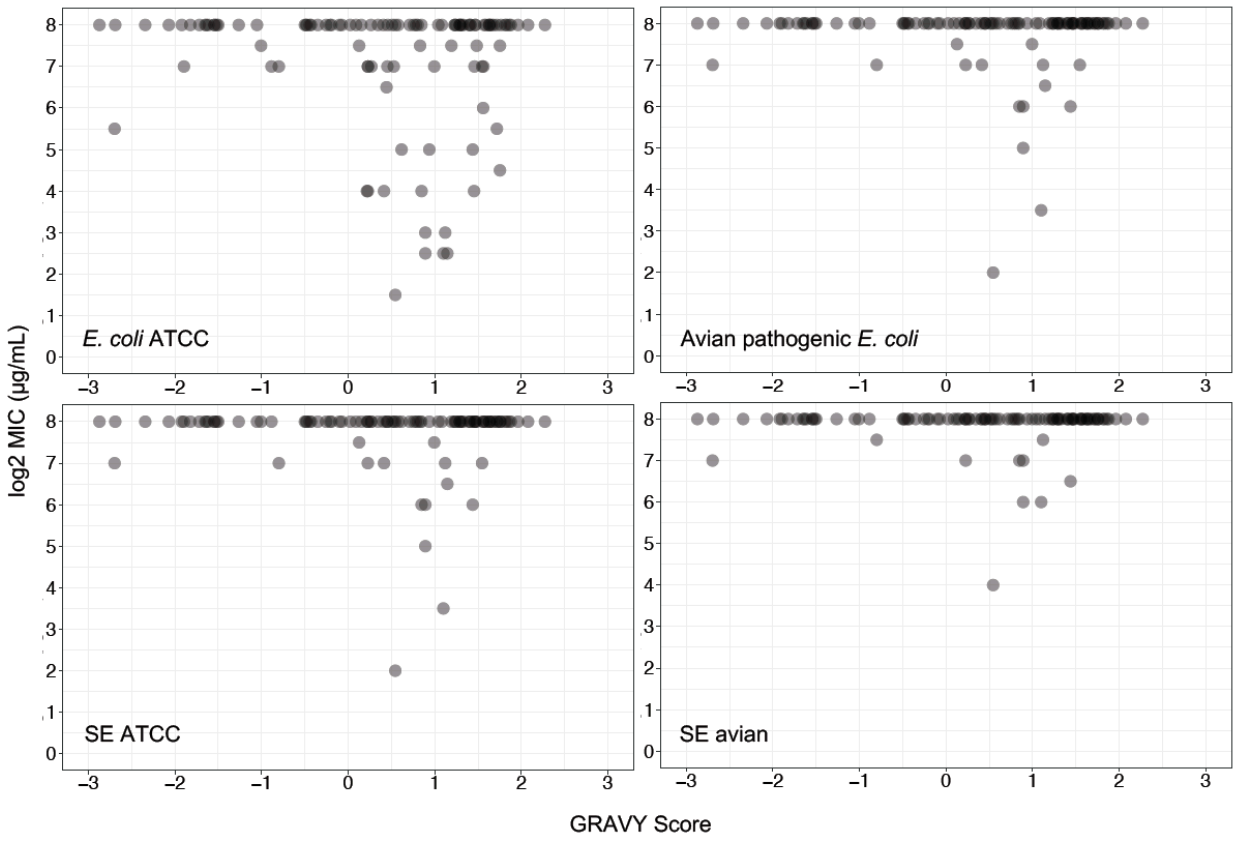

Figure 3.4.2-1 Hydrophobicity of the un-amidated peptides vs growth inhibition for *E. coli* ATCC, APEC, SE ATCC, and SE avian. The Grand Average of Hydropathy (GRAVY) score was calculated for each un-amidated peptide. The GRAVY score vs $\log_2$(median MIC) for each individual peptide is denoted by a semi-transparent point on the x-y figure for each pathogen. The darker the area, the more novel putative AMPs fall at that position. The classifications for activity converted to $\log_2$MIC are "No activity" (MIC > 7), "low" ($7 \geq$ MIC > 5), "moderate" ($5 \geq$ MIC > 2), or "high" (MIC $\leq$ 2).

Increased positive charge is typically linked with greater membrane association due to the electrostatic interactions between the positively charged AMPs and the negatively charged bacterial membrane (Zasloff, 2002). In the present study, we selected for positively charged novel putative AMPs. Charges for the *in vitro* tested novel putative AMPs ranged from +1 to +14 for the natural peptides and +2 to +15 for the amidated peptides due to the +1 charge conferred by amidation (Figure 3.4.2-2). High ($\log_2$MIC $\leq$ 2) and moderate ($5 \geq \log_2$MIC > 2) antimicrobial activity was observed in +1 to +4 charge range for the un-amidated putative AMPs and from +2 to +5 in the amidated AMPs (Figure 3.4.2-2). In the higher charge range (> +5), amidation appeared to increase the number of low activity AMPs observed compared to the small number of

low activity un-amidated AMPs in that range. However, no high to moderate activity was seen in peptides with a charge greater than +5. Overall, moderate to high activity was only observed in the +1 to +5 charge range for these AMPs while no moderate to high activity was associated with the higher charge range (> +5) (Figure 3.4.2-2).

Cell toxicity against PRBC is shown at the bottom of Figure 3.4.2-2. Some low cell toxicity ($8 > \log_2 HC50 \geq 7$) was observed in the PRBCs in the un-amidated peptides at charges of +2 or +4 only. Low ($8 > \log_2 HC50 \geq 7$) to moderate ($7 > \log_2 HC50 \geq 6$) cell toxicity for the amidated peptides was observed between a charge range of +2 to +5. No increase of toxicity was observed in the AMPs with a higher charge (> +5) due to amidation.

In general, low positive charges (+1 to +5) tended to be associated with greater antimicrobial as well as hemolytic activity. Higher positive charges (> +5) had no/low antimicrobial and no hemolytic activity; however, amidation increased activity but not cell toxicity at higher charge ranges (Figure 3.4.2-2). Chung et al. (2020) reported that approximately 50% of naturally occurring AMPs have a charge of +2 to +4 and the Antimicrobial Peptide Database's the average net charge is 3.47 (out of 3705 peptides) (Wang et al., 2015). Therefore, the most active AMPs identified in the present study were consistent with literature values.

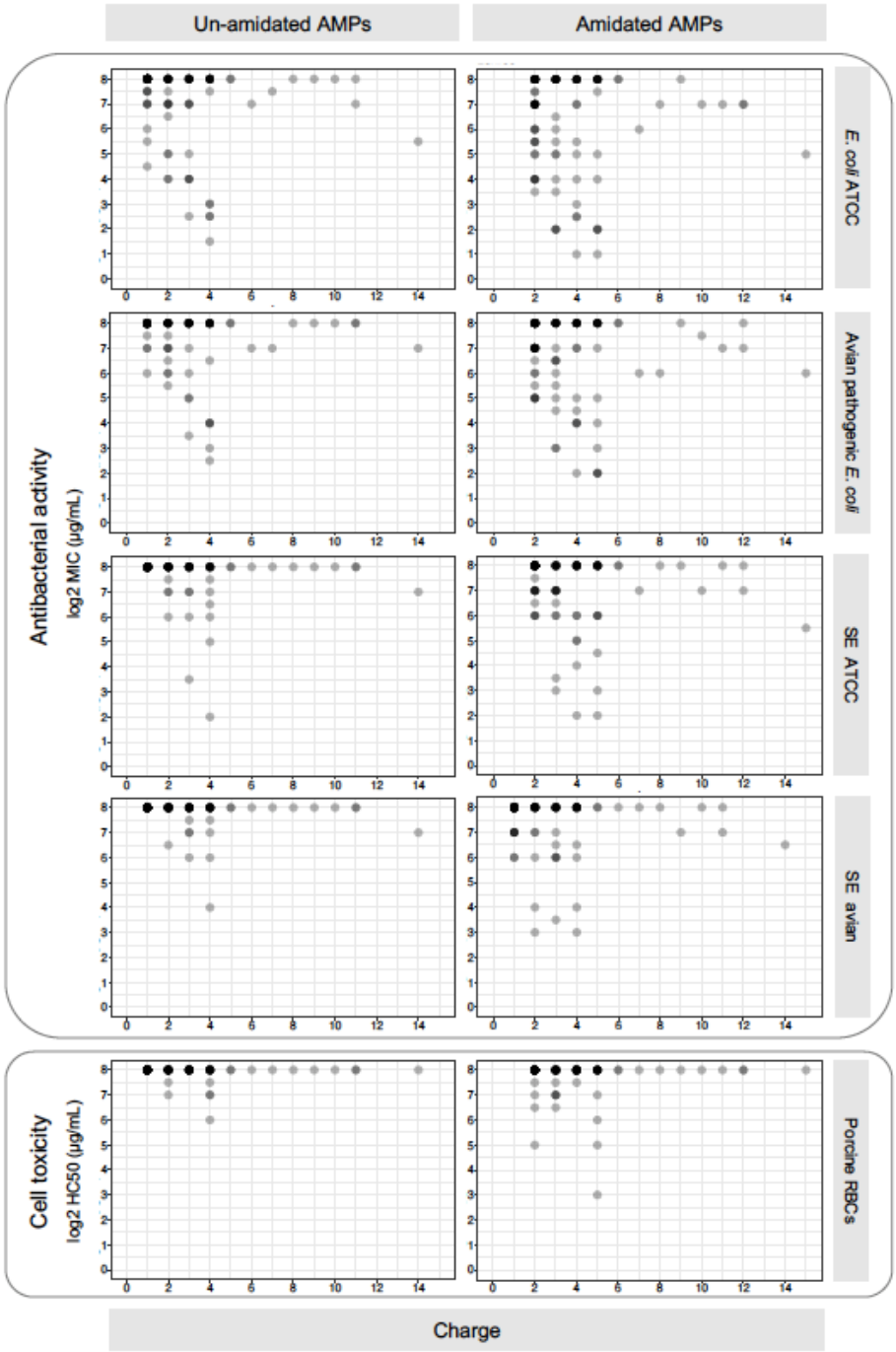

Figure 3.4.2-2 Relationship between charge vs antimicrobial activity for the un-amidated and amidated novel putative AMPs. The positive charge or the length in AAs was plotted vs $\log_2$(median MIC) for each peptide. The darker the area, the more novel putative AMPs fall at that position. The classifications for antimicrobial activity converted to $\log_2$MIC are “No activity” (MIC > 7), “low” (7 ≥ MIC > 5), “moderate” (5 ≥ MIC > 2), or “high” (MIC ≤ 2). The classifications for cytotoxic activity converted to $\log_2$HC50 are none (HC50 = 8), low (8 > HC50 ≥ 7), moderate (7 > HC50 ≥ 6), and high (HC50 < 6).

The length of an AMP can influence peptide activity, the ability to penetrate a membrane, and other physicochemical characteristics (Bahar & Ren, 2013; Wang, 2020). Here we selected for AMPs with a length of 30 AAs or less (range of 7 to 30 AAs). We observed that there was no activity below 10 AAs in length for both the un-amidated and amidated AMPs (Figure 3.4.2-3). It is possible that below 10 AAs was approaching the minimum length needed for peptide activity in our experimental conditions. However, shorter sequences improve synthesis costs for therapeutic development. Therefore, choosing short active peptides or truncating long AMPs and using other methods such as post-translational modification to improve activity and stability could be employed as ways to decrease cost.

More activity was observed in the longer un-amidated peptides (length > 24 AA) compared to the shorter un-amidated peptides (Figure 3.4.2-3). In the amidated AMPs, the trend of longer AMPs having higher activity was also observed with high activity being predominately in amidated AMPs of 22 AAs or more; however, there was a large increase in the number of moderately active AMPs in the 10 to 20 AA range. In terms of length, there appeared to be a general trend towards the longer AMPs having more antimicrobial activity.

In the PRBCs, there was no cell toxicity activity in un-amidated AMPs below 23 AAs. For the amidated peptides there was some toxicity observed in the 12 to 17 AA range, as well as at the longer lengths (Figure 3.4.2-3). Length of AMP has been associated with cytotoxicity, with truncated peptides having significantly less toxicity than their original form (Park et al., 2007; Subbalakshmi et al., 1999). In our data, there was little toxicity observed in AMPs below 24 AAs in length. This is promising for therapeutic development.

Overall, the novel putative AMPs tended to possess higher activity at the longer AA lengths tested. Amidation increased both antimicrobial activity and cell toxicity at the 10 to 21 AA length range; however, the number of AMPs with increased activity in that range was greater than the number of AMPs with increased toxicity.

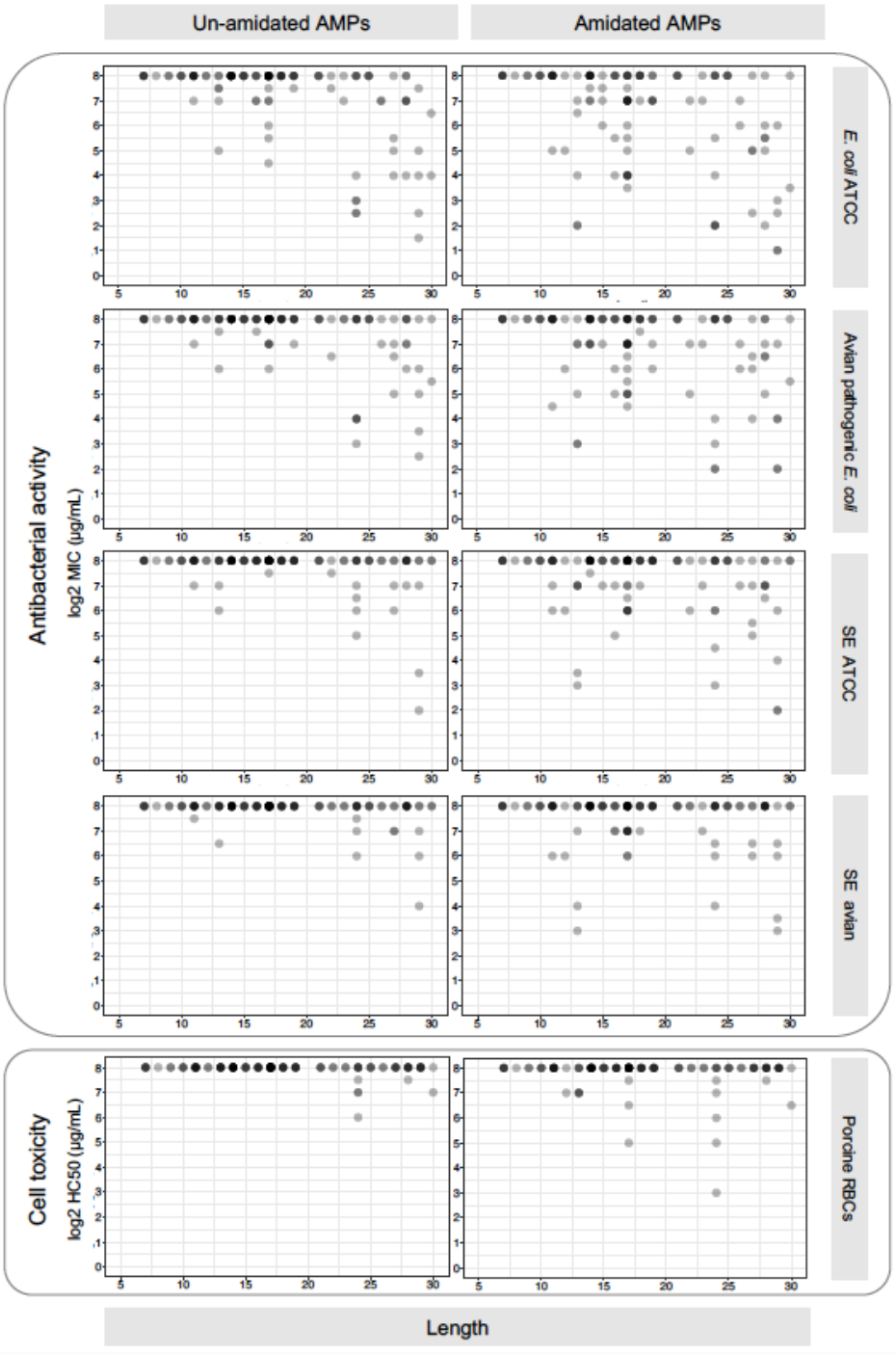

Figure 3.4.2-3 Relationship between length vs antimicrobial activity for the un-amidated and amidated novel putative AMPs. The length in AAs was plotted vs $\log_2$(median MIC) for each peptide. The darker the area, the more novel putative AMPs fall at that position. The classifications for antimicrobial activity converted to $\log_2$MIC are “No activity” (MIC > 7), “low” (7 ≥ MIC > 5), “moderate” (5 ≥ MIC > 2), or “high” (MIC ≤ 2). The classifications for cytotoxic activity converted to $\log_2$HC50 are none (HC50 = 8), low (8 > HC50 ≥ 7), moderate (7 > HC50 ≥ 6), and high (HC50 < 6).

Most active AMPs were clustered at lower positive charges and at longer lengths, as observed in Figure 3.4.2-2 and Figure 3.4.2-3. The physicochemical properties identified here can inform analysis of bioinformatically identified putative AMPs datasets. The novel active AMPs identified in the present study have all been predominately alpha-helical, had hydrophobic properties, and been positively charged. This is consistent with commonly observed amphibian AMP motifs and suggests that these AMPs may be associated with membrane disruption as a potential mechanism of action (Haney et al., 2009; Islam et al., 2023). This remains to be tested on the novel AMPs described herein.

3.4.1. Amidation

C-terminal amidation of AMPs can enhance activity as an antimicrobial agent, making this post-translational modification an area of interest in terms of improving an AMP's activity (Bahar & Ren, 2013; Dennison et al., 2015; Huan et al., 2020; Strandberg et al., 2007; Wang, 2020). C-terminal amidation can increase electrostatic interactions with negatively charged microbial membrane, improve membrane-penetrating abilities, and stabilize the AMP (Mura et al., 2016; Sforça et al., 2004; Shalev et al., 2002). While many studies have looked at the impact of amidation on individual or a small number of peptides (Dennison et al., 2015; Mura et al., 2016; Shahmiri & Mechler, 2020; Shalev et al., 2002), the present study is the first examining amidation of a large dataset of novel putative AMPs (n=111). To elucidate the effect of amidation on AMP activity, all novel putative AMPs were amidated at the C-terminal end and then tested against our pathogen panel. To observe the impact of amidation on AMP activity, we compared the median MICs of the un-amidated versus the amidated AMPs using XY-plots (Figure 3.4.1-1). We also performed a pairwise comparison of the antimicrobial activity of each individual un-amidated and amidated novel AMP pair to observe any significant differences in MICs due to amidation (Table 3.4.1-1; p-value $\leq$ 0.05). See Supplementary Figure 6-6 to Supplementary Figure 6-8 for boxplots of individual pairwise comparisons.

Amidation increased the antimicrobial activity of most novel AMPs. As per Figure 3.4.1-1, there were more AMPs below the center line for each pathogen tested

indicating that amidation decreased the MIC and therefore increased antimicrobial activity of those AMPs. This was also observed in the pairwise comparison where 59.3% of the novel AMP pairs containing at least one active AMP had significantly more antimicrobial activity against both *E. coli* strains in the amidated AMP compared to their un-amidated counterpart (Table 3.4.1-1). A significant increase in activity of the amidated AMP was also observed in 45.8% and 37.3% of the active AMP pairs against SE ATCC and SE avian respectively (Table 3.4.1-1). Overall, there was a significant increase in antimicrobial activity due to C-terminal amidation in 37.3% to 59.3% of all the active AMP pairs tested in the present study. Studies of individual AMPs have noted similar increases in AMP activity due to C-terminal amidation and have shown that the increase stems from stabilized helix formation, improved cell membrane penetration, and increased charge (Dennison & Phoenix, 2011; Mura et al., 2016; Shahmiri & Mechler, 2020; Shalev et al., 2002). While mechanism of action is outside the scope of the present study, we hypothesize that amidation of the C-terminus had a similar impact on the novel AMPs identified here that showed improved activity.

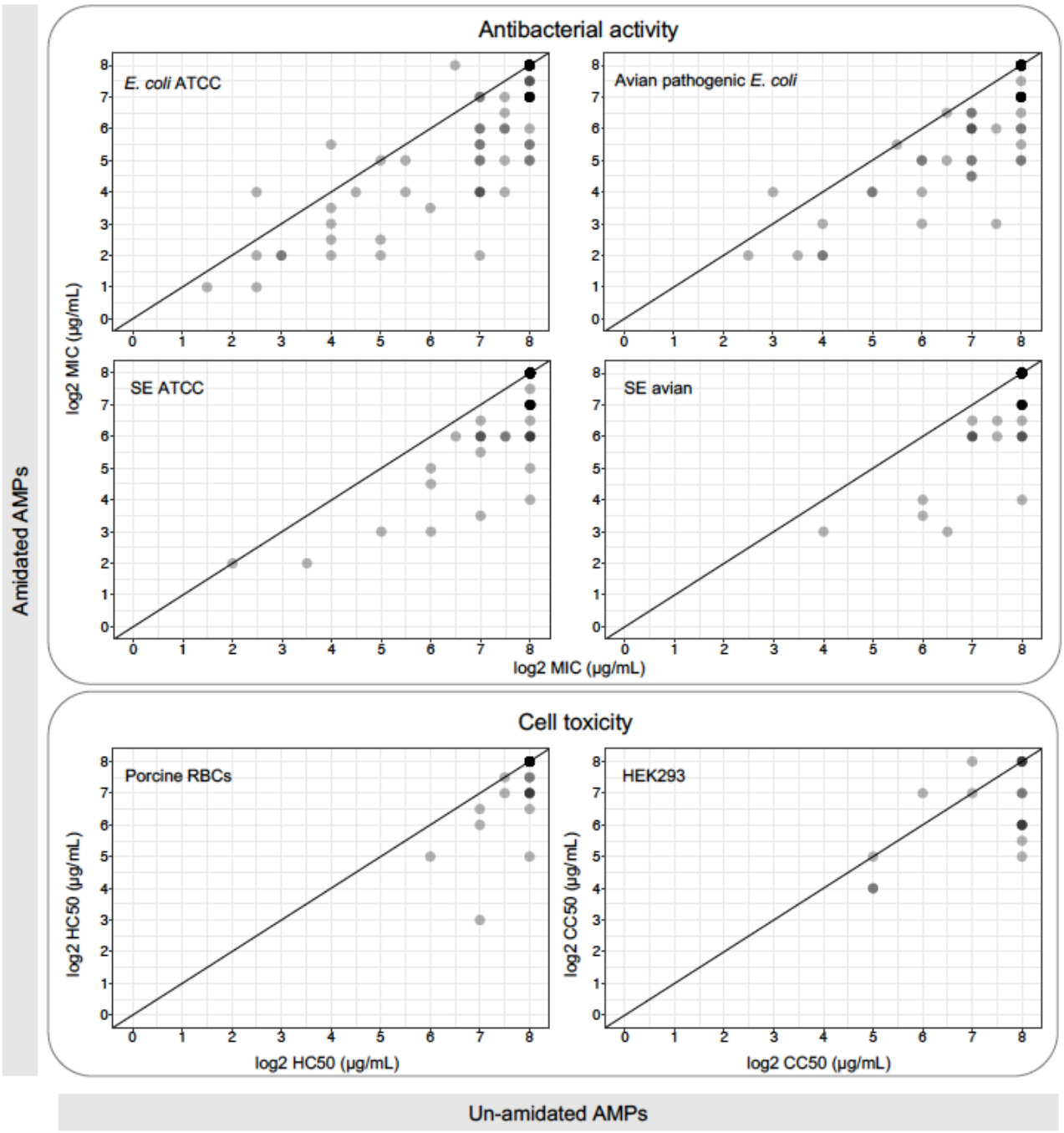

Figure 3.4.1-1 XY-plots comparing the $\log_2$ median MIC or cell toxicity (HC50 or CC50) of un-amidated versus amidated novel putative AMPs. Points that fall on the line indicate no difference between un-amidated and amidated MICs for that putative AMP. Points on the line y = x indicate that $MIC_{un\text{-}amidated} = MIC_{amidated}$ (amidation did not affect MIC), any points in the area below the line indicated that the $MIC_{amidated} < MIC_{un\text{-}amidated}$ (amidation decreased MIC indicating increased antimicrobial activity), and any points in the area above the line indicate $MIC_{un\text{-}amidated} < MIC_{amidated}$ (amidation increased MIC indicating decreased antimicrobial activity). See Figure 3.4.2-1 for a description of the data points.

The XY-plot (Figure 3.4.1-1) and pairwise comparison (Table 3.4.1-1) analyses were also performed for cell toxicity testing. Amidation significantly increased cell toxicity of 13.6% of the novel putative AMPs tested against both PRBCs and HEK293 cells (Table 3.4.1-1), and this trend can be observed in Figure 3.4.1-1. This indicated that amidation may increase the ability of certain AMPs to interact with mammalian membranes. However, many of the AMPs in which cell toxicity was observed only showed toxicity at concentrations well above their MICs (Supplementary Figure 6-8). Interestingly, other studies have shown that C-terminal amidation did not influence AMP selectivity for microbial over eukaryotic cells (Dennison et al., 2009; Pan et al., 2007). Perhaps, because of our larger dataset, we observed an effect of amidation that is not normally seen in more directed studies of individual or small groups of AMPs.

There were rare cases when amidation decreased the ability of the AMP to inhibit growth (CCH-63, -64, and -74 for *E. coli* ATCC and CCH-64 only for APEC; Figure 3.4.1-1). These were only significant against the *E. coli* strains (Table 3.4.1-1). This could be due to the amidation interfering the AMP's mechanism of action or structure and preventing its antimicrobial activity. Finally, amidation also had no effect on the activity of some of the active AMPs (Figure 3.4.1-1: AMPs on the line). While amidation is often associated with increased antimicrobial activity, that is not always the case. Dennison et al. (2009) found that C-terminal amidation had variable effect on the activity and anticancer properties of nine different AMP pairs.

There was a significant increase in antimicrobial activity from C-terminal amidation against all pathogens tested. Cell toxicity of AMPs is a concern when designing therapeutics. While amidation increased the cell toxicity of a small number of the AMPs tested, the majority of the amidated AMPs did not show a significant change in cell toxicity or displayed toxicity at concentrations above their MICs. The mechanisms behind the C-terminal amidation change in membrane affinity is worth further investigation. Overall, these results suggest that, when testing AMPs for therapeutic use, amidating the C-terminus may increase antimicrobial activity of many AMPs.

C-terminal amidation increased the antimicrobial activity against both APEC and SE avian. Amidation significantly increased over half and over a third of the AMP's

activity against both APEC and SE respectively with little (APEC) to no (SE avian) increase in toxicity (Table 3.4.1-1). C-terminal amidation may be a promising route for therapeutic discovery against avian pathogens.

Table 3.4.1-1 Pairwise comparison of antimicrobial activity and cell toxicity of un-amidated vs C-terminal amidated novel putative AMPs. The number of pairs with a significant change, a significant increase, or a significant decrease in activity due to C-terminal amidation (left) and the respective percentage out of the 59 AMP pairs tested that showed some activity and were therefore verified AMPs (right) is shown (p-value ≤ 0.05). One AMP pair was removed from analysis due to the un-amidated version being un-synthesizable. For the HEK293 cell assay, only putative AMPs with high antimicrobial activity and/or hemolytic activity plus the pair (regardless of actively), was tested so the percent on the top is out of the total AMP pairs (59) although not all were tested against HEK293 cells and the percent on the bottom is the activity out of the actual number of AMPs tested (36).

		# of significantly different pairs			**% of total novel active AMPs tested**		
	Pathogen	**Total**	**Increased activity**	**Decreased activity**	**Total**	**Increased activity**	**Decreased activity**
Antimicrobial activity	*E. coli* ATCC	38	35	3	64.4%	59.3%	5.1%
	APEC	36	35	1	61.0%	59.3%	1.7%
	SE ATCC	27	27	-	45.8%	45.8%	-
	SE Avian	22	22	-	37.3%	37.3%	-
Cell toxicity	PRBC	8	8	-	13.6%	13.6%	-
	HEK293	8	8	-	13.6% 22.2%	13.6% 22.2%	-

3.4.2. Activity, predicted structure, and physicochemical property overview

Structural and physicochemical properties such as hydrophobicity, charge, and length influence AMP activity (Torres et al., 2019). In the present study, 111 novel putative AMPs, as well as their C-terminal amidated pair, were chosen to undergo the investigation of these characteristics. The outcome of this in-depth characterization in relation to the antimicrobial activity and cell toxicity of the novel AMP were summarized in Figure 3.4.2-1. The highly and moderately active novel AMPs identified herein (both

un-amidated and amidated) tended to be positively charged (+1 to +5), longer (>22 AA) alpha-helices with hydrophobic properties.

For the other peptides that were bioinformatically identified but that did not show activity in the present study, it is possible that they may be associated with other functions or mechanisms of action other than direct killing of our pathogens of interest (antimicrobial against other pathogens, induce cytokine expression etc.), so the scope of their activity may not have been captured in our analysis. While they were not identified as bioactive in the present study, that does not exclude them from having antimicrobial activity on other pathogens.

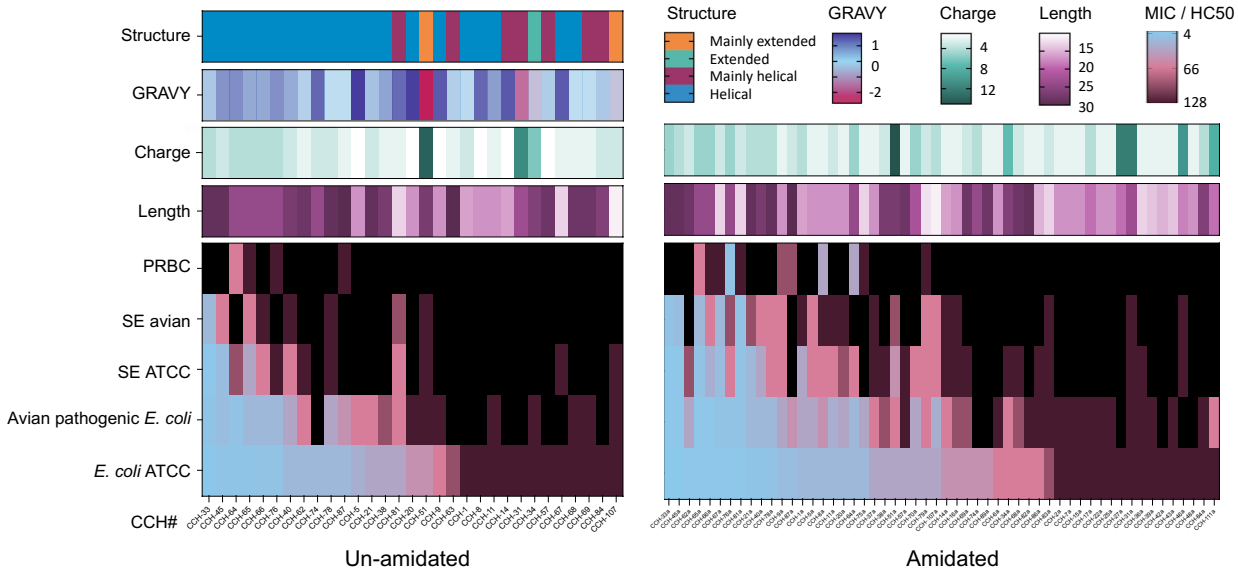

Figure 3.4.2-1 Physicochemical attribute, antimicrobial activity, and cell toxicity overview of the un-amidated (left) and amidated (right) novel AMPs. Predicted secondary structure is shown in the top row (row 1). Physicochemical properties of the AMPs tested (hydrophobicity, charge, and length) are displayed in the 2 - 4 rows. Antimicrobial activity against *E. coli* ATCC, APEC, SE ATCC, and SE avian and cell toxicity against PRBC of all active novel AMPs are shown in the bottom five rows. Legends are found to the right of each respective row.

3.5. Conclusion

AMPs are promising therapeutic candidates that have the potential to mitigate antibiotic use in public health and agricultural sectors. APEC and SE avian are both agriculturally relevant pathogens in the poultry industry that are responsible for large

yearly economic losses and pose public health risks. Here we showed that the bioinformatic AMP identification pipeline, rAMPage, could successfully identify novel AMPs from amphibian RNA-seq datasets that were active against these critical poultry pathogens. To the best of our knowledge the present study is the first comprehensive analysis of a large dataset of novel AMPs in their natural and C-terminal amidated form. Analysis of the physicochemical properties of these novel AMPs showed the most activity trended toward being observed in hydrophobic, alpha-helical peptides with a charge range of +1 to +5. Additionally, we showed that amidation of the C-terminus significantly increases AMP activity against both APEC and SE avian. An increase in cell toxicity due to amidation was also observed, but to a lesser degree than the paired increase in activity. Amidation of the C-terminus of peptides may be a promising way to increase AMP activity in future therapeutic discovery studies. AMP candidates identified here will continue to be investigated as potential antimicrobials for the poultry industry.

4. Conclusions and future directions

TH is a critical regulator of anuran metamorphosis that initiates structural and functional remodeling of the aquatic tadpole tissues into those of the terrestrial frog. This allows the organism to adapt to a new ecological niche associated new environmental and microbial challenges. Amphibian skin is the innate immune system's first line of defense that acts as a physical, chemical, and microbial barrier against the microbially diverse environments that it is continuously interacting with during the anuran life cycle. Skin, like many other amphibian tissues, is remodelled during metamorphosis. However, changes in many of the immune components during metamorphosis are not well understood.

Herein, we expanded upon targeted qPCR-based TH-induction transcriptomic studies of the back skin by performing the first RNA-sequencing analysis of *R. catesbeiana* back skin undergoing natural metamorphosis, as well as induced-metamorphosis in temperature-modulated conditions. GO enrichment analysis provided an overview of the transcriptomic changes occurring during development and in the early stages of TH-induction in the back skin. Upon further analysis, the expression of classic TH-indicator transcripts was observed during natural metamorphosis with the temperature-mediation experiment providing insight into the early transcriptomic initiation events. The early response transcript *thibz* was found to be significantly expressed during the initiation of TH signalling in the back skin. This pattern of *thibz* expression is a common phenomenon across many *R. catesbeiana* tissues and has been identified as a critical component of the molecular memory (Hammond et al., 2016; Hammond et al., 2015; Koide et al., 2022). Identifying the function of this transcript is key to understanding molecular memory and early TH signalling events.

To further understand how the *R. catesbeiana* skin responded to metamorphosis and temperature challenge, the expression of transcripts relating to temperature and immune challenge were profiled. During cutaneous remodelling, the expression of many heat shock proteins, keratin, mucins, and AMPs were modulated by TH. The expression of *hsp30* was developmentally regulated. While *hsp30* expression did not appear to be an early initiator of TH signalling, TH may directly or indirectly influence its expression

and it may be involved in skin development. Understanding role of *hsp30* expression in the back skin, as well as elucidating *hsp30* expression in other metamorphically active tissues are areas of future work. Larval and adult specific keratins were abundantly expressed at their appropriate developmental stages. Later in development however, the expression of adult keratin was organism dependent with either incredibly high or almost non-existent expression levels. Keratin is an important structural component of the back skin so understanding why high levels of variation were present later in development and how they may affect the organism's ability to survive is worth investigating. The mucin and AMP expression profiles shifted during metamorphosis, with certain transcripts being expressed in developmentally regulated patterns. Additionally, temperature influenced mucin-like and AMP transcript abundance. TH induces a biphasic cascade of gene expression that regulates the transformation of the larval back skin into the stratified adult epithelium. During this process, the heat shock proteins, keratin, mucin, and AMP profiles also undergo developmentally regulated changes, allowing the developing frog to adapt to its new environment.

AMP identification has historically been challenging; however, with the emergence of bioinformatic tools, finding novel AMPs has been facilitated. In the present study, we showed that using genomic resources from organisms in different developmental stages or environmental conditions lead to novel AMP profiles. AMP production is an important part of the innate immune system of anurans and expression, especially during development, has not been well studied. Identifying new AMPs is critical for our understanding of the amphibian immune system, but the AMPs identified in amphibians can and have been applied therapeutically elsewhere. A subset of the AMPs that have been identified in our datasets were tested for their effectiveness as potential agricultural therapeutics.

APEC and SE are both agriculturally relevant pathogens that pose significant public health risks and cause large economic losses in the poultry industry. Herein, we successfully bioinformatically identified novel AMPs from unique developmental amphibian transcriptomics resources that are active against these critical poultry pathogens. To the best of our knowledge this study is the first comprehensive analysis of a large dataset of novel AMPs and their C-terminal amidated pair. Physicochemical

analysis of these novel AMPs showed that activity was observed in positively charged (+1 to +5 range), alpha-helical peptides with hydrophobic properties. Additionally, we showed that amidation of the C-terminus significantly increases AMP activity in a large dataset of novel AMPs. Increased toxicity due to C-terminal amidation was also observed, but to a lesser extent. Amidation of the C-terminus of peptides may be a promising way to increase AMP activity in future therapeutic discovery studies. AMP candidates identified here will continue to be investigated as potential antimicrobials for the poultry industry.

5. References

Aberg, K. M., Radek, K. A., Choi, E.-H., Kim, D.-K., Demerjian, M., Hupe, M., . . . Elias, P. M. (2007). Psychological stress downregulates epidermal antimicrobial peptide expression and increases severity of cutaneous infections in mice. *Journal of Clinical Investigation*, *117*(11), 3339-3349. https://doi.org/10.1172/jci31726

Akat Çömden, E., Yenmiş, M., & Çakır, B. (2023). The Complex Bridge between Aquatic and Terrestrial Life: Skin Changes during Development of Amphibians. *Journal of Developmental Biology*, *11*(1), 6. https://doi.org/10.3390/jdb11010006

Alves, R. N., Sundell, K. S., Anjos, L., Sundh, H., Harboe, T., Norberg, B., & Power, D. M. (2018). Structural and functional maturation of skin during metamorphosis in the Atlantic halibut (Hippoglossus hippoglossus). *Cell and Tissue Research*, *372*(3), 469-492. https://doi.org/10.1007/s00441-018-2794-1

Ashley, H., Katti, P., & Frieden, E. (1968). Urea excretion in the bullfrog tadpole: Effect of temperature, metamorphosis, and thyroid hormones. *Developmental Biology*, *17*(3), 293-307. https://doi.org/10.1016/0012-1606(68)90066-3

Bahar, A., & Ren, D. (2013). Antimicrobial Peptides. *Pharmaceuticals*, *6*(12), 1543-1575. https://doi.org/10.3390/ph6121543

Barlam, T. F., & Gupta, K. (2015). Antibiotic Resistance Spreads Internationally across Borders. *The Journal of Law, Medicine & Ethics*, *43*(3_suppl), 12-16. https://doi.org/10.1111/jlme.12268

Bates, K. A., Clare, F. C., O'Hanlon, S., Bosch, J., Brookes, L., Hopkins, K., . . . Harrison, X. A. (2018). Amphibian chytridiomycosis outbreak dynamics are linked with host skin bacterial community structure. *Nature Communications*, *9*(1). https://doi.org/10.1038/s41467-018-02967-w

Bender, M. C., Hu, C., Pelletier, C., & Denver, R. J. (2018). To eat or not to eat: ontogeny of hypothalamic feeding controls and a role for leptin in modulating life-history transition in amphibian tadpoles. *Proceedings of the Royal Society B: Biological Sciences*, *285*(1875), 20172784. https://doi.org/10.1098/rspb.2017.2784

Benincasa, M., Runti, G., Mardirossian, M., Gennaro, R., & Scocchi, M. (2017). Methods for Elucidating the Mechanism of Action of Proline-Rich and Other Non-lytic Antimicrobial Peptides. In *Methods in Molecular Biology* (pp. 283-295). Springer New York. https://doi.org/10.1007/978-1-4939-6737-7_20

Bergh, J. J., Lin, H.-Y., Lansing, L., Mohamed, S. N., Davis, F. B., Mousa, S., & Davis, P. J. (2005). Integrin αVβ3 Contains a Cell Surface Receptor Site for Thyroid Hormone that Is Linked to Activation of Mitogen-Activated Protein Kinase and Induction of Angiogenesis. *Endocrinology*, *146*(7), 2864-2871. https://doi.org/10.1210/en.2005-0102

Brandenburg, L.-O., Merres, J., Albrecht, L.-J., Varoga, D., & Pufe, T. (2012). Antimicrobial Peptides: Multifunctional Drugs for Different Applications. *Polymers*, *4*(1), 539-560. https://doi.org/10.3390/polym4010539

Brogden, K. A., Bates, A. M., & Fischer, C. L. (2016). Antimicrobial Peptides in Host Defense: Functions Beyond Antimicrobial Activity. In *Antimicrobial Peptides* (pp. 129-146). Springer International Publishing. https://doi.org/10.1007/978-3-319-24199-9_9

Brown, D., & Cai, L. (2015). *Amphibian metamorphosis*.

Brumfitt, W., Salton, M. R. J., & Hamilton-Miller, J. M. T. (2002). Nisin, alone and combined with peptidoglycan-modulating antibiotics: activity against methicillin-resistant Staphylococcus aureus and vancomycin-resistant enterococci. *Journal of Antimicrobial Chemotherapy*, *50*(5), 731-734. https://doi.org/10.1093/jac/dkf190

Bryant, D. M., Johnson, K., DiTommaso, T., Tickle, T., Couger, M. B., Payzin-Dogru, D., . . . Whited, J. L. (2017). A Tissue-Mapped Axolotl De Novo Transcriptome Enables Identification of Limb Regeneration Factors. *Cell Reports*, *18*(3), 762-776. https://doi.org/https://doi.org/10.1016/j.celrep.2016.12.063

Buchholz, D. R. (2015). More similar than you think: Frog metamorphosis as a model of human perinatal endocrinology. *Developmental Biology*, *408*(2), 188-195. https://doi.org/10.1016/j.ydbio.2015.02.018

Buchholz, D. R., Heimeier, R. A., Das, B., Washington, T., & Shi, Y. B. (2007). Pairing morphology with gene expression in thyroid hormone-induced intestinal remodeling and identification of a core set of TH-induced genes across tadpole tissues. *Dev Biol*, *303*(2), 576-590. https://doi.org/10.1016/j.ydbio.2006.11.037

Chambers, D. L., Wojdak, J. M., Du, P., & Belden, L. K. (2011). Corticosterone Level Changes throughout Larval Development in the Amphibians Rana sylvatica and Ambystoma jeffersonianum Reared under Laboratory, Mesocosm, or Free-living Conditions. *Copeia*, *2011*(4), 530-538.

Chantziaras, I., Boyen, F., Callens, B., & Dewulf, J. (2014). Correlation between veterinary antimicrobial use and antimicrobial resistance in food-producing animals: a report on seven countries. *J Antimicrob Chemother*, *69*(3), 827-834. https://doi.org/10.1093/jac/dkt443

Chapoval, S. P., Lee, M., Lemmer, A., Ajayi, O., Qi, X., Neuwald, A. F., & Keegan, A. D. (2022). Identifying Function Determining Residues in Neuroimmune Semaphorin 4A. *International Journal of Molecular Sciences*, *23*(6), 3024. https://doi.org/10.3390/ijms23063024

Chen, C. H., Bepler, T., Pepper, K., Fu, D., & Lu, T. K. (2022). Synthetic molecular evolution of antimicrobial peptides. *Current Opinion in Biotechnology*, *75*, 102718. https://doi.org/https://doi.org/10.1016/j.copbio.2022.102718

Chung, C.-R., Jhong, J.-H., Wang, Z., Chen, S., Wan, Y., Horng, J.-T., & Lee, T.-Y. (2020). Characterization and Identification of Natural Antimicrobial Peptides on

Different Organisms. *International Journal of Molecular Sciences*, *21*(3), 986. https://doi.org/10.3390/ijms21030986

Clinical and Laboratory Standards Institute. (2015). Methods for Dilution Antimicrobial Susceptibility Tests for Bacteria That Grow Aerobically:Approved Standards. *Clinical and Laboratory Standards Institute: ayne, PA, USA,*.

Corrie, L. M., Kempe, M. N., Blajkevitch, O., Shang, D., & Helbing, C. C. (2021). Dioctyl Sodium Sulfosuccinate as a Potential Endocrine Disruptor of Thyroid Hormone Activity in American bullfrog, Rana (Lithobates) catesbeiana, Tadpoles. *Archives of Environmental Contamination and Toxicology*, *80*(4), 726-734. https://doi.org/10.1007/s00244-021-00835-1

Crespi, E. J., & Denver, R. J. (2006). Leptin (ob gene) of the South African clawed frog Xenopus laevis. *Proceedings of the National Academy of Sciences*, *103*(26), 10092-10097. https://doi.org/10.1073/pnas.0507519103

Cruz, J., Ortiz, C., Guzmán, F., Fernández-Lafuente, R., & Torres, R. (2014). Antimicrobial peptides: promising compounds against pathogenic microorganisms. *Curr Med Chem*, *21*(20), 2299-2321. https://doi.org/10.2174/09298673216661402171101 55

Das, B., Heimeier, R. A., Buchholz, D. R., & Shi, Y.-B. (2009). Identification of Direct Thyroid Hormone Response Genes Reveals the Earliest Gene Regulation Programs during Frog Metamorphosis. *Journal of Biological Chemistry*, *284*(49), 34167-34178. https://doi.org/10.1074/jbc.m109.066084

Dennison, S. R., Harris, F., Bhatt, T., Singh, J., & Phoenix, D. A. (2009). The effect of C-terminal amidation on the efficacy and selectivity of antimicrobial and anticancer peptides. *Molecular and Cellular Biochemistry*, *332*(1-2), 43-50. https://doi.org/10.1007/s11010-009-0172-8

Dennison, S. R., Mura, M., Harris, F., Morton, L. H. G., Zvelindovsky, A., & Phoenix, D. A. (2015). The role of C-terminal amidation in the membrane interactions of the anionic antimicrobial peptide, maximin H5. *Biochimica et Biophysica Acta (BBA) - Biomembranes*, *1848*(5), 1111-1118. https://doi.org/https://doi.org/10.1016/j.bbamem.2015.01.014

Dennison, S. R., & Phoenix, D. A. (2011). Influence of C-Terminal Amidation on the Efficacy of Modelin-5. *Biochemistry*, *50*(9), 1514-1523. https://doi.org/10.1021/bi101687t

Deutsch, D., Leiser, Y., Shay, B., Fermon, E., Taylor, A., Rosenfeld, E., . . . Mao, Z. (2002). The Human Tuftelin Gene and the Expression of Tuftelin in Mineralizing and Nonmineralizing Tissues. *Connective Tissue Research*, *43*(2-3), 425-434. https://doi.org/10.1080/03008200290001186

Deutsch, D., Silverstein, N., Shilo, D., Lecht, S., Lazarovici, P., & Blumenfeld, A. (2011). Biphasic influence of hypoxia on tuftelin expression in mouse mesenchymal C3H10T1/2 stem cells. *European Journal of Oral Sciences*, *119*, 55-61. https://doi.org/10.1111/j.1600-0722.2011.00861.x

Diarra, M. S., Delaquis, P., Rempel, H., Bach, S., Harlton, C., Aslam, M., . . . Topp, E. (2014). Antibiotic Resistance and Diversity of Salmonella enterica Serovars Associated with Broiler Chickens. *Journal of Food Protection*, *77*(1), 40-49. https://doi.org/https://doi.org/10.4315/0362-028.JFP-13-251

Dobin, A., Davis, C. A., Schlesinger, F., Drenkow, J., Zaleski, C., Jha, S., . . . Gingeras, T. R. (2013). STAR: ultrafast universal RNA-seq aligner. *Bioinformatics*, *29*(1), 15-21. https://doi.org/10.1093/bioinformatics/bts635

Dohrman, A., Miyata, S., Gallup, M., Li, J. D., Chapelin, C., Coste, A., . . . Basbaum, C. (1998). Mucin gene (MUC 2 and MUC 5AC) upregulation by Gram-positive and Gram-negative bacteria. *Biochim Biophys Acta*, *1406*(3), 251-259. https://doi.org/10.1016/s0925-4439(98)00010-6

Domanski, D., & Helbing, C. C. (2007). Analysis of the Rana catesbeiana tadpole tail fin proteome and phosphoproteome during T3-induced apoptosis: identification of a novel type I keratin. *BMC Developmental Biology*, *7*(1), 94. https://doi.org/10.1186/1471-213x-7-94

Dubaissi, E., & Papalopulu, N. (2011). Embryonic frog epidermis: a model for the study of cell-cell interactions in the development of mucociliary disease. *Disease Models & Mechanisms*, *4*(2), 179-192. https://doi.org/10.1242/dmm.006494

Dubaissi, E., Rousseau, K., Hughes, G. W., Ridley, C., Grencis, R. K., Roberts, I. S., & Thornton, D. J. (2018). Functional characterization of the mucus barrier on the Xenopus tropicalis skin surface. *Proceedings of the National Academy of Sciences*, *115*(4), 726-731. https://doi.org/10.1073/pnas.1713539115

Dubaissi, E., Rousseau, K., Lea, R., Soto, X., Nardeosingh, S., Schweickert, A., . . . Papalopulu, N. (2014). A secretory cell type develops alongside multiciliated cells, ionocytes and goblet cells, and provides a protective, anti-infective function in the frog embryonic mucociliary epidermis. *Development*, *141*(7), 1514-1525. https://doi.org/10.1242/dev.102426

Durand, G. A., Raoult, D., & Dubourg, G. (2019). Antibiotic discovery: history, methods and perspectives. *International Journal of Antimicrobial Agents*, *53*(4), 371-382. https://doi.org/https://doi.org/10.1016/j.ijantimicag.2018.11.010

Elass-Rochard, E., Legrand, D., Salmon, V., Roseanu, A., Trif, M., Tobias, P. S., . . . Spik, G. (1998). Lactoferrin Inhibits the Endotoxin Interaction with CD14 by Competition with the Lipopolysaccharide-Binding Protein. *Infection and Immunity*, *66*(2), 486-491. https://doi.org/doi:10.1128/iai.66.2.486-491.1998

Ellison, T. R., Mathisen, P. M., & Miller, L. (1985). Developmental changes in keratin patterns during epidermal maturation. *Developmental Biology*, *112*(2), 329-337. https://doi.org/https://doi.org/10.1016/0012-1606(85)90403-8

Fagerberg, L., Hallström, B. M., Oksvold, P., Kampf, C., Djureinovic, D., Odeberg, J., . . . Uhlén, M. (2014). Analysis of the human tissue-specific expression by genome-wide integration of transcriptomics and antibody-based proteomics. *Mol Cell Proteomics*, *13*(2), 397-406. https://doi.org/10.1074/mcp.M113.035600

Finley, R. L., Collignon, P., Larsson, D. G. J., McEwen, S. A., Li, X.-Z., Gaze, W. H., . . . Topp, E. (2013). The Scourge of Antibiotic Resistance: The Important Role of the Environment. *Clinical Infectious Diseases*, *57*(5), 704-710. https://doi.org/10.1093/cid/cit355

Frieden, E., Wahlborg, A., & Howard, E. (1965). Temperature Control of the Response of Tadpoles to Triiodothyronine. *Nature*, *205*(4977), 1173-1176. https://doi.org/10.1038/2051173a0

Friedrich, C., L., Moyles, D., Beveridge, T., J., & Hancock, R., E. W. (2000). Antibacterial Action of Structurally Diverse Cationic Peptides on Gram-Positive Bacteria. *Antimicrobial Agents and Chemotherapy*, *44*(8), 2086-2092. https://doi.org/10.1128/aac.44.8.2086-2092.2000

Frishman, D., & Argos, P. (1995). Knowledge-based protein secondary structure assignment. *Proteins: Structure, Function, and Genetics*, *23*(4), 566-579. https://doi.org/10.1002/prot.340230412

Fuchs, E. (1988). Keratins as biochemical markers of epithelial differentiation. *Trends in Genetics*, *4*(10), 277-281. https://doi.org/https://doi.org/10.1016/0168-9525(88)90169-2

Furlow, J. D., Berry, D. L., Wang, Z., & Brown, D. D. (1997). A set of novel tadpole specific genes expressed only in the epidermis are down-regulated by thyroid hormone during Xenopus laevis metamorphosis. *Dev Biol*, *182*(2), 284-298. https://doi.org/10.1006/dbio.1996.8478

Furtula, V., Farrell, E. G., Diarrassouba, F., Rempel, H., Pritchard, J., & Diarra, M. S. (2010). Veterinary pharmaceuticals and antibiotic resistance of Escherichia coli isolates in poultry litter from commercial farms and controlled feeding trials. *Poultry Science*, *89*(1), 180-188. https://doi.org/https://doi.org/10.3382/ps.2009-00198

Giangaspero, A., Sandri, L., & Tossi, A. (2001). Amphipathic α helical antimicrobial peptides. *European Journal of Biochemistry*, *268*(21), 5589-5600. https://doi.org/10.1046/j.1432-1033.2001.02494.x

Gosavi, S. M., Gaikwad, P. S., Gramapurohit, N. P., & Kumar, A. R. (2014). Occurrence of parotoid glands in tadpoles of the tropical frog, Clinotarsus curtipes and their role in predator deterrence. *Comp Biochem Physiol A Mol Integr Physiol*, *170*, 31-37. https://doi.org/10.1016/j.cbpa.2014.01.009

Grogan, L. F., Robert, J., Berger, L., Skerratt, L. F., Scheele, B. C., Castley, J. G., . . . McCallum, H. I. (2018). Review of the Amphibian Immune Response to Chytridiomycosis, and Future Directions. *Front Immunol*, *9*, 2536. https://doi.org/10.3389/fimmu.2018.02536

Gunzburger, M. S., & Travis, J. (2005). Critical Literature Review of the Evidence for Unpalatability of Amphibian Eggs and Larvae. *Journal of Herpetology*, *39*(4), 547-571.

Gurrapu, S., & Tamagnone, L. (2016). Transmembrane semaphorins: Multimodal signaling cues in development and cancer. *Cell Adhesion & Migration*, *10*(6), 675-691. https://doi.org/10.1080/19336918.2016.1197479

Hammond, A., Jackman, K. W., Partovi, S. H., Veldhoen, N., & Helbing, C. C. (2016). Identification of organ-autonomous constituents of the molecular memory conferred by thyroid hormone exposure in cold temperature-arrested metamorphosing Rana (Lithobates) catesbeiana tadpoles. *Comparative Biochemistry and Physiology Part D: Genomics and Proteomics*, *17*, 58-65. https://doi.org/https://doi.org/10.1016/j.cbd.2016.01.002

Hammond, S., Veldhoen, N., & Helbing, C. (2015). Influence of temperature on thyroid hormone signaling and endocrine disruptor action in Rana (Lithobates) catesbeiana tadpoles. *General and comparative endocrinology*, *219*, 6-15. https://doi.org/10.1016/j.ygcen.2014.12.001

Hammond, S. A., Warren, R. L., Vandervalk, B. P., Kucuk, E., Khan, H., Gibb, E. A., . . . Birol, I. (2017). The North American bullfrog draft genome provides insight into hormonal regulation of long noncoding RNA. *Nature Communications*, *8*(1). https://doi.org/10.1038/s41467-017-01316-7

Hancock, R. E. W., & Sahl, H.-G. (2006). Antimicrobial and host-defense peptides as new anti-infective therapeutic strategies. *Nature Biotechnology*, *24*(12), 1551-1557. https://doi.org/10.1038/nbt1267

Haney, E. F., Hunter, H. N., Matsuzaki, K., & Vogel, H. J. (2009). Solution NMR studies of amphibian antimicrobial peptides: Linking structure to function? *Biochimica et Biophysica Acta (BBA) - Biomembranes*, *1788*(8), 1639-1655. https://doi.org/https://doi.org/10.1016/j.bbamem.2009.01.002

Heerema, J. L., Jackman, K. W., Miliano, R. C., Li, L., Zaborniak, T. S. M., Veldhoen, N., . . . Helbing, C. C. (2018). Behavioral and molecular analyses of olfaction-mediated avoidance responses of Rana (Lithobates) catesbeiana tadpoles: Sensitivity to thyroid hormones, estrogen, and treated municipal wastewater effluent. *Horm Behav*, *101*, 85-93. https://doi.org/10.1016/j.yhbeh.2017.09.016

Heikkila, J. J. (2003). Expression and function of small heat shock protein genes during Xenopus development. *Seminars in Cell & Developmental Biology*, *14*(5), 259-266. https://doi.org/https://doi.org/10.1016/j.semcdb.2003.09.022

Heikkila, J. J. (2010). Heat shock protein gene expression and function in amphibian model systems. *Comparative Biochemistry and Physiology Part A: Molecular & Integrative Physiology*, *156*(1), 19-33. https://doi.org/https://doi.org/10.1016/j.cbpa.2010.01.024

Helbing, C., Gallimore, C., & Atkinson, B. G. (1996). Characterization of Rana catesbeiana HSP30 gene and its expression in the liver of this amphibian during both spontaneous and thyroid hormone-induced metamorphosis. *Developmental Genetics*, *18*(3), 223-233. https://doi.org/https://doi.org/10.1002/(SICI)1520-6408(1996)18:3<223::AID-DVG3>3.0.CO;2-B

Helbing, C. C., Hammond, S. A., Jackman, S. H., Houston, S., Warren, R. L., Cameron, C. E., & Birol, I. (2019). Antimicrobial peptides from Rana [Lithobates] catesbeiana: Gene structure and bioinformatic identification of novel forms from tadpoles. *Scientific Reports*, *9*(1). https://doi.org/10.1038/s41598-018-38442-1

Huan, Y., Kong, Q., Mou, H., & Yi, H. (2020). Antimicrobial Peptides: Classification, Design, Application and Research Progress in Multiple Fields [Review]. *Frontiers in Microbiology*, *11*. https://doi.org/10.3389/fmicb.2020.582779

Humphries, J. E., Lanctôt, C. M., Robert, J., McCallum, H. I., Newell, D. A., & Grogan, L. F. (2022). Do immune system changes at metamorphosis predict vulnerability to chytridiomycosis? An update. *Developmental & Comparative Immunology*, *136*, 104510. https://doi.org/https://doi.org/10.1016/j.dci.2022.104510

Håversen, L., Ohlsson, B. G., Hahn-Zoric, M., Hanson, L. Å., & Mattsby-Baltzer, I. (2002). Lactoferrin down-regulates the LPS-induced cytokine production in monocytic cells via NF-κB. *Cellular Immunology*, *220*(2), 83-95. https://doi.org/https://doi.org/10.1016/S0008-8749(03)00006-6

Islam, M. M., Asif, F., Zaman, S. U., Arnab, M. K. H., Rahman, M. M., & Hasan, M. (2023). Effect of charge on the antimicrobial activity of alpha-helical amphibian antimicrobial peptide. *Current Research in Microbial Sciences*, *4*, 100182. https://doi.org/https://doi.org/10.1016/j.crmicr.2023.100182

Jackman, S. H., Evans, E. R., Kuecks-Winger, H. N., Corrie, L. M., Imbery, J. J., Miliano, R. C., . . . Helbing, C. C. (2022). Comparison of transcriptome responses of the liver, tail fin, and olfactory epithelium of Rana [Lithobates] catesbeiana tadpoles disrupted by thyroid hormones and estrogen. *Aquatic Toxicology*, *253*. https://doi.org/10.1016/j.aquatox.2022.106344

Jenssen, H. V., Hamill, P., & Hancock, R. E. W. (2006). Peptide Antimicrobial Agents. *Clinical Microbiology Reviews*, *19*(3), 491-511. https://doi.org/10.1128/cmr.00056-05

Jonas, E., Sargent, T. D., & Dawid, I. B. (1985). Epidermal keratin gene expressed in embryos of Xenopus laevis. *Proceedings of the National Academy of Sciences*, *82*(16), 5413-5417. https://doi.org/10.1073/pnas.82.16.5413

Jones, A. T. (2007). Macropinocytosis: searching for an endocytic identity and role in the uptake of cell penetrating peptides. *Journal of Cellular and Molecular Medicine*, *11*(4), 670-684. https://doi.org/10.1111/j.1582-4934.2007.00062.x

Jumper, J., Evans, R., Pritzel, A., Green, T., Figurnov, M., Ronneberger, O., . . . Hassabis, D. (2021). Highly accurate protein structure prediction with AlphaFold. *Nature*, *596*(7873), 583-589. https://doi.org/10.1038/s41586-021-03819-2

Kabir, S. M. L. (2010). Avian Colibacillosis and Salmonellosis: A Closer Look at Epidemiology, Pathogenesis, Diagnosis, Control and Public Health Concerns. *International Journal of Environmental Research and Public Health*, *7*(1), 89-114. https://doi.org/10.3390/ijerph7010089

Katzenback, B. A., Holden, H. A., Falardeau, J., Childers, C., Hadj-Moussa, H., Avis, T. J., & Storey, K. B. (2014). Regulation of the Rana sylvatica brevinin-1SY

antimicrobial peptide during development and in dorsal and ventral skin in response to freezing, anoxia, and dehydration. *Journal of Experimental Biology*, *217*(8), 1392-1401. https://doi.org/10.1242/jeb.092288

Kim, J.-Y., Park, S.-C., Yoon, M.-Y., Hahm, K.-S., & Park, Y. (2011). C-terminal amidation of PMAP-23: translocation to the inner membrane of Gram-negative bacteria. *Amino Acids*, *40*(1), 183-195. https://doi.org/10.1007/s00726-010-0632-1

Koide, E. M., Abbott, E. A., & Helbing, C. C. (2022). Uncovering early thyroid hormone signalling events through temperature-mediated activation of molecular memory in the cultured bullfrog tadpole tail fin. *General and Comparative Endocrinology*, *323-324*, 114047. https://doi.org/https://doi.org/10.1016/j.ygcen.2022.114047

Koncina, E., Roth, L., Gonthier, B., & Bagnard, D. Role of Semaphorins during Axon Growth and Guidance. In *Advances in Experimental Medicine and Biology* (pp. 50-64). Springer New York. https://doi.org/10.1007/978-0-387-76715-4_4

Kragol, G., Lovas, S., Varadi, G., Condie, B. A., Hoffmann, R., & Otvos, L. (2001). The Antibacterial Peptide Pyrrhocoricin Inhibits the ATPase Actions of DnaK and Prevents Chaperone-Assisted Protein Folding. *Biochemistry*, *40*(10), 3016-3026. https://doi.org/10.1021/bi002656a

Krone, P. H. (2003). Heat shock proteins in development, aging, and evolution. *Seminars in Cell & Developmental Biology*, *14*(5), 249. https://doi.org/https://doi.org/10.1016/j.semcdb.2003.09.017

Krynak, K. L., Burke, D. J., & Benard, M. F. (2015). Larval Environment Alters Amphibian Immune Defenses Differentially across Life Stages and Populations. *PLOS ONE*, *10*(6), e0130383. https://doi.org/10.1371/journal.pone.0130383

Kustanovich, I., Shalev, D. E., Mikhlin, M., Gaidukov, L., & Mor, A. (2002). Structural Requirements for Potent Versus Selective Cytotoxicity for Antimicrobial Dermaseptin S4 Derivatives. *Journal of Biological Chemistry*, *277*(19), 16941-16951. https://doi.org/10.1074/jbc.m111071200

Kyte, J., & Doolittle, R. F. (1982). A simple method for displaying the hydropathic character of a protein. *Journal of Molecular Biology*, *157*(1), 105-132. https://doi.org/https://doi.org/10.1016/0022-2836(82)90515-0

Lai, Y., & Gallo, R. L. (2009). AMPed up immunity: how antimicrobial peptides have multiple roles in immune defense. *Trends in Immunology*, *30*(3), 131-141. https://doi.org/10.1016/j.it.2008.12.003

Landeira-Dabarca, A., Abreu, C. S. R., Álvarez, M., & Molist, P. (2021). Changes in marine turbot (Scophthalmus maximus) epidermis and skin mucus composition during development from bilateral larvae to juvenile flat fish. *Journal of Fish Biology*, *99*(6), 2018-2029. https://doi.org/10.1111/jfb.14910

Lang, T., Hansson, G. C., & Samuelsson, T. (2007). Gel-forming mucins appeared early in metazoan evolution. *Proceedings of the National Academy of Sciences*, *104*(41), 16209-16214. https://doi.org/10.1073/pnas.0705984104

Lee, H., Kwang, Lee, G., Dong, Park, Y., Kang, D.-I., Shin, Y., Song, Hahm, K.-S., & Kim, Y. (2006). Interactions between the plasma membrane and the antimicrobial peptide HP (2-20) and its analogues derived from Helicobacter pylori. *Biochemical Journal*, *394*(1), 105-114. https://doi.org/10.1042/bj20051574

Li, C., Sutherland, D., Hammond, S. A., Yang, C., Taho, F., Bergman, L., . . . Birol, I. (2022). AMPlify: attentive deep learning model for discovery of novel antimicrobial peptides effective against WHO priority pathogens. *BMC Genomics*, *23*(1). https://doi.org/10.1186/s12864-022-08310-4

Lillywhite, H. B., & Licht, P. (1975). A comparative study of integumentary mucous secretions in amphibians. *Comparative Biochemistry and Physiology Part A: Physiology*, *51*(4), 937-941. https://doi.org/https://doi.org/10.1016/0300-9629(75)90077-8

Lin, D., Sutherland, D., Aninta, S. I., Louie, N., Nip, K. M., Li, C., . . . Birol, I. (2022). Mining Amphibian and Insect Transcriptomes for Antimicrobial Peptide Sequences with rAMPage. *Antibiotics*, *11*(7), 952. https://doi.org/10.3390/antibiotics11070952

Love, M. I., Huber, W., & Anders, S. (2014). Moderated estimation of fold change and dispersion for RNA-seq data with DESeq2. *Genome Biology*, *15*(12). https://doi.org/10.1186/s13059-014-0550-8

Lu, Q., & Zhu, L. (2020). The Role of Semaphorins in Metabolic Disorders. *International Journal of Molecular Sciences*, *21*(16), 5641. https://doi.org/10.3390/ijms21165641

Lévesque, M., Guimond, J.-C., Pilote, M., Leclerc, S., Moldovan, F., & Roy, S. (2005). Expression of heat-shock protein 70 during limb development and regeneration in the axolotl. *Developmental Dynamics*, *233*(4), 1525-1534. https://doi.org/10.1002/dvdy.20458

Maher, S. K., Wojnarowicz, P., Ichu, T. A., Veldhoen, N., Lu, L., Lesperance, M., . . . Helbing, C. C. (2016). Rethinking the biological relationships of the thyroid hormones, l-thyroxine and 3,5,3'-triiodothyronine. *Comp Biochem Physiol Part D Genomics Proteomics*, *18*, 44-53. https://doi.org/10.1016/j.cbd.2016.04.002

Mahlapuu, M., Håkansson, J., Ringstad, L., & Björn, C. (2016). Antimicrobial Peptides: An Emerging Category of Therapeutic Agents. *Frontiers in Cellular and Infection Microbiology*, *6*. https://doi.org/10.3389/fcimb.2016.00194

Maniero, G. D., & Carey, C. (1997). Changes in selected aspects of immune function in the leopard frog, Rana pipiens , associated with exposure to cold. *Journal of Comparative Physiology B: Biochemical, Systemic, and Environmental Physiology*, *167*(4), 256-263. https://doi.org/10.1007/s003600050072

Mathew, A. G., Cissell, R., & Liamthong, S. (2007). Antibiotic Resistance in Bacteria Associated with Food Animals: A United States Perspective of Livestock Production. *Foodborne Pathogens and Disease*, *4*(2), 115-133. https://doi.org/10.1089/fpd.2006.0066

McCubbin, K. D., Anholt, R. M., de Jong, E., Ida, J. A., Nóbrega, D. B., Kastelic, J. P., . . . Barkema, H. W. (2021). Knowledge Gaps in the Understanding of Antimicrobial Resistance in Canada [Review]. *Frontiers in Public Health*, *9*.

Mirdita, M., Schütze, K., Moriwaki, Y., Heo, L., Ovchinnikov, S., & Steinegger, M. (2022). ColabFold: making protein folding accessible to all. *Nature Methods*, *19*(6), 679-682. https://doi.org/10.1038/s41592-022-01488-1

Miyatani, S., Winkles, J. A., Sargent, T. D., & Dawid, I. B. (1986). Stage-specific keratins in Xenopus laevis embryos and tadpoles: the XK81 gene family. *The Journal of cell biology*, *103*(5), 1957-1965. https://doi.org/10.1083/jcb.103.5.1957

Mochizuki, K., Goda, T., & Yamauchi, K. (2012). Gene expression profile in the liver of Rana catesbeiana tadpoles exposed to low temperature in the presence of thyroid hormone. *Biochemical and Biophysical Research Communications*, *420*(4), 845-850. https://doi.org/https://doi.org/10.1016/j.bbrc.2012.03.085

Moeller, L. C., Cao, X., Dumitrescu, A. M., Seo, H., & Refetoff, S. (2006). Thyroid hormone mediated changes in gene expression can be initiated by cytosolic action of the thyroid hormone receptor β through the phosphatidylinositol 3-kinase pathway. *Nuclear Receptor Signaling*, *4*(1), nrs.04020. https://doi.org/10.1621/nrs.04020

Mookherjee, N., Brown, K. L., Bowdish, D. M. E., Doria, S., Falsafi, R., Hokamp, K., . . . Hancock, R. E. W. (2006). Modulation of the TLR-Mediated Inflammatory Response by the Endogenous Human Host Defense Peptide LL-371. *The Journal of Immunology*, *176*(4), 2455-2464. https://doi.org/10.4049/jimmunol.176.4.2455

Mulchandani, R., Wang, Y., Gilbert, M., & Van Boeckel, T. P. (2023). Global trends in antimicrobial use in food-producing animals: 2020 to 2030. *PLOS Global Public Health*, *3*(2), e0001305. https://doi.org/10.1371/journal.pgph.0001305

Mullur, R., Liu, Y. Y., & Brent, G. A. (2014). Thyroid hormone regulation of metabolism. *Physiol Rev*, *94*(2), 355-382. https://doi.org/10.1152/physrev.00030.2013

Mura, M., Wang, J., Zhou, Y., Pinna, M., Zvelindovsky, A. V., Dennison, S. R., & Phoenix, D. A. (2016). The effect of amidation on the behaviour of antimicrobial peptides. *European Biophysics Journal*, *45*(3), 195-207. https://doi.org/10.1007/s00249-015-1094-x

Murata, T., & Yamauchi, K. (2005). Low-Temperature Arrest of the Triiodothyronine-Dependent Transcription in Rana catesbeiana Red Blood Cells. *Endocrinology*, *146*(1), 256-264. https://doi.org/10.1210/en.2004-1090

Naghmouchi, K., Le Lay, C., Baah, J., & Drider, D. (2012). Antibiotic and antimicrobial peptide combinations: synergistic inhibition of Pseudomonas fluorescens and antibiotic-resistant variants. *Research in Microbiology*, *163*(2), 101-108. https://doi.org/https://doi.org/10.1016/j.resmic.2011.11.002

Nguyen, T. T. T., Allan, B., Wheler, C., Köster, W., Gerdts, V., & Dar, A. (2021). Avian antimicrobial peptides: in vitro and in ovo characterization and protection from

early chick mortality caused by yolk sac infection. *Scientific Reports*, *11*(1). https://doi.org/10.1038/s41598-021-81734-2

Nhung, N., Chansiripornchai, N., & Carrique-Mas, J. (2017). Antimicrobial Resistance in Bacterial Poultry Pathogens: A Review. *Frontiers in Veterinary Sciences*, *4*, 1-17. https://doi.org/10.3389/fvets.2017.00126

Nota, B. (2017). Gogadget: An R Package for Interpretation and Visualization of GO Enrichment Results. *Molecular Informatics*, *36*(5-6), 1600132. https://doi.org/10.1002/minf.201600132

Nussey, S., & Whitehead, S. (2001). *Chapter 3, The thyroid gland*. Oxford: BIOS Scientific Publishers. https://doi.org/https://www.ncbi.nlm.nih.gov/books/NBK28/

Ottesen, O. H., & Olafsen, J. A. (1997). Ontogenetic development and composition of the mucous cells and the occurrence of saccular cells in the epidermis of Atlantic halibut. *Journal of Fish Biology*, *50*(3), 620-633. https://doi.org/10.1111/j.1095-8649.1997.tb01954.x

Pan, Y.-L., Cheng, J. T.-J., Hale, J., Pan, J., Hancock, R. E. W., & Straus, S. K. (2007). Characterization of the Structure and Membrane Interaction of the Antimicrobial Peptides Aurein 2.2 and 2.3 from Australian Southern Bell Frogs. *Biophysical Journal*, *92*(8), 2854-2864. https://doi.org/10.1529/biophysj.106.097238

Park, C. B., Kim, H. S., & Kim, S. C. (1998). Mechanism of Action of the Antimicrobial Peptide Buforin II: Buforin II Kills Microorganisms by Penetrating the Cell Membrane and Inhibiting Cellular Functions. *Biochemical and Biophysical Research Communications*, *244*(1), 253-257. https://doi.org/https://doi.org/10.1006/bbrc.1998.8159

Park, Y., Park, S.-C., Park, H.-K., Shin, S. Y., Kim, Y., & Hahm, K.-S. (2007). Structure-activity relationship of HP (2–20) analog peptide: Enhanced antimicrobial activity by N-terminal random coil region deletion. *Biopolymers*, *88*(2), 199-207. https://doi.org/10.1002/bip.20679

Paul, B., Sterner, Z. R., Buchholz, D. R., Shi, Y.-B., & Sachs, L. M. (2022). Thyroid and Corticosteroid Signaling in Amphibian Metamorphosis. *Cells*, *11*(10), 1595. https://doi.org/10.3390/cells11101595

Pereira, S., Cline, D. L., Glavas, M. M., Covey, S. D., & Kieffer, T. J. (2021). Tissue-Specific Effects of Leptin on Glucose and Lipid Metabolism. *Endocr Rev*, *42*(1), 1-28. https://doi.org/10.1210/endrev/bnaa027

Pertea, M., Pertea, G. M., Antonescu, C. M., Chang, T.-C., Mendell, J. T., & Salzberg, S. L. (2015). StringTie enables improved reconstruction of a transcriptome from RNA-seq reads. *Nature Biotechnology*, *33*(3), 290-295. https://doi.org/10.1038/nbt.3122

Pirtskhalava, M., Vishnepolsky, B., Grigolava, M., & Managadze, G. (2021). Physicochemical Features and Peculiarities of Interaction of AMP with the Membrane. *Pharmaceuticals*, *14*(5), 471. https://doi.org/10.3390/ph14050471

Poulsen, R., Jackman, S. H., Hansen, M., & Helbing, C. C. (2023). Relationship between serum thyroid hormones and their associated metabolites, and gene expression bioindicators in the back skin of Rana [Lithobates] catesbeiana tadpoles and frogs during metamorphosis [Original Research]. *Frontiers in Endocrinology*, *13*. https://doi.org/10.3389/fendo.2022.1103051

Ribas, L., Li, M.-S., Doddington, B. J., Robert, J., Seidel, J. A., Kroll, J. S., . . . Fisher, M. C. (2009). Expression Profiling the Temperature-Dependent Amphibian Response to Infection by Batrachochytrium dendrobatidis. *PLoS ONE*, *4*(12), e8408. https://doi.org/10.1371/journal.pone.0008408

Richter, A., Sutherland, D., Ebrahimikondori, H., Babcock, A., Louie, N., Li, C., . . . Birol, I. (2022). Associating Biological Activity and Predicted Structure of Antimicrobial Peptides from Amphibians and Insects. *Antibiotics*, *11*(12), 1710. https://doi.org/10.3390/antibiotics11121710

Robak, M. J., Reinert, L. K., Rollins-Smith, L. A., & Richards-Zawacki, C. L. (2019). Out in the cold and sick: Low temperatures and fungal infections impair a frog's skin defenses. *Journal of Experimental Biology*, *222*(18), jeb209445. https://doi.org/10.1242/jeb.209445

Robert, J., & Ohta, Y. (2009). Comparative and developmental study of the immune system in Xenopus. *Developmental Dynamics*, *238*(6), 1249-1270. https://doi.org/10.1002/dvdy.21891

Robinson, D. H., & Heintzelman, M. B. (1987). Morphology of ventral epidermis ofRana catesbeiana during metamorphosis. *The Anatomical Record*, *217*(3), 305-317. https://doi.org/10.1002/ar.1092170310

Rollins-Smith, L. A. (1998). Metamorphosis and the amphibian immune system. *Immunological Reviews*, *166*(1), 221-230. https://doi.org/10.1111/j.1600-065x.1998.tb01265.x

Rollins-Smith, L. A. (2017). Amphibian immunity–stress, disease, and climate change. *Developmental & Comparative Immunology*, *66*, 111-119. https://doi.org/https://doi.org/10.1016/j.dci.2016.07.002

Rollins-Smith, L. A., Ramsey, J. P., Pask, J. D., Reinert, L. K., & Woodhams, D. C. (2011). Amphibian Immune Defenses against Chytridiomycosis: Impacts of Changing Environments. *Integrative and Comparative Biology*, *51*(4), 552-562. https://doi.org/10.1093/icb/icr095

Sauer, E. L., Cohen, J. M., Lajeunesse, M. J., Mcmahon, T. A., Civitello, D. J., Knutie, S. A., . . . Rohr, J. R. (2020). A meta-analysis reveals temperature, dose, life stage, and taxonomy influence host susceptibility to a fungal parasite. *Ecology*, *101*(4). https://doi.org/10.1002/ecy.2979

Schreiber, A. M., & Brown, D. D. (2003). Tadpole skin dies autonomously in response to thyroid hormone at metamorphosis. *Proceedings of the National Academy of Sciences*, *100*(4), 1769-1774. https://doi.org/10.1073/pnas.252774999

Seyfi, R., Kahaki, F. A., Ebrahimi, T., Montazersaheb, S., Eyvazi, S., Babaeipour, V., & Tarhriz, V. (2020). Antimicrobial Peptides (AMPs): Roles, Functions and

Mechanism of Action [Article]. *International Journal of Peptide Research and Therapeutics*, *26*(3), 1451-1463. https://doi.org/10.1007/s10989-019-09946-9

Sforça, M. L., Oyama, Sérgio, Canduri, F., Lorenzi, C. C. B., Pertinhez, T. A., Konno, K., . . . Spisni, A. (2004). How C-Terminal Carboxyamidation Alters the Biological Activity of Peptides from the Venom of the Eumenine Solitary Wasp. *Biochemistry*, *43*(19), 5608-5617. https://doi.org/10.1021/bi0360915

Shahmiri, M., & Mechler, A. (2020). The role of C-terminal amidation in the mechanism of action of the antimicrobial peptide aurein 1.2. *The EuroBiotech Journal*, *4*(1), 25-31. https://doi.org/10.2478/ebtj-2020-0004

Shai, Y. (2002). Mode of action of membrane active antimicrobial peptides. *Biopolymers*, *66*(4), 236-248. https://doi.org/10.1002/bip.10260

Shalev, D. E., Mor, A., & Kustanovich, I. (2002). Structural Consequences of Carboxyamidation of Dermaseptin S3. *Biochemistry*, *41*(23), 7312-7317. https://doi.org/10.1021/bi016013m

Shannon, P., Markiel, A., Ozier, O., Baliga, N. S., Wang, J. T., Ramage, D., . . . Ideker, T. (2003). Cytoscape: A Software Environment for Integrated Models of Biomolecular Interaction Networks. *Genome Research*, *13*(11), 2498-2504. https://doi.org/10.1101/gr.1239303

Shi, Y.-B. (2000). *Amphibian metamorphosis: from morphology to molecular biology*. Wiley-Liss.

Shi, Y.-B. (2009). Dual Functions of Thyroid Hormone Receptors in Vertebrate Development: The Roles of Histone-Modifying Cofactor Complexes. *Thyroid*, *19*(9), 987-999. https://doi.org/10.1089/thy.2009.0041

Shi, Y.-B. (2013). Unliganded Thyroid Hormone Receptor Regulates Metamorphic Timing via the Recruitment of Histone Deacetylase Complexes. In *Current Topics in Developmental Biology* (pp. 275-297). Elsevier. https://doi.org/10.1016/b978-0-12-396968-2.00010-5

Shi, Y.-B., Matsuura, K., Fujimoto, K., Wen, L., & Fu, L. (2012). Thyroid hormone receptor actions on transcription in amphibia: The roles of histone modification and chromatin disruption. *Cell & Bioscience*, *2*(1), 42. https://doi.org/10.1186/2045-3701-2-42

Shih, R. J., & Vanable, J. W. (1975). The development of skin mucous glands ofXenopus laevis during metamorphosis. *Wilhelm Roux's Archives of Developmental Biology*, *177*(3), 183-191. https://doi.org/10.1007/bf00848079

Simmaco, M., Mignogna, G., & Barra, D. (1998). Antimicrobial peptides from amphibian skin: What do they tell us? *Peptide Science*, *47*(6), 435-450. https://doi.org/https://doi.org/10.1002/(SICI)1097-0282(1998)47:6<435::AID-BIP3>3.0.CO;2-8

Skirrow, R. C., Veldhoen, N., Domanski, D., & Helbing, C. C. (2008). Roscovitine inhibits thyroid hormone-induced tail regression of the frog tadpole and reveals a role for cyclin C/Cdk8 in the establishment of the metamorphic gene expression

program. *Developmental Dynamics*, *237*(12), 3787-3797. https://doi.org/10.1002/dvdy.21800

Spohn, R., Daruka, L., Lázár, V., Martins, A., Vidovics, F., Grézal, G., . . . Pál, C. (2019). Integrated evolutionary analysis reveals antimicrobial peptides with limited resistance. *Nature Communications*, *10*(1). https://doi.org/10.1038/s41467-019-12364-6

Stothard, P. (2000). The Sequence Manipulation Suite: JavaScript Programs for Analyzing and Formatting Protein and DNA Sequences. *BioTechniques*, *28*(6), 1102-1104. https://doi.org/10.2144/00286ir01

Strandberg, E., Tiltak, D., Ieronimo, M., Kanithasen, N., Wadhwani, P., & Ulrich, A. S. (2007). Influence of C-terminal amidation on the antimicrobial and hemolytic activities of cationic α-helical peptides. *Pure and Applied Chemistry*, *79*(4), 717-728. https://doi.org/doi:10.1351/pac200779040717

Subbalakshmi, C., Nagaraj, R., & Sitaram, N. (1999). Biological activities of C-terminal 15-residue synthetic fragment of melittin: design of an analog with improved antibacterial activity. *FEBS Letters*, *448*(1), 62-66. https://doi.org/10.1016/s0014-5793(99)00328-2

Suzuki, K., Hayashita, H., Yoshizato, K., Bach Kristensen, D., Sato, K., & Katsu, K. (2001). Novel Rana keratin genes and their expression during larval to adult epidermal conversion in bullfrog tadpoles. *Differentiation*, *68*(1), 44-54. https://doi.org/https://doi.org/10.1046/j.1432-0436.2001.068001044.x

Suzuki, K.-I., Machiyama, F., Nishino, S., Watanabe, Y., Kashiwagi, K., Kashiwagi, A., & Yoshizato, K. (2009). Molecular features of thyroid hormone-regulated skin remodeling in Xenopus laevis during metamorphosis. *Development, Growth & Differentiation*, *51*(4), 411-427. https://doi.org/10.1111/j.1440-169x.2009.01100.x

Taylor, A. C., & Kollros, J. J. (1946). Stages in the normal development of *Rana pipiens* larvae. *The Anatomical Record*, *94*, 7-13.

Thambirajah, A. A., Koide, E. M., Imbery, J. J., & Helbing, C. C. (2019). Contaminant and Environmental Influences on Thyroid Hormone Action in Amphibian Metamorphosis. *Frontiers in Endocrinology*, *10*, 276. https://doi.org/10.3389/fendo.2019.00276

Thornton, D. J., Rousseau, K., & Mcguckin, M. A. (2008). Structure and Function of the Polymeric Mucins in Airways Mucus. *Annual Review of Physiology*, *70*(1), 459-486. https://doi.org/10.1146/annurev.physiol.70.113006.100702

Toledo, R. C., & Jared, C. (1995). Cutaneous granular glands and amphibian venoms. *Comparative Biochemistry and Physiology Part A: Physiology*, *111*(1), 1-29. https://doi.org/https://doi.org/10.1016/0300-9629(95)98515-I

Tornesello, A. L., Borrelli, A., Buonaguro, L., Buonaguro, F. M., & Tornesello, M. L. (2020). Antimicrobial Peptides as Anticancer Agents: Functional Properties and Biological Activities. *Molecules*, *25*(12), 2850. https://doi.org/10.3390/molecules25122850

Torres, M. D. T., Sothiselvam, S., Lu, T. K., & De La Fuente-Nunez, C. (2019). Peptide Design Principles for Antimicrobial Applications. *Journal of Molecular Biology*, *431*(18), 3547-3567. https://doi.org/10.1016/j.jmb.2018.12.015

Van Boeckel, T. P., Brower, C., Gilbert, M., Grenfell, B. T., Levin, S. A., Robinson, T. P., . . . Laxminarayan, R. (2015). Global trends in antimicrobial use in food animals. *Proceedings of the National Academy of Sciences*, *112*(18), 5649-5654. https://doi.org/10.1073/pnas.1503141112

Varga, J. F. A., Bui-Marinos, M. P., & Katzenback, B. A. (2019). Frog Skin Innate Immune Defences: Sensing and Surviving Pathogens. *Frontiers in Immunology*, *9*. https://doi.org/10.3389/fimmu.2018.03128

Wang, G. (2020). Bioinformatic Analysis of 1000 Amphibian Antimicrobial Peptides Uncovers Multiple Length-Dependent Correlations for Peptide Design and Prediction. *Antibiotics*, *9*(8), 491. https://doi.org/10.3390/antibiotics9080491

Wang, G., Li, X., & Wang, Z. (2015). APD3: the antimicrobial peptide database as a tool for research and education. *Nucleic Acids Research*, *44*(D1), D1087-D1093. https://doi.org/10.1093/nar/gkv1278

Wang, Z., & Brown, D. D. (1993). Thyroid hormone-induced gene expression program for amphibian tail resorption. *J Biol Chem*, *268*(22), 16270-16278.

Wanninger, M., Schwaha, T., & Heiss, E. (2018). Form and Function of the skin glands in the Himalayan newt Tylototriton verrucosus. *Zoological Letters*, *4*(1). https://doi.org/10.1186/s40851-018-0095-x

Watanabe, Y., Kobayashi, H., Suzuki, K.-i., Kotani, K., & Yoshizato, K. (2001). New epidermal keratin genes from Xenopus laevis: hormonal and regional regulation of their expression during anuran skin metamorphosis. *Biochimica et Biophysica Acta (BBA) - Gene Structure and Expression*, *1517*(3), 339-350. https://doi.org/https://doi.org/10.1016/S0167-4781(00)00281-5

Wickham, H. (2016). ggplot2: Elegant Graphics for Data Analysis. *Springer-Verlag York*.

Woodhams, D. C., Alford, R. A., Antwis, R. E., Archer, H., Becker, M. H., Belden, L. K., . . . Mckenzie, V. (2015). Antifungal isolates database of amphibian skin-associated bacteria and function against emerging fungal pathogens. *Ecology*, *96*(2), 595-595. https://doi.org/10.1890/14-1837.1

Woodhams, D. C., Bell, S. C., Bigler, L., Caprioli, R. M., Chaurand, P., Lam, B. A., . . . Rollins-Smith, L. A. (2016). Life history linked to immune investment in developing amphibians. *Conservation Physiology*, *4*(1), cow025. https://doi.org/10.1093/conphys/cow025

Wright, M. L., Proctor, K. L., & Alves, C. D. (1999). Hormonal profiles correlated with season, cold, and starvation in Rana catesbeiana (bullfrog) tadpoles. *Comparative Biochemistry and Physiology Part C: Pharmacology, Toxicology and Endocrinology*, *124*(1), 109-116. https://doi.org/10.1016/s0742-8413(99)00060-2

Yamamoto, K., Kanski, D., & Frieden, E. (1966). The uptake and excretion of thyroxine, triiodothyronine and iodide in bullfrog tadpoles after immersion or injection at 25° and 6°C. *General and Comparative Endocrinology*, *6*(3), 312-324. https://doi.org/https://doi.org/10.1016/S0016-6480(66)80019-9

Yoshizato, K. (1992). Death and Transformation of Larval Cells during Metamorphosis of Anura. *Development, Growth and Differentiation*, *34*(6), 607-612. https://doi.org/10.1111/j.1440-169x.1992.tb00028.x

You, S. H., Liao, X., Weiss, R. E., & Lazar, M. A. (2010). The interaction between nuclear receptor corepressor and histone deacetylase 3 regulates both positive and negative thyroid hormone action in vivo. *Mol Endocrinol*, *24*(7), 1359-1367. https://doi.org/10.1210/me.2009-0501

Young, M. D., Wakefield, M. J., Smyth, G. K., & Oshlack, A. (2010). Gene ontology analysis for RNA-seq: accounting for selection bias. *Genome Biology*, *11*(2), R14. https://doi.org/10.1186/gb-2010-11-2-r14

Zasloff, M. (2002). Antimicrobial peptides of multicellular organisms. *Nature*, *415*(6870), 389-395. https://doi.org/10.1038/415389a

Zelezetsky, I., Pacor, S., Pag, U., Papo, N., Shai, Y., Sahl, H.-G., & Tossi, A. (2005). Controlled alteration of the shape and conformational stability of α-helical cell-lytic peptides: effect on mode of action and cell specificity. *Biochemical Journal*, *390*(1), 177-188. https://doi.org/10.1042/bj20042138

6. Supplementary Figures

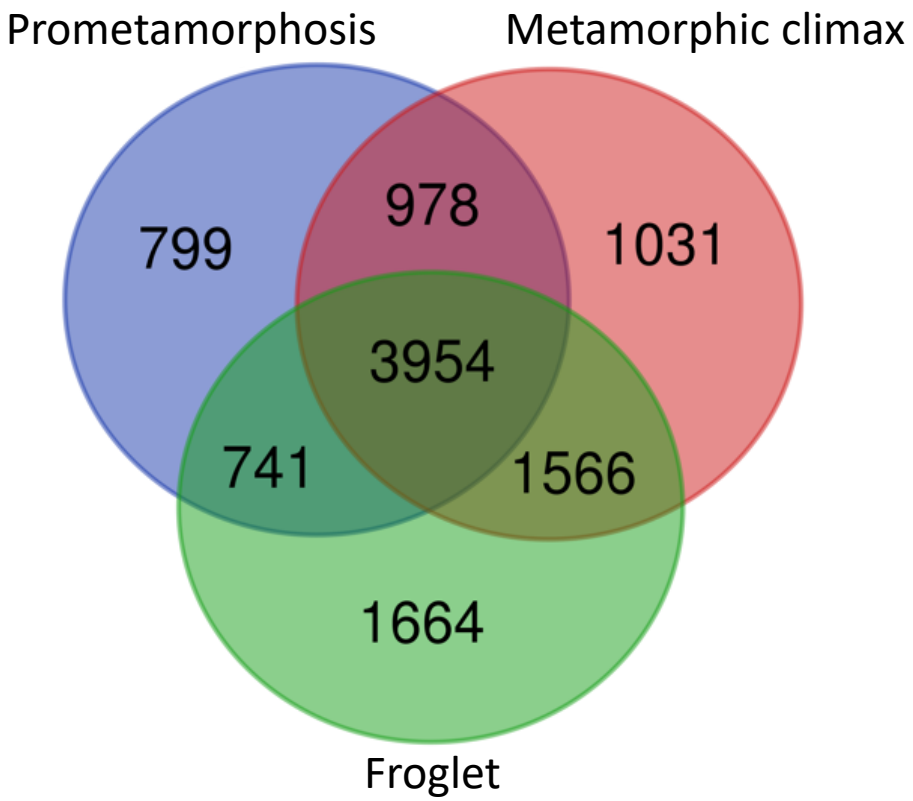

Supplementary Figure 6-1 Comparison of the number of DE genes in the back skin of *R. catesbeiana* undergoing natural metamorphosis. DE ($p_{adj} \leq 0.05$) during prometamorphosis (blue), at metamorphic climax (red), or as froglets (green) compared to premetamorphic tadpoles as identified by DESeq2. DE gene data was used for GO analysis.

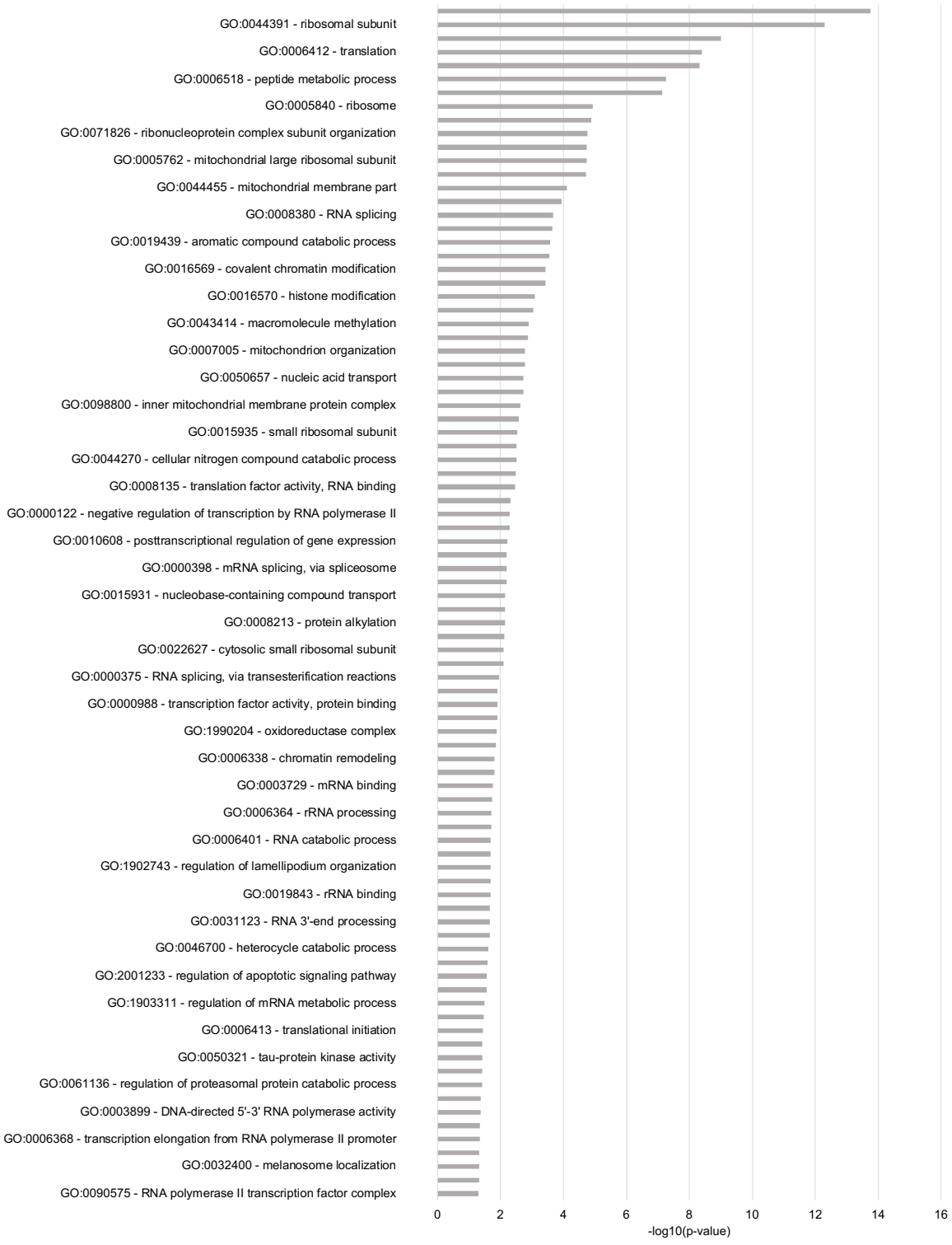

Supplementary Figure 6-2 Natural metamorphosis: The negative $\log_{10}$ of the p-value for all GO terms enriched in *R. catesbeiana* back skin during prometamorphosis compared to the premetamorphic tadpole.

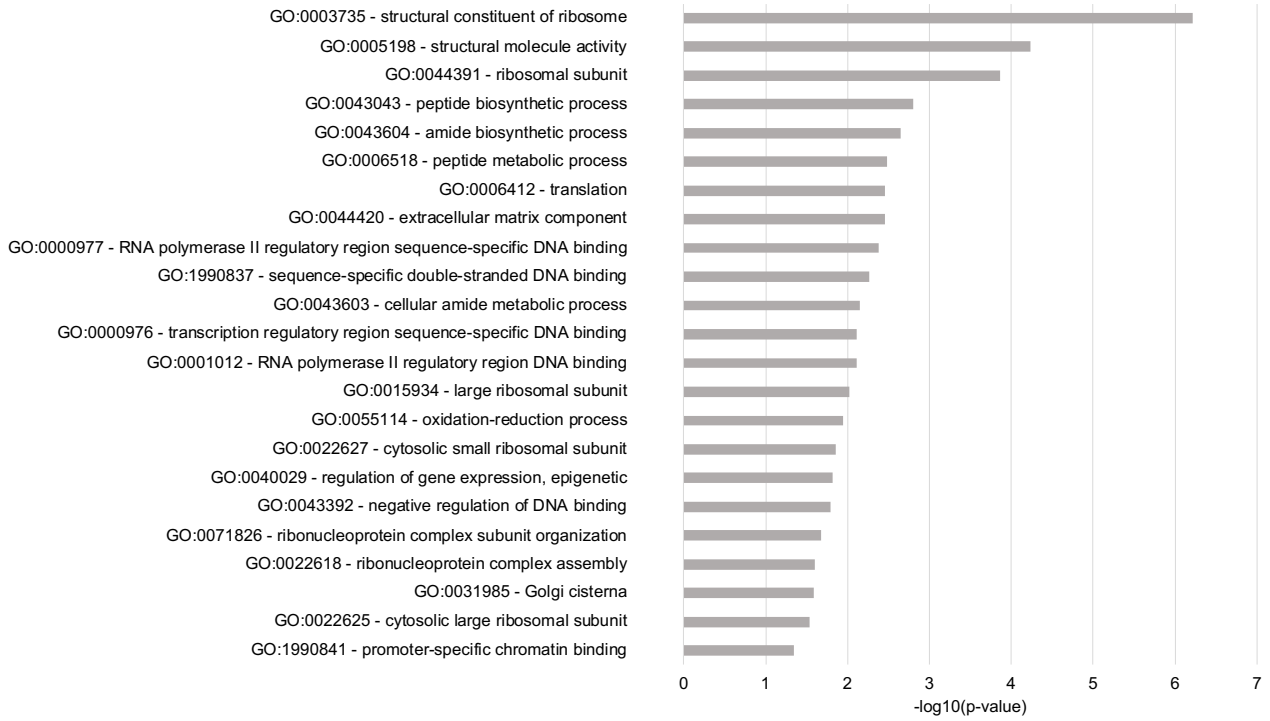

Supplementary Figure 6-3 Natural metamorphosis: The negative $\log_{10}$ of the p-value for all GO terms enriched in *R. catesbeiana* back skin at metamorphic climax compared to the premetamorphic tadpole.

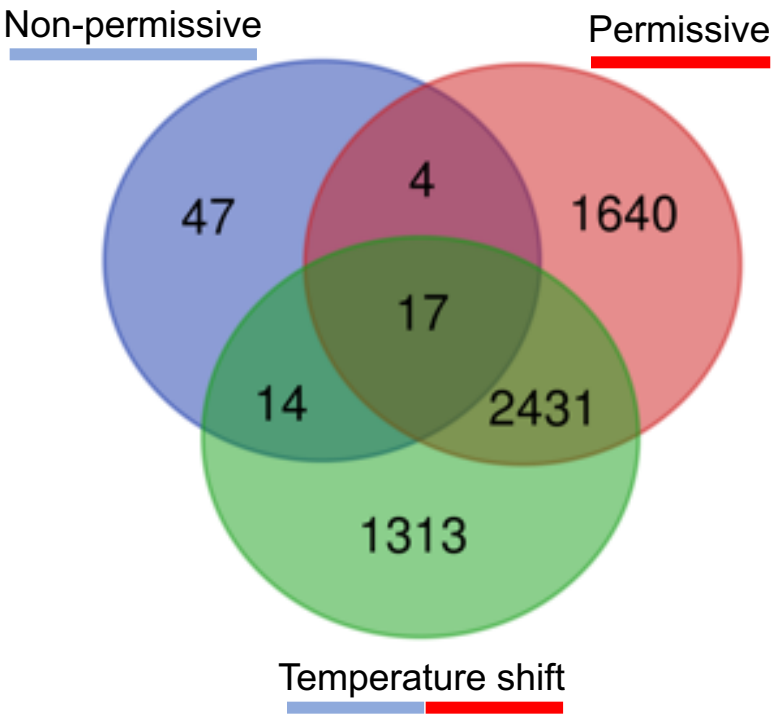

Supplementary Figure 6-4 Comparison of the number of DE genes in the back skin treated of *R. catesbeiana* tadpoles injected with 10 nM T_3. DE ($p_{adj} \leq 0.05$) in response to non-permissive (blue), permissive (red), or shift (green) conditions were identified by DESeq2. DE gene data was used for GO analysis.

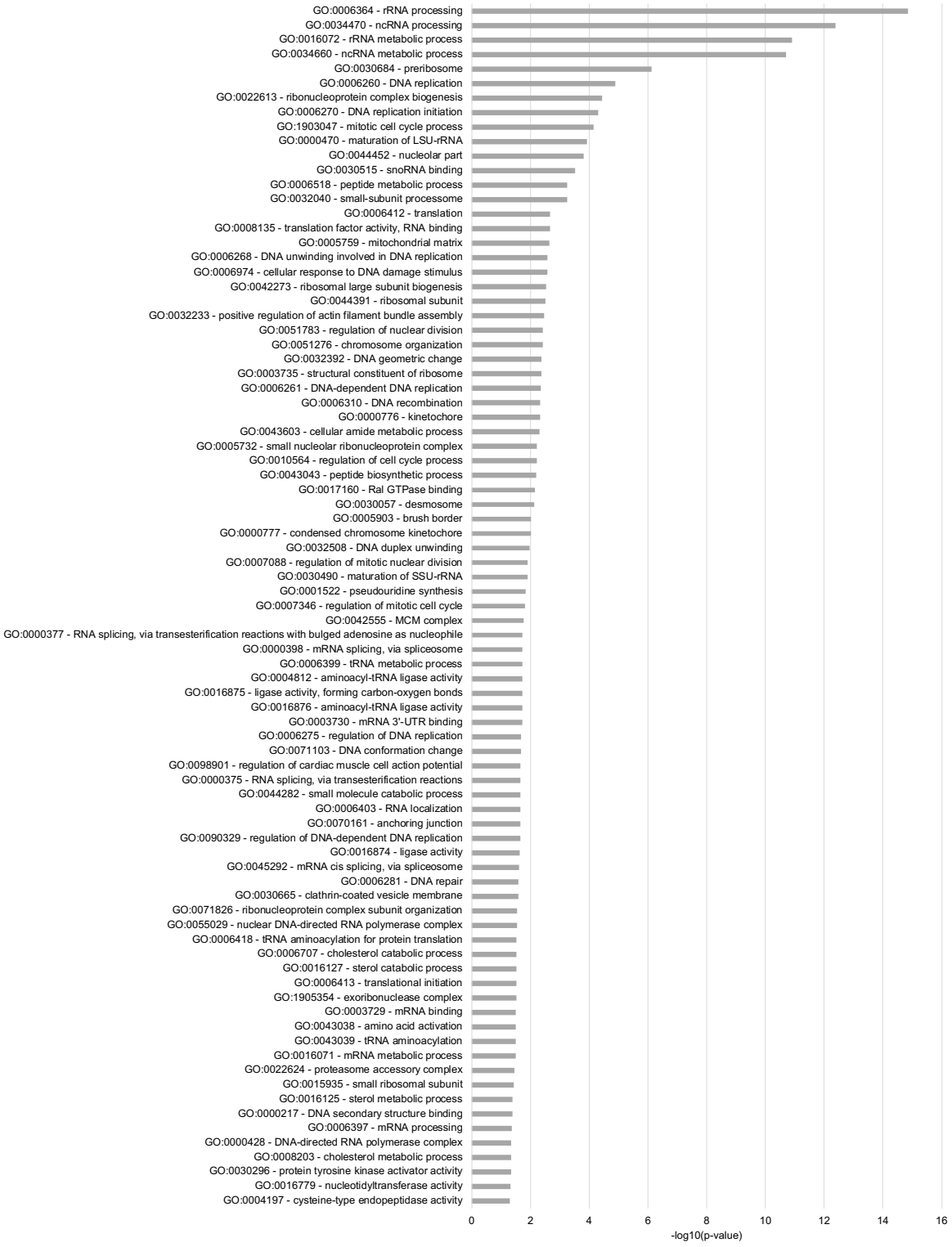

Supplementary Figure 6-5 Temperature mediation: The negative $\log_{10}$ of the p-value for all GO terms enriched in *R. catesbeiana* back skin at permissive temperatures after TH injection.

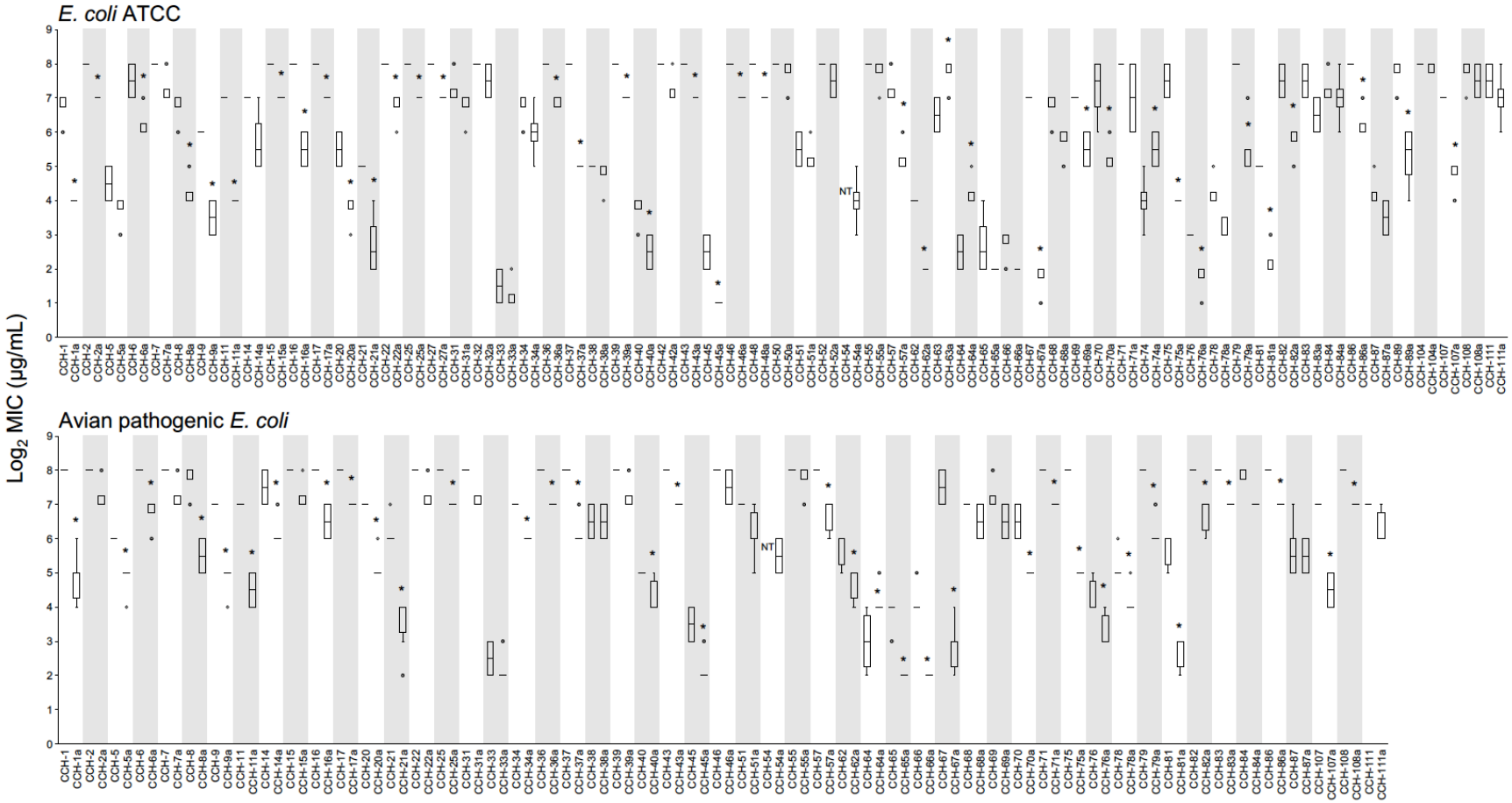

Supplementary Figure 6-6 Pairwise comparison of the antimicrobial activity of the un-amidated and amidated novel AMPs against *E. coli* ATCC and APEC. Only AMPs with activity in at least one of the paired AMPs are shown. The horizontal bars represent the median $\log_2$(MIC). The white and grey sections indicate paired un-amidated and amidated AMPs. An "*" indicates a significant difference of the amidated AMP from the un-amidated version ($p_{adj} \leq 0.05$). CCH-54, which was not synthesizable, is indicated by NT for "Not tested".

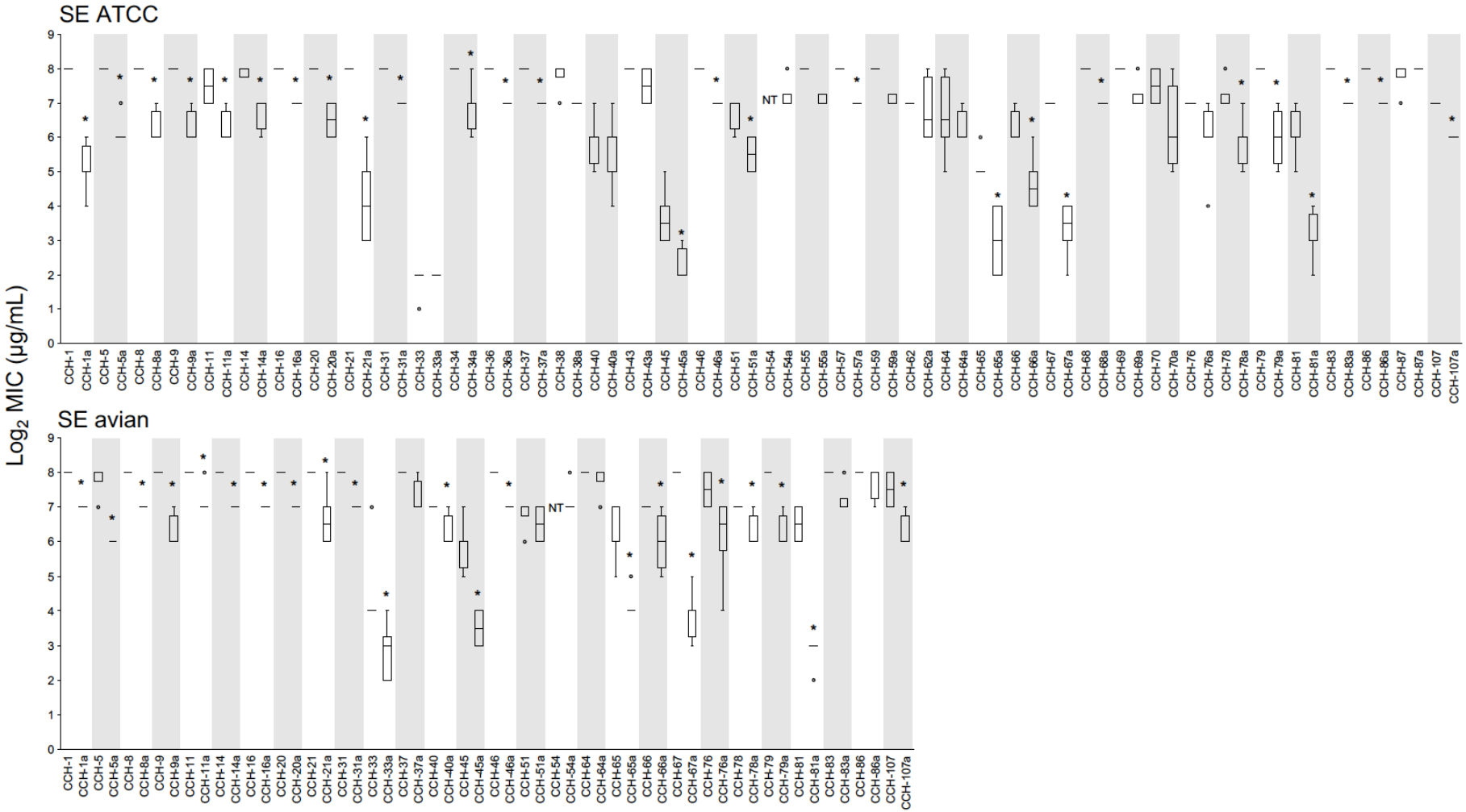

Supplementary Figure 6-7 Pairwise comparison of the antimicrobial activity of the un-amidated and amidated novel AMPs against SE ATCC and SE avian. Only AMPs with activity in at least one of the paired AMPs are shown. See Supplementary Figure 6-6 for more details.

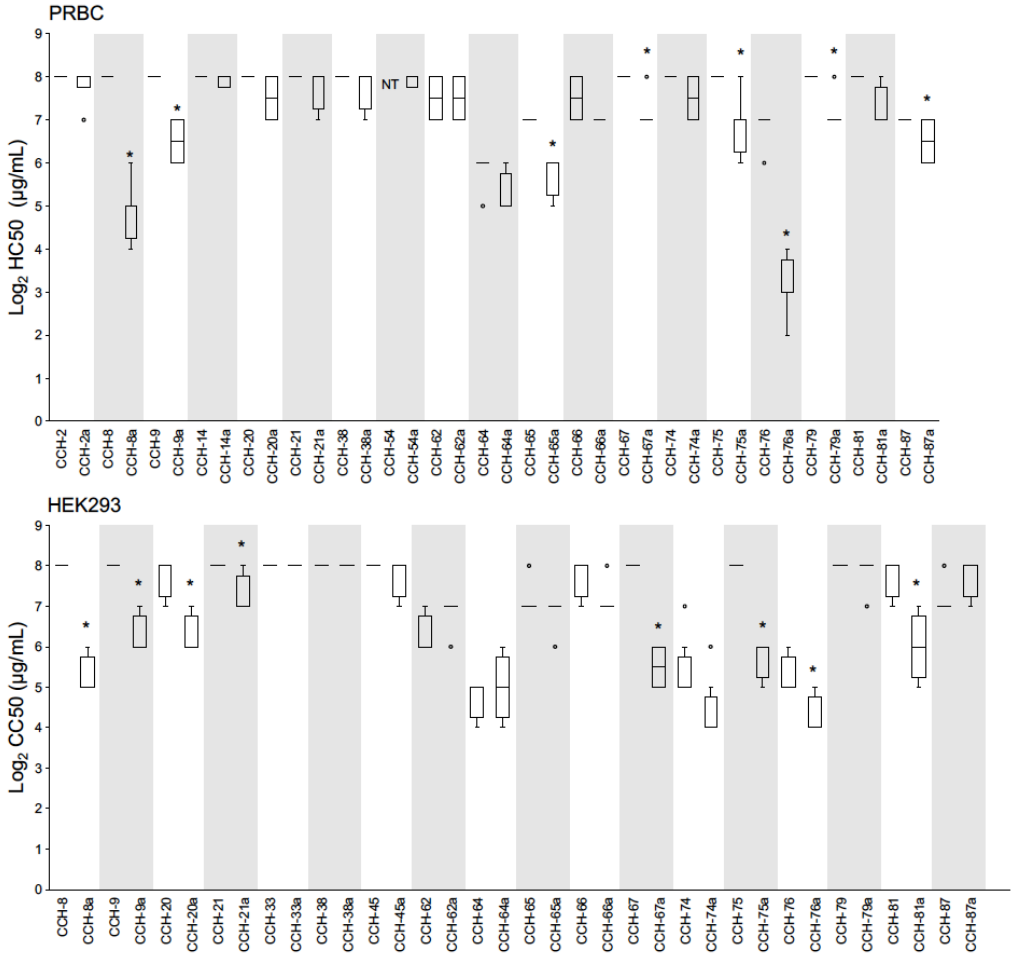

Supplementary Figure 6-8 Pairwise comparison of the hemolytic (PRBC) or cytotoxic (HEK293) activity of the un-amidated and amidated novel AMPs. HC50 is defined as the AMP concentration needed to lyse 50% of the PRBCs. CC50 is defined as the concentration of AMP needed to reduce cell viability of the HEK293 cells by 50%. Only AMPs with activity in at least one of the paired AMPs are shown for the PRBCs. All data is shown for HEK293. The horizontal bars represent the median $\log_2$(HC50 or CC50). See Supplementary Figure 6-6 for more details.

7. Supplementary Tables

Supplementary Table 7-1 150 base pair paired-end reads sequenced from back skin of *R. catesbeiana* tadpoles during natural metamorphosis. The reads were mapped to the *R. catesbeiana* genome (DOI 10.5281/zenodo.8125199). The mean and standard error of the mean (SEM) are shown.

Stage	Animal #	Input Reads	Mapped Reads	% Mapped Reads
Premetamorphosis	1	56,610,494	42,996,025	75.95%
	2	67,783,254	51,708,053	76.28%
	3	78,764,583	60,305,198	76.56%
	4	39,097,022	29,986,944	76.70%
	5	72,799,604	56,791,275	78.01%
Prometamorphosis	1	39,991,791	31,053,041	77.65%
	2	29,974,552	23,465,882	78.29%
	3	32,162,488	25,207,065	78.37%
	4	32,049,590	25,017,349	78.06%
	5	33,146,042	25,804,660	77.85%
	6	34,999,371	27,529,851	78.66%
	7	36,154,095	28,107,655	77.74%
	8	34,777,165	27,289,524	78.47%
	9	38,327,135	29,954,067	78.15%
	10	35,414,789	27,499,366	77.65%
Metamorphic climax	1	52,002,174	41,345,897	79.51%
	2	39,568,532	31,046,581	78.46%
	3	36,780,198	28,722,069	78.09%
	4	27,062,462	21,570,930	79.71%
	5	39,154,157	30,904,475	78.93%
	6	34,414,667	26,887,201	78.13%
	7	36,654,765	28,664,747	78.20%
	8	49,041,173	38,570,427	78.65%
	9	46,727,695	36,605,745	78.34%
	10	39,893,401	31,006,419	77.72%
	11	41,144,381	32,130,337	78.09%
	12	48,919,979	37,688,081	77.04%
	13	39,188,263	30,335,722	77.41%
Froglet	1	52,640,121	41,041,733	77.97%
	2	49,943,998	38,749,207	77.59%
	3	38,311,902	30,382,887	79.30%
	4	46,974,736	36,347,863	77.38%
	5	42,139,160	32,297,378	76.64%
	Mean	43,109,507	33,545,868	77.93%
	SEM	2,077,898	1,579,560	0.0015

Supplementary Table 7-2 150 base pair paired-end reads sequenced from back skin of *R. catesbeiana* tadpoles during temperature modulated TH-induced metamorphosis. See Supplementary Table 7-1 legend for more details.

Condition	Treatment	Animal ID	Input Reads	Mapped Reads	% Mapped Reads
Non-permissive	Control	TS-NP-C-108	68,307,592	53,771,665	78.72%
		TS-NP-C-109	80,802,170	63,590,641	78.70%
		TS-NP-C-112	63,113,496	49,162,534	77.90%
		TS-NP-C-113	63,421,297	49,866,718	78.63%
		TS-NP-C-114	99,757,869	77,733,271	77.92%
	TH	TS-NP-T3-106	48,583,046	37,795,931	77.80%
		TS-NP-T3-110	69,737,293	54,592,275	78.28%
		TS-NP-T3-111	115,264,326	90,029,909	78.11%
		TS-NP-T3-117	74,923,314	58,850,969	78.55%
		TS-NP-T3-120	71,006,287	55,383,755	78.00%
Permissive	Control	TS-P-C-1	39,073,492	30,527,488	78.13%
		TS-P-C-17	60,285,950	47,090,199	78.11%
		TS-P-C-5	48,300,244	38,077,356	78.83%
		TS-P-C-6	46,884,983	36,672,717	78.22%
		TS-P-C-7	42,694,544	33,273,142	77.93%
	TH	TS-P-T3-20	73,724,744	56,992,634	77.30%
		TS-P-T3-3	41,596,873	32,766,559	78.77%
		TS-P-T3-4	39,765,297	31,348,930	78.83%
		TS-P-T3-8	32,464,335	24,683,521	76.03%
		TS-P-T3-9	38,701,703	29,517,105	76.27%
Shift	Control	TS-Sh-C-228	82,853,522	64,652,988	78.03%
		TS-Sh-C-234	83,459,678	65,061,814	77.96%
		TS-Sh-C-235	98,186,817	75,912,504	77.31%
		TS-Sh-C-238	30,687,300	23,716,850	77.29%
		TS-Sh-C-240	65,749,334	50,949,593	77.49%
	TH	TS-Sh-T3-226	57,784,384	43,645,277	75.53%
		TS-Sh-T3-227	54,312,307	42,213,408	77.72%
		TS-Sh-T3-229	67,770,170	51,928,509	76.62%
		TS-Sh-T3-230	86,529,262	66,663,385	77.04%
		TS-Sh-T3-233	58,516,401	44,958,424	76.83%
		Mean	63,475,268	49,381,002	77.76%
		SEM	3,769,194	2,942,223	0.00

Supplementary Table 7-3 List of differentially expressed transcripts and their fold changes (FC) identified in the back skin of *R. catesbeiana* in the non-permissive condition after TH exposure ($p_{adj} \geq 0.05$).

ContigID	FC	Annotation
AB205_0 0398442-RB	840.1	XM_040332469.1_89.893_2246_PREDICTED:_Rana_temporaria_tuftelin_1_ (TUFT1),_transcript_variant_X1,_mRNA
AB205_0 0395826-RA	51.9	MG459289.1_99.598_5963_Rana_catesbeiana_thyroid_hormone-induced_bZip_protein_variant_1_(thibz)_mRNA,_complete_cds
AB205_0 0411257-RA	18.4	XM_040332964.1_93.408_713_PREDICTED:_Rana_temporaria_semaphori n_4A_(SEMA4A),_transcript_variant_X6,_mRNA
AB205_0 0397862-RA	16.0	XM_040354241.1_93.837_1217_PREDICTED:_Rana_temporaria_UBX_dom ain_protein_2B_(UBXN2B),_mRNA
AB205_0 0389089-RA	7.0	XM_040343214.1_91.045_1474_PREDICTED:_Rana_temporaria_leptin_(LO C120931606),_mRNA
AB205_0 0390098-RA	6.0	XM_040348357.1_91.925_1226_PREDICTED:_Rana_temporaria_squalene_ synthase-like_(LOC120936190),_transcript_variant_X1,_mRNA
AB205_0 0402102-RA	4.9	XM_040355183.1_84.097_1157_PREDICTED:_Rana_temporaria_cytochrom e_P450_2C3-like_(LOC120941653),_mRNA
AB205_0 0394707-RA	4.2	XM_040341986.1_87.818_903_PREDICTED:_Rana_temporaria_protein_mo no-ADP-ribosyltransferase_PARP14-like_(LOC120930809),_mRNA
AB205_0 0389227-RA	4.2	XM_040323203.1_93.266_594_PREDICTED:_Rana_temporaria_cytochrome _P450_2G1-like_(LOC120913333),_mRNA
AB205_0 0406042-RA	4.1	XM_040333418.1_92.857_658_PREDICTED:_Rana_temporaria_selenium_b inding_protein_1_(SELENBP1),_mRNA
AB205_0 0396752-RE	4.1	XM_040345361.1_90.634_662_PREDICTED:_Rana_temporaria_ubiquitin_s pecific_peptidase_18_(USP18),_transcript_variant_X3,_mRNA
AB205_0 0401148-RB	3.9	XM_040349600.1_95.799_976_PREDICTED:_Rana_temporaria_receptor-transporting_protein_3-like_(LOC120936871),_mRNA
AB205_0 0410016-RA	3.9	XM_040332243.1_92.586_1160_PREDICTED:_Rana_temporaria_NACHT,_ LRR_and_PYD_domains-containing_protein_3-like_(LOC120920264),_transcript_variant_X5,_mRNA
AB205_0 0402509-RB	3.8	XM_040340633.1_92.889_450_PREDICTED:_Rana_temporaria_sterol_O-acyltransferase_2-like_(LOC120929305),_mRNA
AB205_0 0399765-RA	3.6	XM_040352658.1_96.359_1758_PREDICTED:_Rana_temporaria_frizzled_cl ass_receptor_8_(FZD8),_mRNA
AB205_0 0400821-RA	3.5	XM_040348649.1_94.805_308_PREDICTED:_Rana_temporaria_radical_S-adenosyl_methionine_domain_containing_2_(RSAD2),_mRNA

AB205_0 0406298-RA	3.5	XM_040352720.1_96.407_334_PREDICTED:_Rana_temporaria_insulin_induced_gene_1_(INSIG1),_mRNA
AB205_0 0403422-RB	3.4	XM_040333418.1_92.237_438_PREDICTED:_Rana_temporaria_selenium_binding_protein_1_(SELENBP1),_mRNA
AB205_0 0407024-RA	3.4	XM_040353787.1_93.778_1125_PREDICTED:_Rana_temporaria_SRY-box_transcription_factor_4_(SOX4),_mRNA
AB205_0 0400826-RA	3.3	XM_040324316.1_94.438_809_PREDICTED:_Rana_temporaria_B-box_and_SPRY_domain_containing_(BSPRY),_mRNA
AB205_0 0403854-RB	3.3	XM_040322441.1_90.371_1454_PREDICTED:_Rana_temporaria_interferon-induced_protein_with_tetratricopeptide_repeats_1-like_(LOC120910689),_mRNA
AB205_0 0400465-RA	3.3	XM_040346760.1_93.369_558_PREDICTED:_Rana_temporaria_flavin-containing_monooxygenase_FMO_GS-OX4-like_(LOC120933517),_mRNA
AB205_0 0401147-RA	3.2	XM_040349600.1_93.662_568_PREDICTED:_Rana_temporaria_receptor-transporting_protein_3-like_(LOC120936871),_mRNA
AB205_0 0401148-RA	3.2	XM_040349600.1_95.323_1069_PREDICTED:_Rana_temporaria_receptor-transporting_protein_3-like_(LOC120936871),_mRNA
AB205_0 0400820-RA	3.1	XM_040348649.1_94.819_386_PREDICTED:_Rana_temporaria_radical_S-adenosyl_methionine_domain_containing_2_(RSAD2),_mRNA
AB205_0 0396752-RD	3.0	XM_040345359.1_93.142_1327_PREDICTED:_Rana_temporaria_ubiquitin_specific_peptidase_18_(USP18),_transcript_variant_X1,_mRNA
AB205_0 0409251-RA	3.0	XM_040327065.1_94.184_10781_PREDICTED:_Rana_temporaria_sacsin-like_(LOC120916210),_mRNA
AB205_0 0390275-RA	3.0	XM_040352729.1_96.835_948_PREDICTED:_Rana_temporaria_X-ray_repair_cross_complementing_2_(XRCC2),_transcript_variant_X1,_mRNA
AB205_0 0404665-RA	2.6	XM_040351497.1_98.000_750_PREDICTED:_Rana_temporaria_SERTA_domain_containing_4_(SERTAD4),_transcript_variant_X2,_mRNA
AB205_0 0396766-RB	2.5	XM_040349954.1_89.024_3134_PREDICTED:_Rana_temporaria_cyclic_GMP-AMP_synthase-like_(LOC120937033),_mRNA
AB205_0 0389187-RA	2.5	BT081954.1_100.000_702_Rana_catesbeiana_clone_rcat-evr-521-095_Three_prime_repair_exonuclease_2_putative_mRNA,_complete_cds
AB205_0 0411213-RA	2.5	U08604.1_99.659_879_Rana_catesbeiana_transcription_factor_RcC/EBP-1_mRNA,_complete_cds
AB205_0 0405847-RA	2.4	XM_040355998.1_92.656_4698_PREDICTED:_Rana_temporaria_up-regulator_of_cell_proliferation-like_(LOC120942985),_mRNA
AB205_0 0395809-RA	2.4	XM_040348585.1_97.576_660_PREDICTED:_Rana_temporaria_Rho_associated_coiled-coil_containing_protein_kinase_2_(ROCK2),_transcript_variant_X5,_mRNA

AB205_0 0405354-RA	2.3	XM_040355873.1_93.359_4608_PREDICTED:_Rana_temporaria_interferon-induced_very_large_GTPase_1-like_(LOC120942919),_transcript_variant_X2,_mRNA
AB205_0 0405112-RA	2.3	XM_040339015.1_90.647_417_PREDICTED:_Rana_temporaria_interferon-induced_GTP-binding_protein_Mx2-like_(LOC120927976),_transcript_variant_X2,_mRNA
AB205_0 0392821-RA	2.3	XM_018556033.1_81.356_708_PREDICTED:_Nanorana_parkeri_interferon_regulatory_factor_7-like_(LOC108786686),_mRNA
AB205_0 0400634-RA	2.3	XM_040323183.1_97.736_1767_PREDICTED:_Rana_temporaria_ectoderm-neural_cortex_protein_1-like_(LOC120913314),_mRNA
AB205_0 0409471-RA	2.2	XM_040356180.1_91.087_561_PREDICTED:_Rana_temporaria_nuclear_protein_1,_transcriptional_regulator_(NUPR1),_mRNA
AB205_0 0395931-RA	2.2	XM_040342662.1_97.683_3841_PREDICTED:_Rana_temporaria_semaphorin_6D_(SEMA6D),_transcript_variant_X4,_mRNA
AB205_0 0405954-RA	2.0	XM_040336051.1_93.569_1073_PREDICTED:_Rana_temporaria_aquaporin_3_(Gill_blood_group)_(AQP3),_mRNA
AB205_0 0403343-RA	1.9	XM_040332991.1_95.170_352_PREDICTED:_Rana_temporaria_probable_ATP-dependent_RNA_helicase_DDX60_(LOC120920741),_mRNA
AB205_0 0400819-RA	1.8	BT081933.1_99.843_635_Rana_catesbeiana_clone_rcat-evr-537-364_Probable_thymidylate_kinase_1_putative_mRNA,_complete_cds
AB205_0 0400206-RA	1.8	XM_040323163.1_95.192_936_PREDICTED:_Rana_temporaria_SERTA_domain_containing_1_(SERTAD1),_transcript_variant_X2,_mRNA
AB205_0 0410221-RA	1.8	XM_040356286.1_91.139_790_PREDICTED:_Rana_temporaria_E3_ubiquitin/ISG15_ligase_TRIM25-like_(LOC120943149),_transcript_variant_X2,_mRNA
AB205_0 0402845-RA	1.8	XM_040345609.1_94.154_1762_PREDICTED:_Rana_temporaria_basic_helix-loop-helix_family_member_e41_(BHLHE41),_mRNA
AB205_0 0403885-RA	1.8	XM_040350787.1_93.921_658_PREDICTED:_Rana_temporaria_interferon-induced,_double-stranded_RNA-activated_protein_kinase-like_(LOC120937509),_transcript_variant_X2,_mRNA
AB205_0 0391345-RA	1.7	XM_040324681.1_91.815_1014_PREDICTED:_Rana_temporaria_immediate_early_response_5_like_(IER5L),_mRNA
AB205_0 0392260-RA	1.7	XM_040356946.1_96.541_636_PREDICTED:_Rana_temporaria_suppressor_of_cytokine_signaling_1_(SOCS1),_mRNA
AB205_0 0400876-RA	1.7	XM_040338793.1_93.579_2009_PREDICTED:_Rana_temporaria_lipase_I_(LIPI),_transcript_variant_X1,_mRNA
AB205_0 0406350-RA	1.7	XM_040343659.1_93.776_2378_PREDICTED:_Rana_temporaria_Pim-3_proto-oncogene,_serine/threonine_kinase_(PIM3),_transcript_variant_X1,_mRNA
AB205_0 0395487-RA	1.6	XM_040330190.1_95.607_387_PREDICTED:_Rana_temporaria_probable_ATP-dependent_RNA_helicase_DHX58_(LOC120918553),_transcript_variant_X5,_mRNA

AB205_0 0391962-RB	1.6	XM_040352529.1_96.321_5599_PREDICTED:_Rana_temporaria_Rho_GTPase_activating_protein_21_(ARHGAP21),_transcript_variant_X3,_mRNA
AB205_0 0396395-RB	1.6	XM_040360330.1_93.546_1410_PREDICTED:_Rana_temporaria_DExD/H-box_helicase_58_(DDX58),_mRNA
AB205_0 0408826-RA	1.6	XM_040355832.1_89.865_148_PREDICTED:_Rana_temporaria_kringle_containing_transmembrane_protein_2_(KREMEN2),_mRNA
AB205_0 0401288-RB	1.6	XM_040337869.1_93.842_1153_PREDICTED:_Rana_temporaria_E74_like_ETS_transcription_factor_3_(ELF3),_transcript_variant_X1,_mRNA
AB205_0 0395436-RA	1.6	XR_005743477.1_90.211_1328_PREDICTED:_Rana_temporaria_membrane_transport_protein_XK-like_(LOC120913045),_transcript_variant_X2,_misc_RNA
AB205_0 0399973-RA	1.5	XM_040327831.1_97.159_1901_PREDICTED:_Rana_temporaria_neurexin_2_(NRXN2),_transcript_variant_X7,_mRNA
AB205_0 0402110-RA	1.4	XM_040345984.1_92.780_1953_PREDICTED:_Rana_temporaria_uncharacterized_LOC120933038_(LOC120933038),_transcript_variant_X4,_mRNA
AB205_0 0394314-RA	1.4	XM_018569227.1_91.183_1792_PREDICTED:_Nanorana_parkeri_NEDD4_binding_protein_3_(N4BP3),_mRNA
AB205_0 0407660-RA	1.4	XM_040357482.1_95.370_1296_PREDICTED:_Rana_temporaria_BRCA1_associated_RING_domain_1_(BARD1),_transcript_variant_X2,_mRNA
AB205_0 0392299-RA	1.3	No_Annotation
AB205_0 0399019-RA	1.2	XM_040346056.1_96.632_1247_PREDICTED:_Rana_temporaria_ubiquitin_conjugating_enzyme_E2_D4_(putative)_(UBE2D4),_mRNA
AB205_0 0396247-RB	0.9	XM_040353012.1_97.128_1184_PREDICTED:_Rana_temporaria_DNA_topoisomerase_II_beta_(TOP2B),_transcript_variant_X5,_mRNA
AB205_0 0400810-RA	0.7	XM_040346326.1_92.079_808_PREDICTED:_Rana_temporaria_centromere_protein_E_(CENPE),_mRNA
AB205_0 0396908-RA	0.6	XM_040359891.1_94.014_4026_PREDICTED:_Rana_temporaria_assembly_factor_for_spindle_microtubules_(ASPM),_mRNA
AB205_0 0389998-RB	0.5	XM_040332030.1_94.724_417_PREDICTED:_Rana_temporaria_IQ_motif_containing_GTPase_activating_protein_3_(IQGAP3),_mRNA
AB205_0 0400122-RA	0.5	XM_040359859.1_91.194_670_PREDICTED:_Rana_temporaria_kinesin_family_member_14_(KIF14),_mRNA
AB205_0 0391758-RC	0.5	XM_040350983.1_95.334_3922_PREDICTED:_Rana_temporaria_signal_induced_proliferation_associated_1_like_2_(SIPA1L2),_transcript_variant_X1,_mRNA
AB205_0 0394920-RA	0.4	XM_040352410.1_90.285_2594_PREDICTED:_Rana_temporaria_integrin_subunit_alpha_8_(ITGA8),_mRNA

AB205_0 0404227-RA	0.4	XM_040362310.1_93.593_874_PREDICTED:_Rana_temporaria_DNA_damage_inducible_transcript_4_(DDIT4),_mRNA
AB205_0 0395803-RB	0.3	XM_040346149.1_93.218_1622_PREDICTED:_Rana_temporaria_nudix_hydrolase_18_(NUDT18),_mRNA
AB205_0 0388682-RA	0.3	XM_040324011.1_96.731_826_PREDICTED:_Rana_temporaria_F-box_and_WD_repeat_domain_containing_2_(FBXW2),_transcript_variant_X2,_mRNA
AB205_0 0391173-RA	0.3	XM_040344317.1_96.007_1753_PREDICTED:_Rana_temporaria_sodium-coupled_monocarboxylate_transporter_1-like_(LOC120932143),_mRNA
AB205_0 0394324-RB	0.3	XM_040346826.1_90.460_1153_PREDICTED:_Rana_temporaria_uncharacterized_LOC120933565_(LOC120933565),_mRNA
AB205_0 0397156-RB	0.2	XM_040341225.1_97.266_768_PREDICTED:_Rana_temporaria_trafficking_regulator_and_scaffold_protein_tamalin_(TAMALIN),_mRNA
AB205_0 0399019-RB	0.2	XM_040346056.1_96.632_1247_PREDICTED:_Rana_temporaria_ubiquitin_conjugating_enzyme_E2_D4_(putative)_(UBE2D4),_mRNA
AB205_0 0402831-RA	0.2	XM_040339420.1_90.000_1330_PREDICTED:_Rana_temporaria_mucin-2-like_(LOC120928323),_mRNA
AB205_0 0403291-RA	0.2	XM_040337898.1_93.403_1728_PREDICTED:_Rana_temporaria_pancreatic_secretory_granule_membrane_major_glycoprotein_GP2-like_(LOC120927314),_mRNA
AB205_0 0391874-RE	0.1	XM_040347282.1_93.820_890_PREDICTED:_Rana_temporaria_Rab_interacting_lysosomal_protein_like_1_(RILPL1),_transcript_variant_X4,_mRNA
AB205_0 0400615-RA	0.1	BT081728.1_98.925_93_Rana_catesbeiana_clone_rcat-evr-507-254_Glutathione_S-transferase_P_1_putative_mRNA,_complete_cds
AB205_0 0390252-RF	0.00	XM_040331617.1_97.082_514_PREDICTED:_Rana_temporaria_matrilin_4_(MATN4),_transcript_variant_X3,_mRNA
AB205_0 0394776-RB	0.00	XM_040324599.1_95.287_1167_PREDICTED:_Rana_temporaria_NADPH_dependent_diflavin_oxidoreductase_1_(NDOR1),_transcript_variant_X3,_mRNA

Supplementary Table 7-4 List of differentially expressed genes and their fold changes (FC) identified in the back skin of *R. catesbeiana* in the non-permissive condition after TH exposure ($p_{adj} \geq 0.05$).

ContigID	FC	Annotation
AB205_0039 5826	52.0	MG459289.1_99.598_5963_Rana_catesbeiana_thyroid_hormone-induced_bZip_protein_variant_1_(thibz)_mRNA,_complete_cds
RACA.6504	18.3	XM_040332964.1_93.408_713_PREDICTED:_Rana_temporaria_semaphorin_4A_(SEMA4A),_transcript_variant_X6,_mRNA
RACA.539	7.0	XM_040343214.1_91.045_1474_PREDICTED:_Rana_temporaria_leptin_(LOC120931606),_mRNA
RACA.27	6.0	XM_040348357.1_91.925_1226_PREDICTED:_Rana_temporaria_squalene_synthase-like_(LOC120936190),_transcript_variant_X1,_mRNA
RACA.6617	4.9	XM_040355183.1_84.097_1157_PREDICTED:_Rana_temporaria_cytochrome_P450_2C3-like_(LOC120941653),_mRNA
RACA.2321	4.2	XM_040341986.1_87.818_903_PREDICTED:_Rana_temporaria_protein_mono-ADP-ribosyltransferase_PARP14-like_(LOC120930809),_mRNA
RACA.6215	4.1	XM_040333418.1_92.857_658_PREDICTED:_Rana_temporaria_selenium_binding_protein_1_(SELENBP1),_mRNA
RACA.6534	3.9	XM_040332243.1_92.586_1160_PREDICTED:_Rana_temporaria_NACHT,_LRR_and_PYD_domains-containing_protein_3-like_(LOC120920264),_transcript_variant_X5,_mRNA
AB205_0038 9227	3.8	XM_040323207.1_89.607_356_PREDICTED:_Rana_temporaria_cytochrome_P450_2G1-like_(LOC120913337),_mRNA
RACA.6531	3.6	XM_040326301.1_94.131_426_PREDICTED:_Rana_temporaria_indolethylamine_N-methyltransferase-like_(LOC120915632),_mRNA
RACA.3005	3.6	XM_040352658.1_96.359_1758_PREDICTED:_Rana_temporaria_frizzled_class_receptor_8_(FZD8),_mRNA
AB205_0040 0821	3.5	XM_040348649.1_94.805_308_PREDICTED:_Rana_temporaria_radical_S-adenosyl_methionine_domain_containing_2_(RSAD2),_mRNA
RACA.4606	3.5	XM_040352720.1_96.407_334_PREDICTED:_Rana_temporaria_insulin_induced_gene_1_(INSIG1),_mRNA
RACA.5155	3.5	XM_040333418.1_92.237_438_PREDICTED:_Rana_temporaria_selenium_binding_protein_1_(SELENBP1),_mRNA

RACA.2853	3.4	XM_040353787.1_93.778_1125_PREDICTED:_Rana_temporaria_SRY-box_transcription_factor_4_(SOX4),_mRNA
AB205_0040 0826	3.3	XM_040324316.1_94.438_809_PREDICTED:_Rana_temporaria_B-box_and_SPRY_domain_containing_(BSPRY),_mRNA
RACA.4181	3.3	XM_040322441.1_90.371_1454_PREDICTED:_Rana_temporaria_interferon-induced_protein_with_tetratricopeptide_repeats_1-like_(LOC120910689),_mRNA
AB205_0040 0465	3.3	XM_040346760.1_93.369_558_PREDICTED:_Rana_temporaria_flavin-containing_monooxygenase_FMO_GS-OX4-like_(LOC120933517),_mRNA
RACA.2764	3.2	XM_040349600.1_93.662_568_PREDICTED:_Rana_temporaria_receptor-transporting_protein_3-like_(LOC120936871),_mRNA
RACA.2765	3.2	XM_040349600.1_95.323_1069_PREDICTED:_Rana_temporaria_receptor-transporting_protein_3-like_(LOC120936871),_mRNA
RACA.2223	3.1	XM_040348649.1_94.819_386_PREDICTED:_Rana_temporaria_radical_S-adenosyl_methionine_domain_containing_2_(RSAD2),_mRNA
RACA.5170	3.0	XM_040327065.1_94.184_10781_PREDICTED:_Rana_temporaria_sacsin-like_(LOC120916210),_mRNA
AB205_0039 0275	3.0	XM_040352729.1_96.835_948_PREDICTED:_Rana_temporaria_X-ray_repair_cross_complementing_2_(XRCC2),_transcript_variant_X1,_mRNA
AB205_0039 1885	2.9	XM_040332971.1_96.958_1808_PREDICTED:_Rana_temporaria_probable_ATP-dependent_RNA_helicase_DDX60_(LOC120920724),_transcript_variant_X2,_mRNA
AB205_0039 9482	2.8	XM_040340038.1_97.865_890_PREDICTED:_Rana_temporaria_kelch_like_family_member_35_(KLHL35),_mRNA
AB205_0039 6752	2.8	XM_040345361.1_90.634_662_PREDICTED:_Rana_temporaria_ubiquitin_specific_peptidase_18_(USP18),_transcript_variant_X3,_mRNA
RACA.4568	2.6	XM_040327404.1_93.864_1206_PREDICTED:_Rana_temporaria_interferon-inducible_GTPase_5-like_(LOC120916436),_mRNA
RACA.3421	2.6	XM_040351497.1_98.000_750_PREDICTED:_Rana_temporaria_SERTA_domain_containing_4_(SERTAD4),_transcript_variant_X2,_mRNA
AB205_0039 2374	2.5	No_Annotation

RACA.718	2.5	BT081954.1_100.000_702_Rana_catesbeiana_clone_rcat-evr-521-095_Three_prime_repair_exonuclease_2_putative_mRNA,_complete_cds
RACA.2509	2.5	XM_040349954.1_89.024_3134_PREDICTED:_Rana_temporaria_cyclic_GMP-AMP_synthase-like_(LOC120937033),_mRNA
RACA.6292	2.5	U08604.1_99.659_879_Rana_catesbeiana_transcription_factor_RcC/EBP-1_mRNA,_complete_cds
RACA.2571	2.4	XM_040355998.1_92.857_4550_PREDICTED:_Rana_temporaria_up-regulator_of_cell_proliferation-like_(LOC120942985),_mRNA
RACA.1611	2.4	XM_040346213.1_85.027_748_PREDICTED:_Rana_temporaria_RING_finger_protein_112-like_(LOC120933167),_transcript_variant_X1,_mRNA
AB205_0040 5354	2.3	XM_040355873.1_93.359_4608_PREDICTED:_Rana_temporaria_interferon-induced_very_large_GTPase_1-like_(LOC120942919),_transcript_variant_X2,_mRNA
RACA.3211	2.3	XM_040353346.1_97.271_1942_PREDICTED:_Rana_temporaria_nuclear_receptor_subfamily_4_group_A_member_3_(NR4A3),_mRNA
AB205_0039 2449	2.3	XM_040348156.1_91.709_591_PREDICTED:_Rana_temporaria_alpha-1,4-N-acetylglucosaminyltransferase-like_(LOC120936057),_transcript_variant_X2,_mRNA
AB205_0040 5112	2.3	XM_040339015.1_90.647_417_PREDICTED:_Rana_temporaria_interferon-induced_GTP-binding_protein_Mx2-like_(LOC120927976),_transcript_variant_X2,_mRNA
AB205_0039 2821	2.3	XM_018556033.1_81.356_708_PREDICTED:_Nanorana_parkeri_interferon_regulatory_factor_7-like_(LOC108786686),_mRNA
RACA.3639	2.3	XM_040323183.1_97.736_1767_PREDICTED:_Rana_temporaria_ectoderm-neural_cortex_protein_1-like_(LOC120913314),_mRNA
RACA.6520	2.2	XM_040356180.1_91.087_561_PREDICTED:_Rana_temporaria_nuclear_protein_1,_transcriptional_regulator_(NUPR1),_mRNA
AB205_0040 4583	2.0	No_Annotation
RACA.3988	2.0	XM_040336051.1_93.569_1073_PREDICTED:_Rana_temporaria_aquaporin_3_(Gill_blood_group)_(AQP3),_mRNA
AB205_0040 3343	1.9	XM_040332991.1_95.170_352_PREDICTED:_Rana_temporaria_probable_ATP-dependent_RNA_helicase_DDX60_(LOC120920741),_mRNA

AB205_0039 2065	1.8	XM_040354022.1_98.253_229_PREDICTED:_Rana_temporaria_TGFB_induced_factor_homeobox_1_(TGIF1),_transcript_variant_X2,_mRNA
RACA.1970	1.8	XM_040323163.1_95.192_936_PREDICTED:_Rana_temporaria_SERTA_domain_containing_1_(SERTAD1),_transcript_variant_X2,_mRNA
AB205_0040 0819	1.8	BT081933.1_99.843_635_Rana_catesbeiana_clone_rcat-evr-537-364_Probable_thymidylate_kinase_1_putative_mRNA,_complete_cds
RACA.5138	1.8	XM_040356286.1_91.139_790_PREDICTED:_Rana_temporaria_E3_ubiquitin/ISG15_ligase_TRIM25-like_(LOC120943149),_transcript_variant_X2,_mRNA
AB205_0040 3885	1.8	XM_040350787.1_93.921_658_PREDICTED:_Rana_temporaria_interferon-induced,_double-stranded_RNA-activated_protein_kinase-like_(LOC120937509),_transcript_variant_X2,_mRNA
AB205_0040 2845	1.8	XM_040345609.1_94.154_1762_PREDICTED:_Rana_temporaria_basic_helix-loop-helix_family_member_e41_(BHLHE41),_mRNA
RACA.9	1.7	XM_040324681.1_91.815_1014_PREDICTED:_Rana_temporaria_immediate_early_response_5_like_(IER5L),_mRNA
RACA.2063	1.7	XM_040356946.1_96.541_636_PREDICTED:_Rana_temporaria_suppressor_of_cytokine_signaling_1_(SOCS1),_mRNA
RACA.3609	1.7	XM_040343659.1_93.776_2378_PREDICTED:_Rana_temporaria_Pim-3_proto-oncogene,_serine/threonine_kinase_(PIM3),_transcript_variant_X1,_mRNA
AB205_0040 0876	1.6	XM_040338793.1_93.579_2009_PREDICTED:_Rana_temporaria_lipase_I_(LIPI),_transcript_variant_X1,_mRNA
AB205_0038 9845	1.6	XM_018569121.1_86.740_543_PREDICTED:_Nanorana_parkeri_interferon_regulatory_factor_5-like_(LOC108797512),_mRNA
AB205_0039 5487	1.6	XM_040330190.1_95.607_387_PREDICTED:_Rana_temporaria_probable_ATP-dependent_RNA_helicase_DHX58_(LOC120918553),_transcript_variant_X5,_mRNA
AB205_0039 6395	1.6	XM_040360330.1_97.308_520_PREDICTED:_Rana_temporaria_DExD/H-box_helicase_58_(DDX58),_mRNA
AB205_0040 8826	1.6	XM_040355832.1_89.865_148_PREDICTED:_Rana_temporaria_kringle_containing_transmembrane_protein_2_(KREMEN2),_mRNA

RACA.1969	1.6	XM_040337869.1_93.842_1153_PREDICTED:_Rana_temporaria_E74_like_ETS_transcription_factor_3_(ELF3),_transcript_variant_X1,_mRNA
AB205_0039 5436	1.6	XR_005743477.1_90.211_1328_PREDICTED:_Rana_temporaria_membrane_transport_protein_XK-like_(LOC120913045),_transcript_variant_X2,_misc_RNA
RACA.3825	1.5	XM_040327831.1_97.159_1901_PREDICTED:_Rana_temporaria_neurexin_2_(NRXN2),_transcript_variant_X7,_mRNA
AB205_0040 2110	1.4	XM_040345984.1_92.780_1953_PREDICTED:_Rana_temporaria_uncharacterized_LOC120933038_(LOC120933038),_transcript_variant_X4,_mRNA
RACA.2091	1.4	XM_018569227.1_91.183_1792_PREDICTED:_Nanorana_parkeri_NEDD4_binding_protein_3_(N4BP3),_mRNA
RACA.659	1.4	XM_040340693.1_94.980_2291_PREDICTED:_Rana_temporaria_Sp1_transcription_factor_(SP1),_mRNA
RACA.5854	1.4	XM_040357482.1_95.370_1296_PREDICTED:_Rana_temporaria_BRCA1_associated_RING_domain_1_(BARD1),_transcript_variant_X2,_mRNA
AB205_0039 2299	1.3	No_Annotation
AB205_0039 9019	1.2	XM_040346056.1_96.632_1247_PREDICTED:_Rana_temporaria_ubiquitin_conjugating_enzyme_E2_D4_(putative)_(UBE2D4),_mRNA
AB205_0039 4237	0.8	XM_040354892.1_91.964_1991_PREDICTED:_Rana_temporaria_TATA-box_binding_protein_associated_factor_2_(TAF2),_transcript_variant_X2,_mRNA
AB205_0040 0810	0.7	XM_040346326.1_92.079_808_PREDICTED:_Rana_temporaria_centromere_protein_E_(CENPE),_mRNA
AB205_0039 6908	0.6	XM_040359891.1_94.014_4026_PREDICTED:_Rana_temporaria_assembly_factor_for_spindle_microtubules_(ASPM),_mRNA
RACA.3957	0.6	XM_040346149.1_93.313_1660_PREDICTED:_Rana_temporaria_nudix_hydrolase_18_(NUDT18),_mRNA
RACA.3269	0.6	XM_040322830.1_93.870_832_PREDICTED:_Rana_temporaria_TSC22_domain_family_protein_3-like_(LOC120913115),_transcript_variant_X2,_mRNA
AB205_0038 9998	0.6	XM_040332030.1_94.724_417_PREDICTED:_Rana_temporaria_IQ_motif_containing_GTPase_activating_protein_3_(IQGAP3),_mRNA
AB205_0040 0122	0.5	XM_040359859.1_91.194_670_PREDICTED:_Rana_temporaria_kinesin_family_member_14_(KIF14),_mRNA
AB205_0039 4920	0.4	XM_040352410.1_90.285_2594_PREDICTED:_Rana_temporaria_integrin_subunit_alpha_8_(ITGA8),_mRNA

RACA.4700	0.4	XM_040362310.1_93.593_874_PREDICTED:_Rana_temporaria_DNA_damage_inducible_transcript_4_(DDIT4),_mRNA
AB205_0039 1173	0.3	XM_040344317.1_95.905_1685_PREDICTED:_Rana_temporaria_sodium-coupled_monocarboxylate_transporter_1-like_(LOC120932143),_mRNA
AB205_0039 4324	0.3	XM_040346826.1_90.546_1026_PREDICTED:_Rana_temporaria_uncharacterized_LOC120933565_(LOC120933565),_mRNA
AB205_0040 2831	0.2	XM_040339420.1_90.000_1330_PREDICTED:_Rana_temporaria_mucin-2-like_(LOC120928323),_mRNA
RACA.6757	0.1	XM_040337898.1_93.403_1728_PREDICTED:_Rana_temporaria_pancreatic_secretory_granule_membrane_major_glycoprotein_GP2-like_(LOC120927314),_mRNA
AB205_0040 0615	0.1	BT081728.1_98.925_93_Rana_catesbeiana_clone_rcat-evr-507-254_Glutathione_S-transferase_P_1_putative_mRNA,_complete_cds
RACA.511	0.003	XM_040346655.1_84.951_1422_PREDICTED:_Rana_temporaria_venom_factor-like_(LOC120933438),_mRNA

Supplementary Table 7-5 *rak* transcript counts for each biological replicate during natural metamorphosis. There is a large discrepancy in the metamorphic climax and froglet counts (either very high or very low).

	***rak* transcript counts**		
	Premetamorphosis (n = 5)		
Control	49277	55803	54346
	147970	171247	162940
	258890	300249	284586
	41613	48409	46239
	92500	106449	102625
	Prometamorphosis (n = 10)	Metamorphic climax (n = 13)	Froglet (n = 5)
Treatment	708376	481204	524004
	810614	687823	3
	361342	708262	0
	696869	989457	4
	680844	896583	681735
	557683	701081	
	510669	4	
	677488	470616	
	538425	658695	
	1093707	622010	
		11	
		8	
		622054	
Median control	92500	106449	102625
Median treatment	679166	622054	4
Fold change	7.3	5.8	0.0
p_{adj}	3.90E-08	0.29	0.78
Significant?	Yes	No	No

Supplementary Table 7-6 Characteristics of 111 novel putative AMPs including organism of origin, sequence, AMPlify score, length, and charge.

Organism	CCH ID	Predicted Mature Peptide Sequence	AMPlify Score	Length	Charge
Alytes multensis	CCH-1	GIKDILKAGFGSLVKK	54.2	16	3
Alytes multensis	CCH-2	ILGAILPLVSGLRSHLG	43.4	17	1
Alytes multensis	CCH-3	ILGAILPLVSGLRSHL	40.8	16	1
Alytes multensis	CCH-4	IIGALLSAATGLRSHLG	39.4	17	1
Alytes multensis	CCH-5	ILGKIIPLVSVLLSHLG	39.3	17	1
Alytes multensis	CCH-6	ILVKIIPLVSGLLSHLG	39.0	17	1
Alytes multensis	CCH-7	IRGALLSAATGLLSHLG	39.0	17	1
Alytes multensis	CCH-8	ILGKILPLVGGLLNNLC	35.9	17	1
Alytes multensis	CCH-9	ILGAILPLVSGLLRHLG	34.7	17	1
Alytes multensis	CCH-10	ILGARLPLVSGLLSHLG	31.3	17	1
Alytes multensis	CCH-11	IRGKIIPLVSGLLSHLG	30.0	17	2
Alytes multensis	CCH-12	ILGKIIP	27.9	7	1
Alytes multensis	CCH-13	ILGKILPLV	26.3	9	1
Alytes multensis	CCH-14	ILGKILPLVSGLLGNL	25.3	16	1
Alytes multensis	CCH-15	IIGKILPLVGGLLNNLG	25.2	17	1
Alytes multensis	CCH-16	ILGKIIPLVSGLLSNLG	25.2	17	1
Alytes multensis	CCH-17	AGLGSLVKNIAAQVANGKR	25.1	19	3
Alytes multensis	CCH-18	ILGKILPL	24.8	8	1
Alytes multensis	CCH-19	ILGKILPLVG	24.0	10	1
Alytes multensis	CCH-20	ILGKILPLVGVLLSNLG	23.7	17	1
Alytes multensis	CCH-21	KNIAAHVANGKRIIGALLSAATGLLSHLG	23.7	29	3
Alytes multensis	CCH-22	ILGAILPLVSGLLSHRG	22.9	17	1
Alytes multensis	CCH-23	GLGSLVKNIAAHEANGKR	21.5	18	2
Alytes multensis	CCH-24	ILGKILPLVGG	20.7	11	1
Alytes multensis	CCH-25	ILGKIVPLVGGLLSNLG	20.3	17	1
Alytes multensis	CCH-26	ILGKILPLVFWITW	20.1	14	1
Alytes multensis	CCH-27	KKKKKKKKKIAAHVANGKR	19.9	19	11
Alytes multensis	CCH-28	ILGKILPLVSG	19.8	11	1
Alytes multensis	CCH-29	GLGSLVINIAAHVANGKR	19.2	18	2
Alytes multensis	CCH-30	ILGKILPFGFWLTW	19.0	14	1
Alytes multensis	CCH-31	GNPKSVRRRKHKQILGRRKKTRI	18.7	23	11
Alytes multensis	CCH-32	ILGKIVPLVGGLLNNLG	18.5	17	1
Alytes multensis	CCH-33	KNIAAHVANGKRILGKILPLVSGLLGNLG	17.8	29	4
Alytes multensis	CCH-34	RIRCFISSSLFPEGFNVKEPSKKKRR	17.5	26	6
Alytes multensis	CCH-35	RFPKRKR	17.4	7	5
Alytes multensis	CCH-36	ILGKILPLVGGLL	16.5	13	1
Alytes multensis	CCH-37	ILGKILPLVSGLLVNLG	16.2	17	1
Alytes multensis	CCH-38	IAAHVANGKRIIGALLSAATGLLSHLG	16.1	27	2
Alytes multensis	CCH-39	ILGKILPLVGGLLN	15.8	14	1
Alytes multensis	CCH-40	VAAHVANGKRILGKILPLVSGLLGNLG	15.7	27	3

Alytes multensis	CCH-41	ILGKIIPLVSG	15.3	11	1
Alytes multensis	CCH-42	ILGKILPLVGGLLSN	15.3	15	1
Alytes multensis	CCH-43	ILGKILPLVGGLLS	14.9	14	1
Alytes multensis	CCH-44	ILGKIIPLVS	14.7	10	1
Alytes multensis	CCH-45	GSLVKGIAAHVANGKRILGAILPLVSGLL	14.7	29	3
Alytes multensis	CCH-46	GAQRGQRRRGAQRGRRKR	14.6	18	9
Alytes multensis	CCH-47	SWFRKSCERYSSSLANGKR	14.2	19	4
Alytes multensis	CCH-48	IRGAILPLVSGLLGNLG	13.4	17	1
Alytes multensis	CCH-49	GTGLSCEKRKAYNWRVTFCCY	13.4	21	3
Alytes multensis	CCH-50	KLVNKTADLKKKKKNIAAHVANGKR	13.4	25	8
Alytes multensis	CCH-51	GAQRGRRKRGAQRGQRRRGAQRGRRKR	13.3	27	14
Alytes multensis	CCH-52	ILGKILPLVGGLLNN	12.9	15	1
Alytes multensis	CCH-53	RFPKSKR	12.8	7	4
Alytes multensis	CCH-54	VDNGKRILGAILPLFSGLLSHLG	12.4	23	1
Alytes multensis	CCH-55	FLGKYISTISRLG	10.8	13	2
Alytes multensis	CCH-56	ILGFLIYVCKI	10.3	11	1
Rana catesbeiana	CCH-57	GFLDNVKSAATSIVDLLLCKMNAACTHK	34.2	28	1
Rana catesbeiana	CCH-58	FPAIICKVSKKLLKLWKLELEII	30.3	23	3
Rana catesbeiana	CCH-59	SMLSVLKRCSP	29.4	11	2
Rana catesbeiana	CCH-60	GLKKLESLRPGLKIHT	25.6	16	3
Rana catesbeiana	CCH-61	FPAIICKVSKNC	24.1	12	2
Rana catesbeiana	CCH-62	EEERFLPFIARLAAKVFPSIICSVTKKC	16.1	28	2
Rana catesbeiana	CCH-63	FLPIIGKILSTVFGKKPRNVETLKMELEII	15.8	30	2
Rana catesbeiana	CCH-64	FLTFIARLAAKVFPSIICSVTKKC	58.4	24	4
Rana catesbeiana	CCH-65	FLPFIARLAAKVFPSITCSVTKKC	55.0	24	4
Rana catesbeiana	CCH-66	FLPFTARLAAKVFPSIICSVTKKC	51.9	24	4
Rana catesbeiana	CCH-67	FLPFIARLAAKVF	29.8	13	2
Rana catesbeiana	CCH-68	EEERFLPFIARLAAKVFPSITCSVTKKC	19.9	28	2
Rana catesbeiana	CCH-69	EEERFLPFTARLAAKVFPSIICSVTKKC	16.8	28	2
Rana catesbeiana	CCH-70	IIDGYRKRLISLIFSKGCATKY	13.6	22	4
Rana catesbeiana	CCH-71	KPKAGKNKLLKKKTTKLSRSSR	12.3	22	10
Rana catesbeiana	CCH-72	FLPNVGSSGGWRSKSSIAATMPIKRCH	11.5	27	4
Rana catesbeiana	CCH-73	SRRSMSPRGAFPVSFVHFFVE	11.2	21	2
Rana catesbeiana	CCH-74	FLPFIALLAAKVFPSIICSVTKKC	54.5	24	3
Rana catesbeiana	CCH-75	FLFPLITSFLSKF	47.1	13	1

Rana catesbeiana	CCH-76	FLPFIARLAAKVFPSIICSVTKKF	46.1	24	4
Rana catesbeiana	CCH-77	GLFLDTLKGAAKNV	45.8	14	1
Rana catesbeiana	CCH-78	GLFLDTLKGAAKDVAGKLLEGLKCKITRM	45.4	29	3
Rana catesbeiana	CCH-79	FLPFIARLAAKL	34.8	12	2
Rana catesbeiana	CCH-80	GLFLDTLKGAAKDVAGEIAGRSKM	34.4	24	1
Rana catesbeiana	CCH-81	FLPFIARLAAKFF	33.3	13	2
Rana catesbeiana	CCH-82	FLPFIARLAAKVFPSIICSVTKNVETLET	32.8	29	1
Rana catesbeiana	CCH-83	FLPFIARLAAKGF	28.7	13	2
Rana catesbeiana	CCH-84	FFPRVLPLANKFLPTIYCALPKSVGN	28.2	26	3
Rana catesbeiana	CCH-85	SMLSLLNNLGKVGP	26.9	14	1
Rana catesbeiana	CCH-86	GVFLDTLKGLAGKML	22.2	15	1
Rana catesbeiana	CCH-87	DNPDERFLPFIARLAAKVFPSIICSVTKKC	21.0	30	2
Rana catesbeiana	CCH-88	SAIQKWKKK	18.7	9	4
Rana catesbeiana	CCH-89	EEERFLPFIALLAAKVFPSIICSVTKKC	15.0	28	1
Rana catesbeiana	CCH-90	AGLQVPVGRIHRHLKTR	14.5	17	4
Rana catesbeiana	CCH-91	SLNSIVSHLKG	14.3	11	1
Rana catesbeiana	CCH-92	TKRWLPHRTR	14.2	10	4
Rana catesbeiana	CCH-93	GAETHKVWGKRGAETHNVRGKRSP	13.1	24	4
Rana catesbeiana	CCH-94	GAETHNVRGKRSPRSPRG	12.4	18	4
Rana catesbeiana	CCH-95	CQVRSKR	12.2	7	3
Rana catesbeiana	CCH-96	FLGGLIKIVPAMFC	12.0	14	1
Rana catesbeiana	CCH-97	GAETHKVWGKRSPRGAETHNVRGKR	11.8	25	5
Rana catesbeiana	CCH-98	GAETHKVWGKRSPRSP	11.4	16	3
Rana catesbeiana	CCH-99	GAETHKVWGKRSPRSPR	11.1	17	4
Rana catesbeiana	CCH-100	FLPFIARLAAKVFSINYLFSNQKML	11.0	25	3
Rana catesbeiana	CCH-101	GAETHKVWGKRSPRSPGGAETHNVWDKR	10.9	28	3
Rana catesbeiana	CCH-102	FLGGLIKIVPAMFW	10.6	14	1
Rana catesbeiana	CCH-103	SNIVIHCDLVLRASSELNSKRCKR	10.2	24	3
Rana catesbeiana	CCH-104	GQYTVLRTGVCKLLIRVT	27.3	18	3
Rana catesbeiana	CCH-105	VKAVLEKIGGHTKY	22.1	14	2

Rana catesbeiana	CCH-106	SRSSRFYTTYLGCNCWSCWGS	19.9	21	2
Rana catesbeiana	CCH-107	LNIWWKHSIKR	16.3	11	3
Rana catesbeiana	CCH-108	ILLAARPIRSRSGR	14.9	14	4
Rana catesbeiana	CCH-109	GILTLKNTLSFSQKP	10.8	15	2
Rana catesbeiana	CCH-110	QKRFYTTYLGCNCWSCWGS	10.7	19	2
Rana catesbeiana	CCH-111	GLYGRVARRKPLLSARNRK	10.2	19	7